2014

GUMBOS- and Ionic Liquid-Coated Quartz Crystal Microbalance Sensors for Detection and Molecular Weight Determination of Organic Vapors

Bishnu Prasad Regmi
Louisiana State University and Agricultural and Mechanical College, bishnu.regmi@alumni.lsu.edu

GUMBOS- AND IONIC LIQUID-COATED QUARTZ CRYSTAL MICROBALANCE SENSORS FOR DETECTION AND MOLECULAR WEIGHT DETERMINATION OF ORGANIC VAPORS

A Dissertation

Submitted to the Graduate Faculty of the
Louisiana State University and
Agricultural and Mechanical College
in partial fulfillment of the
requirements of the degree
Doctor of Philosophy
in
The Department of Chemistry

by
Bishnu P. Regmi
M.S., Utah State University, 2008
M.Sc., Tribhuvan University, 1997
B.Sc., Tribhuvan University, 1993
August 2014

I would like to dedicate my dissertation to

my parents
my siblings
my wife
and
my lovely kids

FOR

their

endless love, support, patience, and encouragement.

ACKNOWLEDGEMENTS

My PhD studies have been a wonderful journey, and I am indebted to many people who helped me in the successful pursuit of the graduate education.

First and foremost, I am deeply grateful to my advisor, Professor Isiah M. Warner. It has always been exciting times in working with you. Thank you for your time, ideas, advice, encouragements, and financial support to make my PhD education very productive. Your door was always open for me for stimulating discussions. Your insightful comments have always helped me to strengthen my knowledge in Chemistry. I learned not only chemical science but also interpersonal skills by being a member of your research group. I feel I am very fortunate to have you as my advisor, and the Warner Research Group has been a turning point in my career. Thank you for being an amazing mentor!

I would like to express sincere gratitude to my PhD committee members, Prof. Doug Gilman, Prof. Megan Macnaughtan, Prof. Daniel Hayes, and Prof. Keith Gonthier for their time, encouragements, valuable inputs, insightful questions, and interesting discussions. Thank you for making my PhD education enjoyable!

It was very exciting to work on diverse projects with a lot of collaborators. Your ideas, critical comments, suggestions, encouragements, and assistance in data generation and interpretation helped me to strengthen my research as well as broaden my horizons. In this regard, I am truly grateful to Prof. Kermit Murray, Prof. Francisco Hung, Prof. Daniel Hayes, Prof. Bilal El-Zahab, Dr. Joshua Monk, Dr. Paula Berton, Dr. Noureen Siraj, Dr. Arther Gates, Indika Galpothdeniya, Nicholas Speller, Yonathan Merid, Hashim Algafly, Paulina Kolic, Nimisha Bhattarai, and Tony Karam. I am truly grateful to Puspa Adhikari for helping in

statistical analysis. I am grateful to wonderful summer undergraduate students, Michael Anderson, Marc Webb, and Jean Olivier Brutus for their valuable inputs in my research. I gratefully acknowledge all the members of the Warner Research Group for their friendship, help, discussions, and collaborations.

Last but not least, I wish to thank all my family members for their love, support, and encouragements. I am deeply indebted to my mother and siblings who are eagerly waiting for successful completion of my studies. I am intensely grateful to my wife Sabina, and children Shambhawi and Binay who remained with me all these years with great patience!

Bishnu Regmi

Louisiana State University

June 2014

TABLE OF CONTENTS

ABSTRACT

There has been an ever-increasing demand for the development of high-performance sensing devices for detection and discrimination of volatile organic compounds (VOCs) present in different environments. Among a number of sensing devices currently available, sorption-based sensors are particularly attractive because they are simple and inexpensive, require low power, and are appropriate for fabrication of multisensor arrays. A sorption-based sensor is comprised of a chemically active coating immobilized on the surface of a physical transducer. The chemically active film interacts with analytes, and the transducer converts the binding event into an electrical signal. This dissertation is focused on a sorption-based sensor prepared by using ionic liquids (ILs) and a group of uniform materials based on organic salts (GUMBOS) as the sensing materials and the quartz crystal microbalance (QCM) as the transducer.

ILs are defined as organic salts which melt below 100 °C, and similar organic salts with melting point between 25 and 250 °C are defined as GUMBOS. In this research, a series of films comprising binary blends of an IL (or GUMBOS) and polymer are deposited onto the QCM surface in order to evaluate their vapor-sensing characteristics. The QCM sensors on exposure to organic vapors displayed a change in frequency and motional resistance, and both of these parameters were simultaneously measured. Examination of the data revealed an interesting relationship between the QCM parameters and the molecular weight of the absorbed vapors. The initial findings are reported in Chapter 2 of this dissertation. Additional studies were conducted in an effort to fully understand the interesting behavior of this type of material. More elaborate studies along with the theoretical rationale for the relationship between the QCM parameters and the molecular weight of vapors are presented in Chapter 3.

Another important aspect of this dissertation is the design of highly sensitive materials for vapor-sensing applications. Toward this end, two representative GUMBOS were synthesized using porphyrin and phthalocyanine derivatives. The QCM device coated with these GUMBOS exhibited a rapid response and high sensitivity toward different organic vapors. Altogether, these studies demonstrate the true potential of this type of materials for vapor-sensing applications.

CHAPTER 1 INTRODUCTION

1.1 Volatile Organic Compounds and the Need for Monitoring

1.1.1. Volatile Organic Compounds

Volatile organic compounds (VOCs) constitute a large group of organic chemicals that evaporate easily under normal conditions of temperature and pressure. VOCs are emitted in the atmosphere from a wide variety of natural and anthropogenic sources. The natural sources of VOCs are plants, animals, natural forest fires, and anaerobic processes in certain natural environments; and the major human activities that release VOCs include transportation, industrial activities, biomass burning, solvent use, and agricultural activities.[1-3] The biogenic emissions of VOCs are much greater than the anthropogenic emissions. At the global level, approximately 1300 Tg of carbon per year in the form of VOCs is emitted; and the biogenic emission accounts for 1150 Tg of C/year, while anthropogenic emission accounts for 142 Tg of C/year.[4] It is quite surprising that more than 1000 VOCs containing only one carbon atom may be found in the atmosphere.[4] Some VOCs have no adverse health effects, while some are toxic and/or carcinogenic to animals.[5]

1.1.2 The Need for VOC Measurements

The characterization of VOCs emitted from different sources is currently a topic of intense research. VOC monitoring is essential to many fields ranging from biomedical diagnostics to environmental monitoring. VOC sensors are particularly attractive in biomedical research.[6-20] More specifically, it has been demonstrated that VOCs in breath contain biomarkers for cancer and certain other diseases, and in this regard VOC profiling is useful in disease diagnosis and monitoring.[15-20] Altered patterns of VOCs in a diseased state as opposed to normal state are due to changes in the metabolic activity owing to pathological conditions. In addition to

breath, VOCs emitted from urine, skin, and blood also reflect medical status.[20] Several studies have demonstrated that the VOC profile has potential for the detection and discrimination bacterial species,[21-23] assessment of food quality,[24,25] environmental monitoring,[26] detection of diseased plants,[27] and detection of explosives,[28-31]

1.1.3 Common VOC-Detection Technologies

The most commonly employed conventional technique for VOC detection is GC-MS; however, the instrument is expensive, bulky, and requires skilled workers for operation. Other commonly used techniques are ion mobility spectrometry,[32] flame ionization detector,[33,34] and photoionization detector.[34] Recently, there has been upsurge of interest in the development of simple, facile, and low cost detection technology to monitor VOCs. In this regard, sorption-based vapor sensors have gained considerable momentum because they are compact and inexpensive, require low power, and are amenable to the creation of sensor arrays.[35,36] A sorption-based sensor comprises a chemically selective material coated on the surface of a non-selective physical transducer. In other words, a sensor is comprised of two essential components: 1) a chemically active sensing material that binds with the anlytes of interest and determines the chemical selectivity of the sensor and 2) a transducer that converts the binding interactions into an electronic signal. Acoustic wave devices, chemicapacitors, and chemiresistors are among the most common transducers employed to fabricate sorption-based sensors.[36] The most popular acoustic wave device is the quartz crystal microbalance (QCM). It must be noted that an optimal combination of sensing materials and transducer is critical to achieve best sensing performance. The properties of the sensing materials are modulated during vapor sorption, and the transducer converts this change into a useful analytical signal. More specifically, chemicapacitors measure

changes in dielectric properties.[36,37] chemiresistors measure the changes in electric resistance,[38,39] and the QCM measures the changes in mass and/or viscoelasticity.[40,41]

1.2 Quartz Crystal Microbalance and its Operating Principle

The QCM is a simple, cost effective, and highly sensitive mass sensing technique the heart of which is an AT-cut quartz crystal with the operating principle based on piezoelectricity. The technique is discussed in more detail below.

1.2.1 Piezoelectric Effect

Piezoelectric effect was discovered by Pierre and Jacques Curie in 1880. The Curie brothers observed that certain crystals on mechanical deformation produce an electric voltage, and this effect was named as the piezoelectric effect which means pressure-electric effect. Alternatively, the application of an electric field produces a mechanical deformation, and this effect is known as converse piezoelectric effect. In fact, the piezoelectric effect is exhibited by certain compounds containing asymmetric crystalline structures such as quartz, Rochelle salt, ammonium dihydrogen phosphate, and piezoelectric ceramics such as lead titanate-zirconate.[42] Crystalline quartz is the most common piezoelectric material.

1.2.2 Quartz Cuts

A quartz crystal can be cut in different orientations with respect to the crystallographic axes, and the type of cut determines the physical and electrical properties. The most popular types of cut are AT- and BT-cuts; the cutting schemes are displayed in Figure 1.1. A QCM is comprised of an AT-cut crystal which is inserted between two metallic electrodes, usually gold, as shown in Figures 1.2(a-c). In this figure, (**a**) is the top view of the quartz crystal which shows a circular gold electrode in the center, and (**b)** is the bottom view of the crystal. The electrode on

the bottom side is also circular but smaller than the top electrode. The electrical contact to both the electrodes is provided from the bottom side. Figure 1.2b is the side view of the crystal, and the resonance frequency depends on the thickness (t_q) of the crystal.

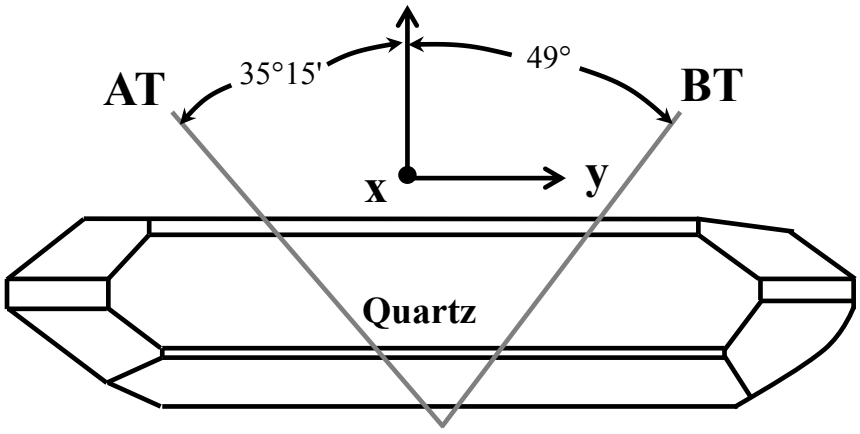

Figure 1.1 Diagram illustrating the methods to get AT- and BT-cut crystal plates from a natural crystal. The lines represent the saw cut positions. This figure is adapted and modified from http://www.4timing.com/techcrystal.htm (accessed May 12, 2014).

(a) (b) (c)

Figure 1.2 Typical quartz crystal resonator used in a QCM; (a) top view, (b) bottom view, and (c) side view (t_q represents the thickness of the quartz wafer).

1.2.3 Shear Waves

When an AC voltage is applied across the electrodes, the quartz crystal undergoes oscillations in the thickness shear mode. Hence, the QCM is more correctly referred to as thickness shear mode (TSM) resonator. The direction of the particle displacement is parallel to the surface of the crystal, while the direction of wave propagation is perpendicular to the surface. The antinodes of the shear waves lie at the surfaces, while the nodes lie inside the crystal as shown in Figures 1.3 (a-b).[43] Since the nodes lie at the surface of the crystal, the crystal vibrates only at odd harmonics. The wavelength of the wave depends on the thickness of the crystal. The oscillation frequency is in the megahertz (MHz) region, and this is a critical parameter for analytical applications. In fact, resonances can occur only at those frequencies where the wavelength is an odd multiple of half wavelength.[43,44] Under resonance conditions, $t_q = \frac{n\lambda}{2}$ (1.1) where t_q is the thickness of the crystal, n is the harmonic number which can be only an odd number, and λ is the wavelength of the shear wave. For the first harmonic, $n = 1$ and t_q is $\frac{\lambda}{2}$ (Figure 1.3a). For the third harmonic, $n = 3$ and t_q is $\frac{3\lambda}{2}$ (Figure 1.3b). For an AT-cut quartz crystal with a thickness 333 μm, the fundamental frequency will be 5 MHz. The AT-cut crystals are preferred for the QCM because they exhibit higher frequency stability and very low temperature coefficient with vibrations in pure thickness-shear mode.[45,46]

1.2.4 Mechanical and Electrical Models for a QCM

A QCM resonator can be represented by a mechanical model as well as an equivalent electrical model. The mechanical model is shown in Figure 1.4a which is comprised of mass attached to a spring and a piston. The overall response depends on the mass (m) of the system, compliance (C_m) of the spring, and coefficient of friction (r_f) of the piston. The piston represents

the energy loss during oscillations. Because of the piezoelectric characteristics of quartz, the mechanical model can be represented by an equivalent electrical model comprising different lumped parameters as shown in Figure 1.4b. The model is also known as the Butterworth-van Dyke (BVD) electrical model, and this model has been widely used to simulate the system near series resonance. The BVD model is comprised of two branches, namely, static and motional branches. The motional arm consists of resistor (R_m), capacitor (C_m), and inductor (L_m) in series. R_m represents the dissipation of oscillation energy, L_m is related to the displaced mass during oscillation, and C_m corresponds to energy stored during oscillation.[47] The static arm is parallel to the motional arm, and this comprises the static capacitance (C_o) produced due to the presence of two electrodes on opposite sides of the dielectric quartz crystal.[47,48]

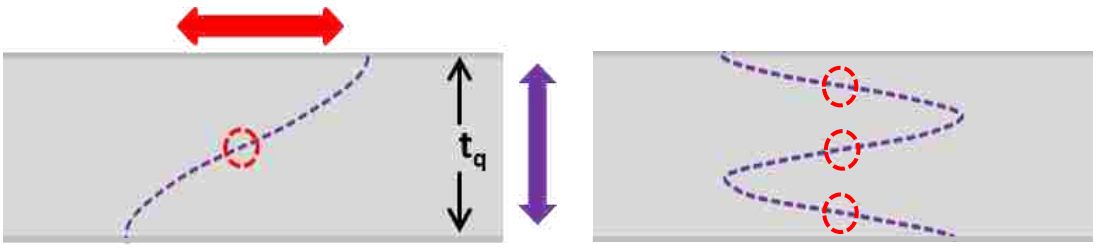

Figure 1.3 Schematic of acoustic shear waves in a TSM resonator displaying (a) fundamental mode and (b) third harmonic. The red double-headed block arrow shows the direction of particle displacement, while the purple arrow indicates the direction of wave propagation, red circles indicate nodes, and t_q represents the thickness of the piezoelectric material. The figures are adapted and modified from reference 43.

1.2.5 Interface Electronics for a QCM

The resonance behavior of a quartz crystal resonator can be described by two essential parameters, namely, series resonance frequency (f) and motional resistance.[48-50] The series resonance frequency (hereafter simply referred to as resonance frequency) is a frequency near the minimum of electrical impedance (or maximum of electrical admittance) of the quartz

resonator.[48] In sensing applications, it is in fact the resonance frequency change (Δf) and motional resistance shift (ΔR) due to interactions of coating with analyte are important. Three

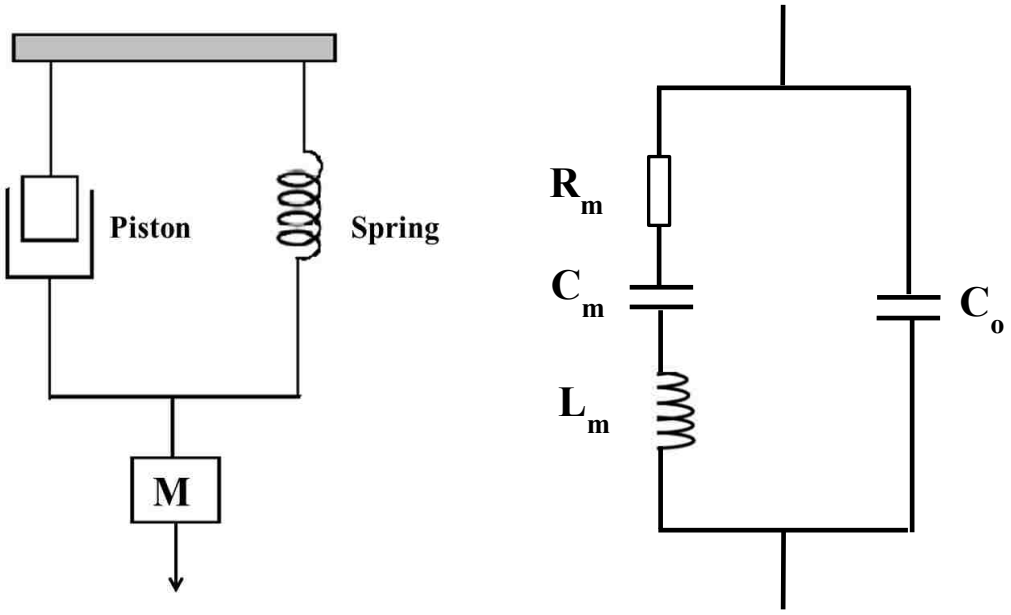

(a) (b)

Figure 1.4 (a) Mechanical model of a TSM resonator (b) Butterworth-van Dyke model of the unperturbed resonator.

types of interface electronic systems are commonly employed to measure the resonance parameters of a QCM resonator.[48,51,52] A simple, economical, and the most common way to measure the QCM parameters is by using oscillator circuit which gives resonance frequency and motional resistance as the output parameters.[48,51-53] The quartz crystal is integrated to an electrical oscillating circuit, and C_o is cancelled to achieve the parameters at series resonance.[53] The main limitation of an oscillator circuit is that it is restricted to only one harmonic, which makes it difficult to interpret the acquired data. However, recently a dual-harmonic oscillator capable of operating at the first and third harmonics has been described.[54]

Another improved approach that has been widely used to measure QCM parameters is a network analyzer which is used to monitor electrical impedance or admittance over a range of frequencies.[55-58] Impedance (Z) refers to the opposition to the flow of AC current through a device or circuit. It is a complex quantity given as: $Z = R + jX$, where the real part is resistance, R, and the imaginary part is reactance, X, and j is the imaginary unit. The reciprocal of impedance is admittance (Y) which is defined as: $Y = G + jB$, where G is conductance and B is susceptance. In practice, the complex admittance or impedance of the resonator in a narrow range of frequency near the resonance is measured by using an impedance analyzer. In Figure 1.5, for instance, the variation of conductance (the real part of the admittance) as a function of oscillation frequency is displayed. The frequency corresponding to the maximum of the conductance-versus-frequency curve is resonance frequency, and the bandwith or the full width at half maximum (2Γ) is related to energy dissipation or motional resistance.[51,58,59] The motional resistance is taken as the inverse of the conductance peak value.[48,60] Motional resistance and bandwidth are equivalent, and they can be derived from each other.[61] The network analyzers can be used to monitor admittance spectra at several harmonics, and these devices provide more information compared to the oscillator circuits.

A third approach to acquire the QCM resonance parameters is by using a ring-down-based technique introduced by Kasemo and coworkers.[62,63] This is a relatively new approach which allows the measurement of the series resonance frequency and the series dissipation factor (D) at multiple harmonics. The dissipation factor (D) is defined as:[62]

$$D = \frac{E_{\text{dissipated}}}{2\pi E_{\text{stored}}} \qquad (1.2)$$

where $E_{\text{dissipated}}$ is the energy lost per oscillation cycle, and E_{stored} is the total energy stored in the oscillation system. The measuring principle of this approach involves abruptly switching off the driving power to the resonator and measuring the amplitude of the freely decaying oscillator. The schematic of oscillation decay as a function of time is shown in Figure 1.6. The amplitude decay is governed by the following equation:[62]

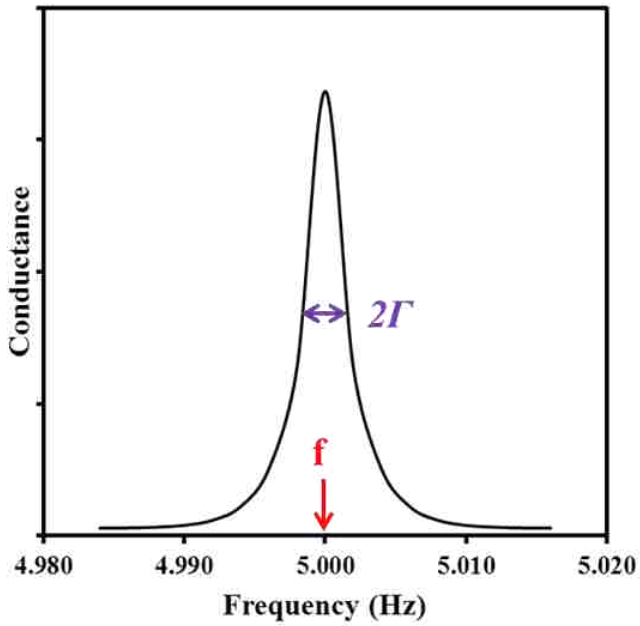

Figure 1.5 Variation of electrical conductance as a function of excitation frequency. The resonance frequency corresponds to the peak of the curve and bandwidth is the full width at half maximum as illustrated. The reciprocal of the conductance peak value is motional resistance.

$$A_t = A_o e^{-\frac{t}{\tau}} \sin(\omega t+\varphi) + \text{ constant}, \quad t \geq 0, \qquad (1.3)$$

Where A_t is the amplitude at time t, A_o is the amplitude $t = 0$, τ is the decay time constant, ω is the angular frequency, φ is the phase, and 'constant' is the dc offset. The dissipation factor is then calculated as:

$$D = \frac{2}{\omega\tau} \qquad (1.4)$$

The dissipation factor can be related to bandwidth and motional resistance by the following equations:[61,62]

$$D = \frac{2\Gamma}{f} \quad (1.5)$$

$$D = \frac{R_m}{2\pi f L_m} \quad (1.6)$$

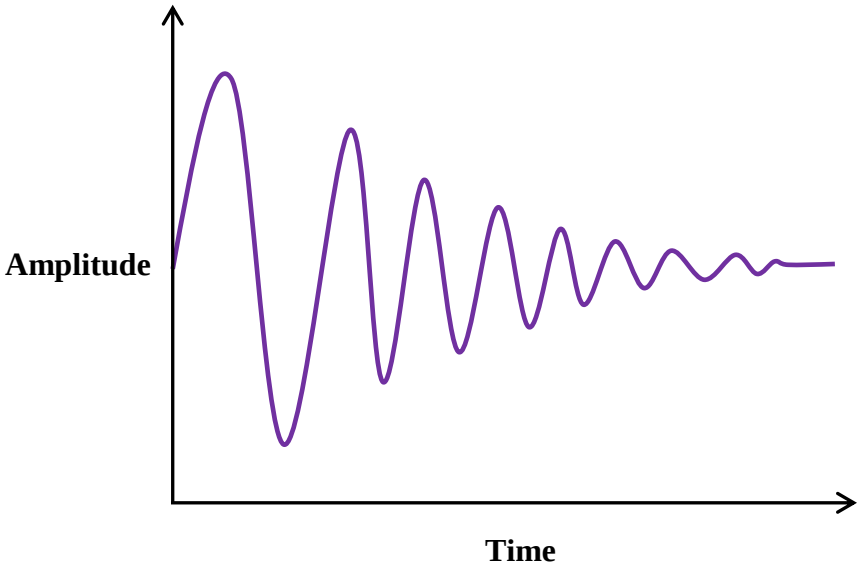

Figure 1.6 Schematic showing the decay of voltage amplitude as a function of time after the driving voltage is switched off.

1.2.6 QCM Responses under Various Mass Loads

The use of a quartz crystal resonator for mass sensing was first realized in 1959 by a German physicist, G. Sauerbrey, who discovered that mass deposition on the surface of the resonator leads to a decrease in its resonance frequency.[41] This discovery led to the development of TSM device as a sensitive analytical tool for detection of chemical and biological species, as well as for probing interfacial properties and phenomena. The Sauerbrey equation states that the magnitude of the frequency shift (Δf) is directly proportional to the amount of mass deposited on

the surface of the resonator. It must remembered that this is true for rigid, thin, and uniform films adsorbed on the surface. Mathematically, the Sauerbrey equation is expressed as:[41]

$$\Delta f = -\frac{n}{C}\Delta m = -\frac{n}{C}\rho_f t_f \qquad (1.7)$$

where Δm is mass per unit area of the film (in air or vacuum), ρ_f is the density of the film, t_f is the thickness of the film, n is the harmonic number which can only be an odd integer, and C is the mass sensitivity or Sauerbrey constant which depends on the fundamental resonance frequency and properties of the quartz (C = 17.7 $ng.cm^{-2}.Hz^{-1}$ for a 5 MHz AT-cut quartz crystal). In the case of rigid mass deposits, the motional resistance change (ΔR) will be zero.[64]

In the 1960s and 1970s, the QCM was used for monitoring of film thickness in gas phase and vacuum. The general belief in those days was that the quartz resonator would not oscillate in the liquid phase. However, in 1982 Nomura and Okuhara[65] from Shinshu University in Japan demonstrated that a QCM can be operated in liquid phase, and the authors reported that the frequency shift is dependent on the viscosity and density of the liquid. This discovery led to a dramatic increase in the use of QCM in liquid phase-based applications, particularly in biosensing.[45,66] In order to explain the resonant behavior of a QCM operating in liquid phase or non-rigid overlayers, several theoretical models have been developed depending on the type of the environment.

It is believed that the Sauerbrey equation is still applicable if a rigid mass is added or removed from the surface of the resonator that is immersed in a liquid.[67] Another commonly observed case in one where one face of the quartz resonator is completely immersed in a Newtonian liquid. The mathematical relationship for such a case was derived by Kanazawa and

Gordon,[68] and the authors demonstrated that the frequency shift is dependent on the viscosity and density of the liquid. The Kanazawa-Gordon equation can be expressed as:

$$\Delta f = -f^{\frac{3}{2}}\left(\frac{\eta_L \rho_L}{\pi \mu_q \rho_q}\right)^{\frac{1}{2}} \qquad (1.8)$$

where f is the resonance frequency of the free crystal, η_L and ρ_L are the absolute viscosity and density of the liquid, respectively, and μ_q and ρ_q are the shear modulus and density of the quartz, respectively. From this equation, it is evident that the decrease in frequency is directly proportional to the square root of viscosity-density product. The motional resistance in this case increases, and this increase is again directly proportional to the square root of viscosity-density product.[69-71]

In many chemical and biological sensing applications, thin viscoelastic films are very common. Viscoelastic materials show both elastic and viscous properties. The rheological behavior of viscoelastic materials can be described by a complex shear modulus (G^*), and thus $G^* = G' + jG''$, where G' (or μ) is the elastic shear modulus and G'' is the loss modulus. In order to explain the viscoelastic characteristics of these materials, a number of mathematical models have been proposed. Two commonly used models in this regard are the Maxwell model, which is made up of a series combination of a spring and a dashpot, and the Kelvin-Voigt model, which comprises a parallel combination of a spring and a dashpot. For a thin layer of Kelvin-Voigt viscoelastic materials in vacuum, Δf and dissipation change (ΔD) are given as:[72,73]

$$\Delta f \approx -\frac{t_f \rho_f \omega}{2\pi \rho_q t_q}\left(1+\frac{t_f^2 \rho_f \omega^2}{3\delta^2(1+\chi^2)}\right) \qquad (1.9)$$

$$\Delta D \approx \frac{2t_f^3 \rho_f \omega}{3\pi f \rho_q t_q}\frac{1}{3\delta^2(1+\chi^2)}, \qquad \chi = \frac{\mu_f}{\omega \eta_f}, \quad \delta = \left(\frac{2\eta_f}{\rho_f \omega}\right)^{\frac{1}{2}} \qquad (1.10)$$

where the subscript f refers to the film, subscript q refers to the quartz, ω is the measured angular frequency, χ is the viscoelastic ratio (ratio of storage modulus and loss modulus), and δ is the viscous penetration depth. For a thin film obeying the Maxwell viscoelastic model, Δf and ΔD are given as:[74]

$$\Delta f \approx -\frac{t_f \rho_f \omega}{2\pi \rho_q t_q}\left(1+\frac{t_f^2 \rho_f \omega^2}{3\mu_f}\right) \qquad (1.11)$$

$$\Delta D \approx \frac{2t_f^3 \rho_f^2 \omega}{3\rho_q t_q \eta} \qquad (1.12)$$

The films are assumed to be thin if the thickness of the film is much less than the penetration depth (δ).[72] The penetration depth can be understood as follows. As shown in Figure 1.7, the shear wave propagates perpendicular to the surface of the resonator, and its amplitude diminishes with distance in the surrounding medium. The penetration depth is defined as the distance at which the amplitude of the wave decays to $\frac{1}{e}$ of the amplitude at the oscillator surface.[75] It is evident from equation 1.10 that the penetration depth depends on the viscosity and density of the medium, and the frequency of the wave. For instance, the penetration depth of a wave at 5 MHz frequency in water at room temperature is approximately 252 nm. The penetration depth is much higher in ionic liquids because of high viscosity of these compounds. For example, 1-butyl-3-methylimidazolium hexafluorophosphate has viscosity 371 mPa.s and density of 1373 $kg.m^{-3}$ at 20 °C.[76] The penetration depth at 5 MHz will be approximately 4.15 μm. It should be emphasized that the penetration depth decreases with an increase in frequency.

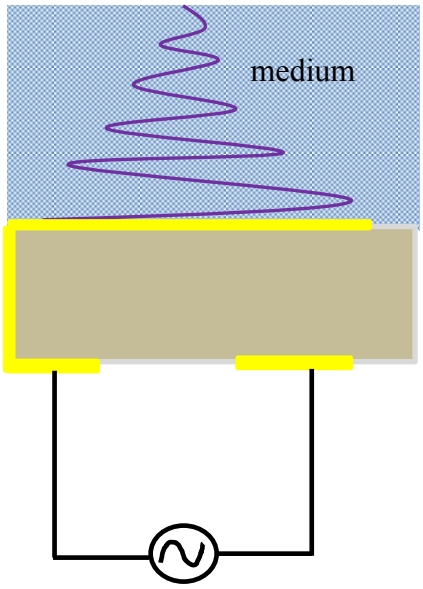

Figure 1.7 Schematic showing the propagation and decay of shear wave in the surrounding medium.

1.3 Sensing Materials for QCM Chemical Sensor

Sensing materials are essential components of chemical sensors, and the chemical sensitivity and selectivity of a sensor depends on the sensing materials, while the transducer as such is non-selective. Hence, most of the current studies focus in designing novel or improved sensing materials. Two approaches have been used in designing sensing materials.[77,78] The first approach is to design materials which exhibit highly selective response to an analyte of interest, and the materials in this category include molecularly imprinted polymers, zeolites, cavitands, and others.[77] However, the synthesis of highly selective sensing materials is challenging; in addition, this method not useful to analyze complex mixtures.[78] The second approach is to design sensing materials exhibiting broad and partial selectivity to different chemical species. The idea is to create an array of sensors (i.e. electronic nose) using these materials to discriminate individual or complex mixture of chemical species. In other words, an electronic nose comprises a group of cross-reactive sensing elements. The responses obtained from a sensor array are then

analyzed using various pattern recognition techniques such as principal component analysis (PCA), linear discriminant analysis (LDA), and artificial neural network (ANN). The electronic nose to discriminate between complex odorant mixtures was first reported by Persaud and Dodd in 1982.[79,80] These days, there is an increasing interest in the use of sensor arrays in multitude of applications.

As discussed above, the QCM sensor comprises a chemosensitive thin film immobilized on the surface of the quartz resonator. The interaction of the coating with analyte(s) of interest causes a change in mass and/or viscoelastic properties of the film which in turn leads to a change in frequency and/or dissipation of the QCM sensor. In vapor sensing studies, Δf as a function of vapor concentration is monitored. Only in rare cases, both Δf and ΔR as a function of analyte concentration have been monitored.[81,82] However, measuring two parameters is much more informative in vapor analysis. It must be emphasized that a selection of suitable sensing material is critical to access both of these parameters. A wide array of materials has been utilized to prepare chemosensitive coatings for QCM sensors to detect and discriminate different organic vapors. These sensing materials include ordinary polymers,[83,84] molecularly imprinted polymers,[85-87] calixarenes,[82,88] carbon nanotubes,[89] metalloporphyrins,[90] various nanocomposites,[91] organic dendrimers,[92] peptides and proteins,[93,94] ceramic materials,[95] and others. In the last decade, a class of materials that has captured increasing attention to prepare QCM sensing films is ionic liquids.[96-112]

1.4 An Overview of Ionic Liquids and GUMBOS, and Their Applications in QCM Devices

Ionic liquids (ILs) are organic salts with melting points below 100 °C.[113] ILs that remain in the liquid state below 25 °C are commonly referred to as room temperature ionic liquids (RTILs), while those that are solid at room temperature are known as frozen ionic liquids. ILs

contain bulky and asymmetric ions with large size differences between cations and anions which ultimately lead to frustrated packing thereby resulting in low melting points.[114] A wide range of cations and anions can be combined to produce potentially 10^{18} ionic liquids.[115] The common ions used to prepare ILs are given in Figure 1.8. ILs possess outstanding physicochemical properties such as high thermal and electrochemical stability, broad liquid range, negligible vapor pressure, high ionic conductivity, and exceptional tunability that make them excellent candidates for industrial applications.[113,116] The Warner Research Group is currently investigating numerous applications of ionic liquids and similar organic salts with melting points extending beyond 100 °C. The organic salts with melting points between 25 and 250 °C have been recently named as a Group of Uniform Materials Based on Organic Salts (GUMBOS).[117] We have recently synthesized ILs and GUMBOS using various dye ions;[118,119] some of these ions are shown in Figure 1.9. Interestingly, GUMBOS can be easily converted into nanomaterials which are known as nanoGUMBOS.[117,120] GUMBOS/nanoGUMBOS have shown promising applications in biomedical imaging,[121] selective killing of cancer cells,[119] organic light emitting diodes,[122] dye-sensitized solar cells,[123] and vapor sensing.[107,108]

The first use of ILs as QCM coating materials to detect organic vapors was reported by Liang and coworkers in almost a decade ago.[96] The authors coated a QCM resonator with a relatively thick layer of an IL, and exposed the sensor toward a number of organic compounds. The frequency change due to vapor absorption was found to be positive. The response was fast with an average response time of 2 s, and the vapor absorption was completely reversible. According to the Sauerbrey equation, the change in frequency during vapor absorption is expected to be negative. The authors explained the positive change in frequency by using the

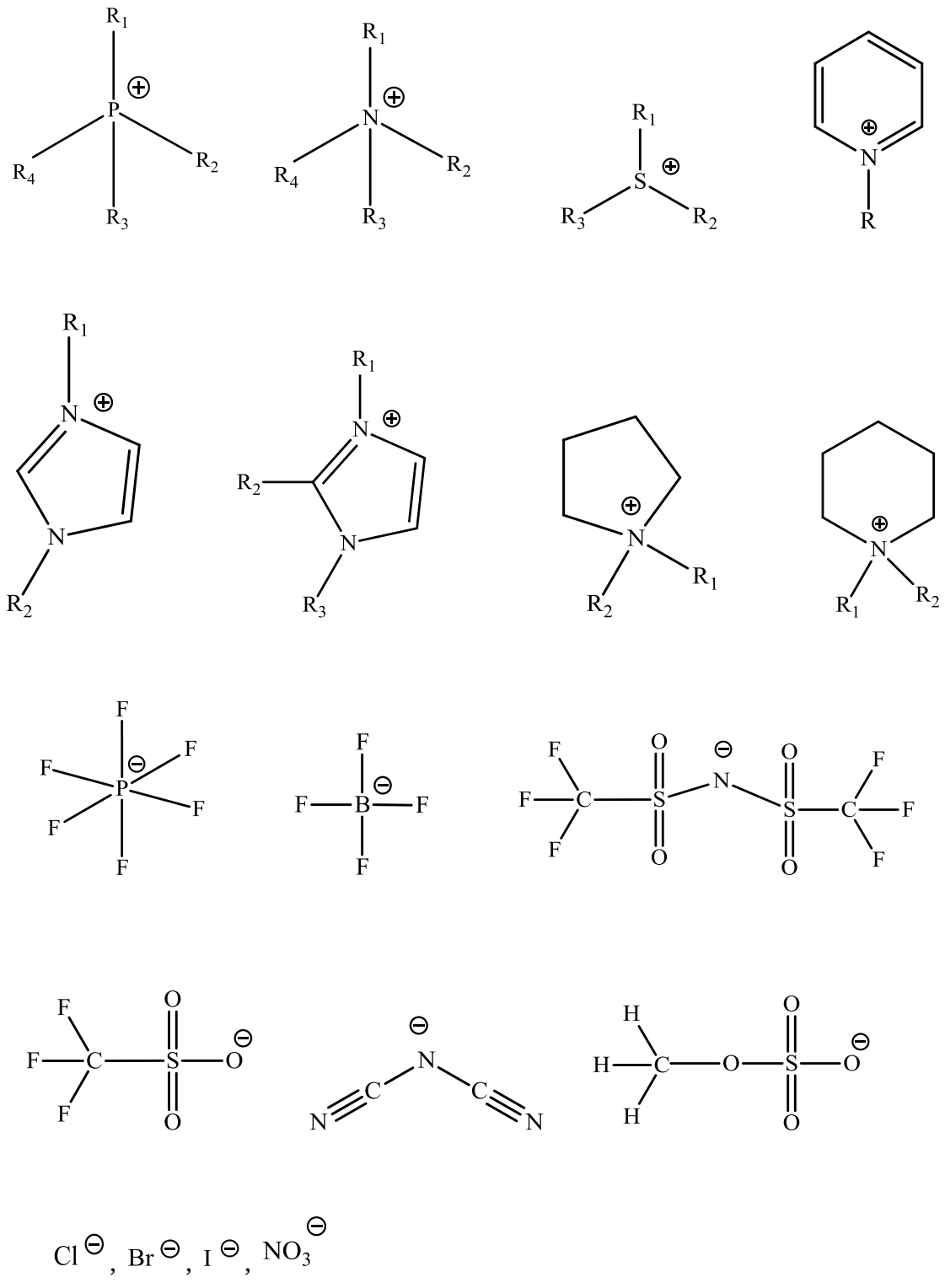

Figure 1.8 Some common cations and anions used to prepare ionic liquids and GUMBOS.

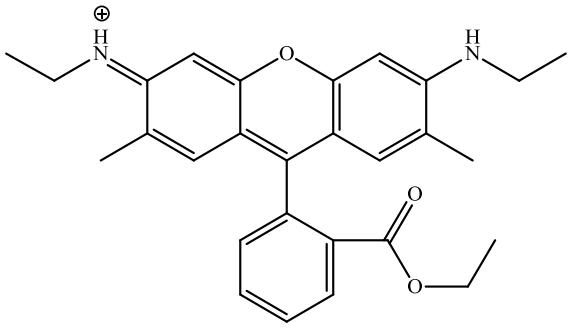

Rhodamine 6G cation

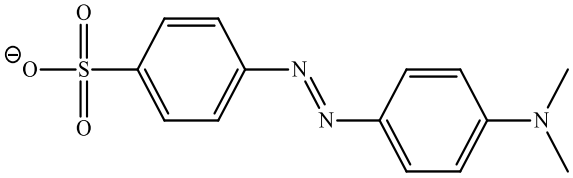

Methyl orange anion

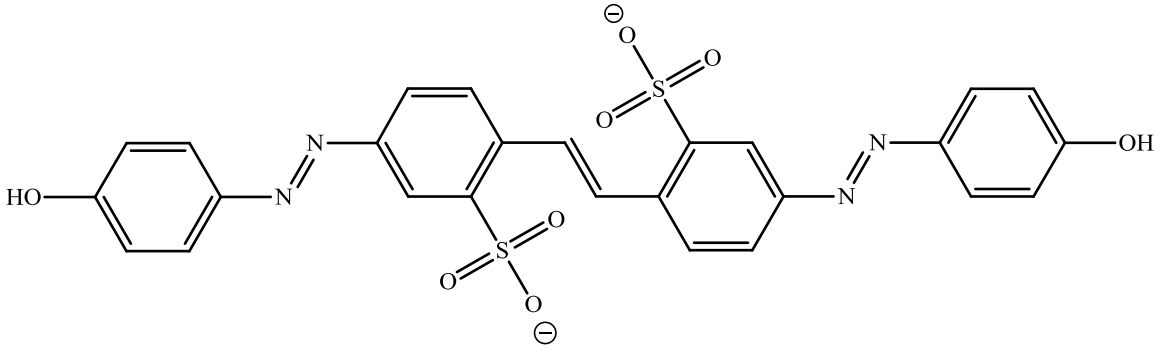

Brilliant yellow anion

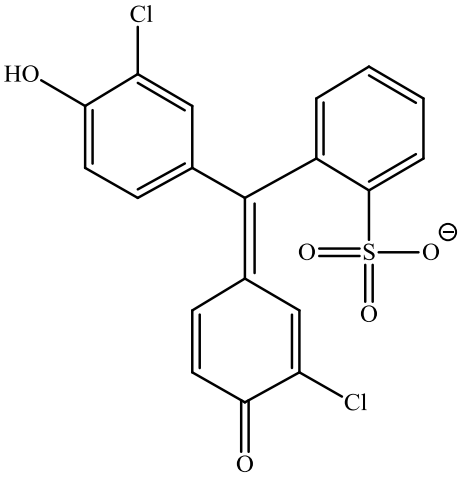

Chlorophenol red anion

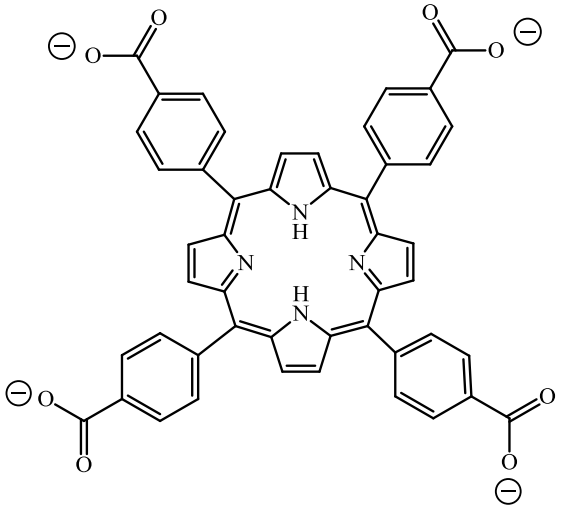

meso-Tetra(4-carboxyphenyl)porphyrin anion

Figure 1.9 Some dye ions used to prepare ionic liquids and GUMBOS

Kanazawa-Gordon equation (equation 1.8). In fact, the absorption of vapors by an ionic liquid results in a decrease in viscosity and density of the ionic liquid thereby leading to an increase in frequency. A number of different forces including dispersion interactions, hydrogen bonding, dipolar, and π-π interactions exist between ionic liquids and the organic compounds, and the extent of these interactions depend on the structures of cations and anions of the ionic liquids. Therefore, ionic liquids are expected to show partial selectivity to different organic vapors, and the selectivity can be fine-tuned by changing or modifying cation and anion.

The use of ILs as sensing materials for a QCM device continued to grow. In this regard, Goubaidoulline and coworkers presented the concept of immobilizing ILs inside nanopores of an alumina layer deposited on the electrode of the quartz resonator.[97] This approach eliminated the problems associated with dewetting and viscoelasticity; however, desorption of vapor was found to be slow due to the confinement of ILs inside the nanopores. Jin et al.[98] developed a QCM/IL sensor array using seven room temperature ionic liquids to detect organic vapors at ambient and high temperatures. The sensor array data were subjected to linear discriminant analysis (LDA) which showed an excellent discrimination between a number of organic vapors. Similarly, Xu et al.[99] devised a QCM/IL sensor array to analyze several organic vapors. The sensor array data were analyzed using an artificial neural network (ANN) method, and the accuracy of identification was found to be 100 %. In a separate study, the same research group evaluated the sensing performance of six imidazolium-based ILs using the QCM, and demonstrated that imidazolium halides exhibit good selectivity for alcohol vapors.[100] Recently, Toniolo et al.[101] developed a QCM sensor array using different RTILs and analyzed 31 VOCs belonging to several chemical classes. The data were analyzed using principal component analysis (PCA), and separate clusters for each class of compounds were obtained. In order to demonstrate that such

sensor array can be useful for discrimination of closely related mixtures, headspaces from two varieties of cinnamon samples were analyzed. Statistical analysis of the data showed a clear distinction between these two samples of food.

ILs in the form of composites have also been used to improve the sensing performance of QCM sensor. In this regard, Seyama et al.[102] designed a sensor array by incorporating an IL into a plasma polymerized film that was prepared using D-phenylalanine. A sensor array was created by using four sensors. The first sensor contained only the polymer film, while the other three sensors contained different concentrations of 1-ethyl-3-methylimidazolium tetrafluoroborate incorporated into the polymer film. The sensor array was then utilized to discriminate four different n-alcohol vapors. In another study, Jin et al.[104] immobilized an IL on a polyaniline template on the QCM surface, and this greatly improved the sensitivity to methane detection. The immobilization of ILs on a polyaniline template improved the wettability of ILs on the surface as well as increased the amount of IL deposits. Ji et al.[105] prepared a layered film using graphene-ionic liquid composite for highly selective sensing of aromatic vapors.

In all the studies discussed above, organic vapors are absorbed reversibly to the IL films due to relatively weak vapor-IL interactions. However, the weak interactions limit the sensitivity. Recently, there have been several attempts to design ILs that exhibit chemical reactions with specific analytes.[110-112] This approach greatly enhances the sensitivity and selectivity of the sensor; however, the binding of analyte to the IL is irreversible, and hence the IL film is required to remove by washing and replace by a new film for each measurement. The foregoing discussion clearly demonstrates that ILs and GUMBOS are very promising materials to be used as chemosensitive film for a QCM device. In this regard, further studies are necessary to fully exploit the potential of these material as chemical recognition elements.

1.5 Scope of this Dissertation

The objective of this research was to investigate in detail the vapor-sensing applications of GUMBOS and ILs using the QCM transducer. The QCM is typically used as a very sensitive mass sensor; however, during the course of this study, very remarkable sensing behavior was discovered which for the first time shows that QCM can be used for an estimation of molecular weight of organic vapors. The second chapter of this dissertation is the description of the initial studies on preparation, characterization, and vapor-sensing applications of a composite film prepared by using 1-butyl-2,3-dimethylimidazolium hexafluorophosphate and cellulose acetate. The composite film coated QCM sensor exhibits excellent sensing characteristics, and moreover, the Δf-to-ΔR ratio, under low vapor concentrations, is directly proportional to the molecular weight of vapor analytes. A preliminary explanation for this observation is presented.

The third chapter is description of the follow-up studies primarily aimed at understanding the theoretical basis for the relationship between the QCM parameters and molecular weight of organic vapors. A number of binary blends of an IL and polymer are prepared on the QCM surface, and the vapor-sensing characteristics the sensors are evaluated over a wider range of analyte concentrations. In addition, the response of the sensor at different harmonics are monitored using a QCM-D system. Based on these data, a more plausible explanation focusing on how the changes in QCM parameters can be related with the molecular weight of the vapors is provided.

The fourth chapter is focused on the synthesis of porphyrin- and phthalocyanine-based GUMBOS and evaluation of these GUMBOS as QCM-coating materials for detection of a number of organic vapors. A remarkable improvement in sensitivity and other sensing characteristics are observed. The potential of these GUMBOS for electronic nose applications is

discussed. The fifth chapter concludes the dissertation by summarizing the important findings, their implications and the possible avenues for future research.

1.6 References

(1) Derwent, R. I. Sources, distributions, and fates of VOCs in the atmosphere. In *volatile organic compounds in the athmosphere*; Editors Hester, R. E., Harrison, R. M; Royal Society of Chemistry; Cambridge, UK, **1995**; Vol. 4, pp. 1-16.

(2) Guenther, A.; Hewitt, C. N.; Erickson, D.; Fall, R.; Geron, C.; Graedel, T.; Harley, P.; Klinger, L.; Lerdau, M.; McKay, W.: A global model of natural volatile organic compound emissions. *Journal of Geophysical Research* **1995**, *100*, 8873-8892.

(3) Kansal, A.: Sources and reactivity of NMHCs and VOCs in the atmosphere: A review. *Journal of Hazardous Materials* **2009**, *166*, 17-26.

(4) Goldstein, A. H.; Galbally, I. E.: Known and unexplored organic constituents in the earth's atmosphere. *Environmental Science & Technology* **2007**, *41*, 1514-1521.

(5) United States Environmental Protection Agency. An introduction to indoor air quality. *http://www.epa.gov/iaq/voc.html* (accessed June 7, 2014).

(6) Baranska, A.; Tigchelaar, E.; Smolinska, A.; Dallinga, J. W.; Moonen, E. J. C.; Dekens, J. A. M.; Wijmenga, C.; Zhernakova, A.; van Schooten, F. J.: Profile of volatile organic compounds in exhaled breath changes as a result of gluten-free diet. *Journal of Breath Research* **2013**, *7*, 037104.

(7) Broza, Y. Y.; Haick, H.: Nanomaterial-based sensors for detection of disease by volatile organic compounds. *Nanomedicine* **2013**, *8*, 785-806.

(8) Alkhouri, N.; Cikach, F.; Eng, K.; Patel, N.; Yan, C.; Brindle, A.; Rome, E. S.; Grove, D.; Hanouneh, I. A.; Lopez, R.; Hazen, S. L.; Dweik, R. A.: Analysis of breath volatile organic compounds as a noninvasive tool to diagnose nonalcoholic fatty liver disease in obese children. *Gastroenterology* **2013**, *144*, S947-S948.

(9) Peled, N.; Barash, O.; Tisch, U.; Ionescu, R.; Broza, Y. Y.; Ilouze, M.; Mattei, J.; Bunn, P. A., Jr.; Hirsch, F. R.; Haick, H.: Volatile fingerprints of cancer specific genetic mutations. *Nanomedicine-Nanotechnology Biology and Medicine* **2013**, *9*, 758-766.

(10) Sethi, S.; Nanda, R.; Chakraborty, T.: Clinical application of volatile organic compound analysis for detecting infectious diseases. *Clinical Microbiology Reviews* **2013**, *26*, 462-475.

(11) Walton, C.; Fowler, D. P.; Turner, C.; Jia, W.; Whitehead, R. N.; Griffiths, L.; Dawson, C.; Waring, R. H.; Ramsden, D. B.; Cole, J. A.; Cauchi, M.; Bessant, C.; Hunter, J. O.:

Analysis of volatile organic compounds of bacterial origin in chronic gastrointestinal diseases. *Inflammatory Bowel Diseases* **2013**, *19*, 2069-2078.

(12) Xu, Y.; Lee, H.; Hu, Y.; Huang, J.; Kim, S.; Yun, M.: Detection and identification of breast cancer volatile organic compounds biomarkers using highly-sensitive single nanowire array on a chip. *Journal of Biomedical Nanotechnology* **2013**, *9*, 1164-1172.

(13) Robroeks, C. M.; van Berkel, J. J.; Jobsis, Q.; van Schooten, F.-J.; Dallinga, J. W.; Wouters, E. F.; Dompeling, E.: Exhaled volatile organic compounds predict exacerbations of childhood asthma in a 1-year prospective study. *European Respiratory Journal* **2013**, *42*, 98-106.

(14) Phillips, M.; Byrnes, R.; Cataneo, R. N.; Chaturvedi, A.; Kaplan, P. D.; Libardoni, M.; Mehta, V.; Mundada, M.; Patel, U.; Ramakrishna, N.; Schiff, P. B.; Zhang, X.: Detection of volatile biomarkers of therapeutic radiation in breath. *Journal of Breath Research* **2013**, *7*, 036002.

(15) Phillips, M.; Basa-Dalay, V.; Bothamley, G.; Cataneo, R. N.; Lam, P. K.; Natividad, M. P. R.; Schmitt, P.; Wai, J.: Breath biomarkers of active pulmonary tuberculosis. *Tuberculosis* **2010**, *90*, 145-151.

(16) Wang, Y.; Hu, Y.; Wang, D.; Yu, K.; Wang, L.; Zou, Y.; Zhao, C.; Zhang, X.; Wang, P.; Ying, K.: The analysis of volatile organic compounds biomarkers for lung cancer in exhaled breath, tissues and cell lines. *Cancer Biomarkers* **2012**, *11*, 129-137.

(17) Buszewski, B.; Grzywinski, D.; Ligor, T.; Stacewicz, T.; Bielecki, Z.; Wojtas, J.: Detection of volatile organic compounds as biomarkers in breath analysis by different analytical techniques. *Bioanalysis* **2013**, *5*, 2287-2306.

(18) Sarbach, C.; Stevens, P.; Whiting, J.; Puget, P.; Humbert, M.; Cohen-Kaminsky, S.; Postaire, E.: Evidence of endogenous volatile organic compounds as biomarkers of diseases in alveolar breath. *Annales Pharmaceutiques Francaises* **2013**, *71*, 203-215.

(19) Boursier, J.; Rawls, J. F.; Diehl, A. M.: Obese humans with nonalcoholic fatty liver disease display alterations in fecal microbiota and volatile organic compounds. *Clinical Gastroenterology and Hepatology* **2013**, *11*, 876-878.

(20) Shirasu, M.; Touhara, K.: The scent of disease: volatile organic compounds of the human body related to disease and disorder. *Journal of Biochemistry* **2011**, *150*, 257-266.

(21) Wang, D. D.; Ding, X. D.; Rather, P. N.: Indole can act as an extracellular signal in *Escherichia coli*. *Journal of Bacteriology* **2001**, *183*, 4210-4216.

(22) Zhu, J.; Bean, H. D.; Kuo, Y.-M.; Hill, J. E.: Fast detection of volatile organic compounds from bacterial cultures by secondary electrospray ionization-mass spectrometry. *Journal of Clinical Microbiology* **2010**, *48*, 4426-4431.

(23) Trefz, P.; Koehler, H.; Klepik, K.; Moebius, P.; Reinhold, P.; Schubert, J. K.; Miekisch, W.: Volatile emissions from mycobacterium avium subsp paratuberculosis mirror bacterial growth and enable distinction of different strains. *Plos One* **2013**, *8*, e76868.

(24) Lloyd, S. W.; Grimm, C. C.; Klich, M. A.; Beltz, S. B.: Fungal infections of fresh-cut fruit can be detected by the gas chromatography-mass spectrometric identification of microbial volatile organic compounds. *Journal of Food Protection* **2005**, *68*, 1211-1216.

(25) Barie, N.; Bucking, M.; Rapp, M.: A novel electronic nose based on miniaturized SAW sensor arrays coupled with SPME enhanced headspace-analysis and its use for rapid determination of volatile organic compounds in food quality monitoring. *Sensors and Actuators B: Chemical* **2006**, *114*, 482-488.

(26) Srivastava, A. K.: Detection of volatile organic compounds (VOCs) using SnO2 gas-sensor array and artificial neural network. *Sensors and Actuators B: Chemical* **2003**, *96*, 24-37.

(27) Sankaran, S.; Mishra, A.; Ehsani, R.; Davis, C.: A review of advanced techniques for detecting plant diseases. *Computers and Electronics in Agriculture* **2010**, *72*, 1-13.

(28) Lin, H.; Suslick, K. S.: A colorimetric sensor array for detection of triacetone triperoxide vapor. *Journal of the American Chemical Society* **2010**, *132*, 15519-15521.

(29) Ewing, R. G.; Clowers, B. H.; Atkinson, D. A.: Direct real-time detection of vapors from explosive compounds. *Analytical Chemistry* **2013**, *85*, 10977-10983.

(30) Hu, Z.; Pramanik, S.; Tan, K.; Zheng, C.; Liu, W.; Zhang, X.; Chabal, Y. J.; Li, J.: Selective, sensitive, and reversible detection of vapor-phase high explosives via two-dimensional mapping: a new strategy for MOF-based sensors. *Crystal Growth & Design* **2013**, *13*, 4204-4207.

(31) Ewing, R. G.; Atkinson, D. A.; Clowers, B. H.: Direct real-time detection of RDX vapors under ambient conditions. *Analytical Chemistry* **2013**, *85*, 389-397.

(32) Westhoff, M.; Litterst, P.; Freitag, L.; Urfer, W.; Bader, S.; Baumbach, J. I.: Ion mobility spectrometry for the detection of volatile organic compounds in exhaled breath of patients with lung cancer: results of a pilot study. *Thorax* **2009**, *64*, 744-748.

(33) Faiola, C.; Erickson, M.; Fricaud, V.; Jobson, B.; VanReken, T.: Quantification of biogenic volatile organic compounds with a flame ionization detector using the effective carbon number concept. *Atmospheric Measurement Techniques Discussions* **2012**, *5*, 2415-2447.

(34) Nyquist, J. E.; Wilson, D. L.; Norman, L. A.; Gammage, R. B.: Decreased sensitivity of photoionization detector total organic vapor detectors in the presence of methane. *The American Industrial Hygiene Association Journal* **1990**, *51*, 326-330.

(35) Grate, J. W.; Abraham, M. H.; Wise, B. M.: Design and information content of arrays of sorption-based vapor sensors using solubility interactions and linear solvation energy relationships. In *Computational Methods for Sensor Material Selection*; Editors Ryan, M. A., Shevade A. V., Taylor, C. J., Homer, M. L., Blanco M., Sttter, J. R.; Springer, New York, **2010**; pp. 193-218.

(36) Snow, E.; Perkins, F.; Houser, E.; Badescu, S.; Reinecke, T.: Chemical detection with a single-walled carbon nanotube capacitor. *Science* **2005**, *307*, 1942-1945.

(37) Mlsna, T. E.; Cemalovic, S.; Warburton, M.; Hobson, S. T.; Mlsna, D. A.; Patel, S. V.: Chemicapacitive microsensors for chemical warfare agent and toxic industrial chemical detection. *Sensors and Actuators B: Chemical* **2006**, *116*, 192-201.

(38) Dobrokhotov, V.; Larin, A.; Sowell, D.: Vapor trace recognition using a single nonspecific chemiresistor. *Sensors* **2013**, *13*, 9016-9028.

(39) Abraham, J. K.; Philip, B.; Witchurch, A.; Varadan, V. K.; Reddy, C. C.: A compact wireless gas sensor using a carbon nanotube/PMMA thin film chemiresistor. *Smart Materials & Structures* **2004**, *13*, 1045-1049.

(40) Lucklum, R.; Hauptmann, P.: The quartz crystal microbalance: mass sensitivity, viscoelasticity and acoustic amplification. *Sensors and Actuators B: Chemical* **2000**, *70*, 30-36.

(41) Sauerbrey, G.: The use of quartz oscillators for weighing thin layers and for microweighing. *Zeitschrift Fur Physik* **1959**, *155*, 206-222.

(42) Jaffe, H.; Berlinco, D. A.: Piezoelectric transducer materials. *Proceedings of the IEEE* **1965**, *53*, 1372-1386.

(43) Banicia, F-G.: *Chemical Sensors and Biosensors: Fundamentals and Applications*; John Wiley & Sons, West Sussex, United Kingdom, **2012**; pp. 473-506.

(44) Martin, S. J.; Bandey, H. L.; Cernosek, R. W.; Hillman, A. R.; Brown, M. J.: Equivalent-circuit model for the thickness-shear mode resonator with a viscoelastic film near film resonance. *Analytical Chemistry* **2000**, *72*, 141-149.

(45) Janshoff, A.; Galla, H. J.; Steinem, C.: Piezoelectric mass-sensing devices as biosensors-an alternative to optical biosensors? *Angewandte Chemie-International Edition* **2000**, *39*, 4004-4032.

(46) Dixon, M. C.: Quartz crystal microbalance with dissipation monitoring: enabling real-time characterization of biological materials and their interactions. *Journal of Biomolecular Techniques* **2008**, *19*, 151-158.

(47) Buttry, D. A.; Ward, M. D.: Measurement of interfacial processes at electrode surfaces with the electrochemical quartz crystal microbalance. *Chemical Reviews* **1992**, *92*, 1355-1379.

(48) Arnau, A.: A review of interface electronic systems for AT-cut quartz crystal microbalance applications in liquids. *Sensors* **2008**, *8*, 370-411.

(49) Lucklum, R.; Hauptmann, P.: The Δf-ΔR QCM technique: an approach to an advanced sensor signal interpretation. *Electrochimica Acta* **2000**, *45*, 3907-3916.

(50) Schröder, J.; Borngräber, R.; Eichelbaum, F.; Hauptmann, P.: Advanced interface electronics and methods for QCM. *Sensors and Actuators A: Physical* **2002**, *97*, 543-547.

(51) Yoon, S. M.; Cho, N. J.; Kanazawa, K.: Analyzing spur-distorted impedance spectra for the QCM. *Journal of Sensors* **2009**, *2009*, article ID 259746.

(52) Eichelbaum, F.; Borngraber, R.; Schroder, J.; Lucklum, R.; Hauptmann, P.: Interface circuits for quartz-crystal-microbalance sensors. *Review of Scientific Instruments* **1999**, *70*, 2537-2545.

(53) Lee, S-W.; Hinsberg, W. D.; Kanazawa, K. K.: Determination of the viscoelastic properties of polymer films using a compensated phase-locked oscillator circuit. *Analytical Chemistry* **2002**, *74*, 125-131.

(54) Ferrari, M.; Ferrari, V.; Kanazawa, K.: Dual-harmonic oscillator for quartz crystal resonator sensors. *Sensors and Actuators A: Physical* **2008**, *145*, 131-138.

(55) Beck, R.; Pittermann, U.; Weil, K. G.: Impedance analysis of quartz oscillators, contacted on one side with a liquid. *Berichte der Bunsengesellschaft für physikalische Chemie* **1988**, *92*, 1363-1368.

(56) Schroder, J.; Borngraber, R.; Lucklum, R.; Hauptmann, P.: Network analysis based interface electronics for quartz crystal microbalance. *Review of Scientific Instruments* **2001**, *72*, 2750-2755.

(57) Reviakine, I.; Johannsmann, D.; Richter, R. P.: Hearing what you cannot see and visualizing what you hear: interpreting quartz crystal microbalance data from solvated interfaces. *Analytical Chemistry* **2011**, *83*, 8838-8848.

(58) DeNolf, G. C.; Haack, L.; Holubka, J.; Straccia, A.; Blohowiak, K.; Broadbent, C.; Shull, K. R.: High frequency rheometry of viscoelastic coatings with the quartz crystal microbalance. *Langmuir* **2011**, *27*, 9873-9879.

(59) Johannsmann, D.: Viscoelastic, mechanical, and dielectric measurements on complex samples with the quartz crystal microbalance. *Physical Chemistry Chemical Physics* **2008**, *10*, 4516-4534.

(60) Johannsmann, D.; Heim, L-O.: A simple equation predicting the amplitude of motion of quartz crystal resonators. *Journal of Applied Physics* **2006**, *100*, 094505.1-094505.5.

(61) Johannsmann, D.; Reviakine, I.; Richter, R. P.: Dissipation in films of adsorbed nanospheres studied by quartz crystal microbalance (QCM). *Analytical Chemistry* **2009**, *81*, 8167-8176.

(62) Rodahl, M.; Hook, F.; Krozer, A.; Brzezinski, P.; Kasemo, B.: Quartz crystal microbalance setup for frequency and Q-factor measurements in gaseous and liquid environments. *Review of Scientific Instruments* **1995**, *66*, 3924-3930.

(63) Rodahl, M.; Kasemo, B.: A simple setup to simultaneously measure the resonant frequency and the absolute dissipation factor of a quartz crystal microbalance. *Review of Scientific Instruments* **1996**, *67*, 3238-3241.

(64) Bandey, H. L.; Martin, S. J.; Cernosek, R. W.; Hillman, A. R.: Modeling the responses of thickness-shear mode resonators under various loading conditions. *Analytical Chemistry* **1999**, *71*, 2205-2214.

(65) Nomura, T.; Okuhara, M.: Frequency shifts of piezoelectric quartz crystals immersed in organic liquids. *Analytica Chimica Acta* **1982**, *142*, 281-284.

(66) Wangchareansak, T.; Sangma, C.; Ngernmeesri, P.; Thitithanyanont, A.; Lieberzeit, P. A.: Self-assembled glucosamine monolayers as biomimetic receptors for detecting WGA lectin and influenza virus with a quartz crystal microbalance. *Analytical and Bioanalytical Chemistry* **2013**, *405*, 6471-6478.

(67) Rodahl, M.; Höök, F.; Fredriksson, C.; Keller, C. A.; Krozer, A.; Brzezinski, P.; Voinova, M.; Kasemo, B.: Simultaneous frequency and dissipation factor QCM measurements of biomolecular adsorption and cell adhesion. *Faraday Discussions* **1997**, *107*, 229-246.

(68) Keiji Kanazawa, K.; Gordon II, J. G.: The oscillation frequency of a quartz resonator in contact with liquid. *Analytica Chimica Acta* **1985**, *175*, 99-105.

(69) Muramatsu, H.; Tamiya, E.; Karube, I.: Computation of equivalent circuit parameters of quartz crystals in contact with liquids and study of liquid properties. *Analytical Chemistry* **1988**, *60*, 2142-2146.

(70) Martin, S. J.; Spates, J. J.; Wessendorf, K. O.; Schneider, T. W.; Huber, R. J.: Resonator/oscillator response to liquid loading. *Analytical Chemistry* **1997**, *69*, 2050-2054.

(71) Cho, N-J.; D'Amour, J. N.; Stalgren, J.; Knoll, W.; Kanazawa, K.; Frank, C. W.: Quartz resonator signatures under Newtonian liquid loading for initial instrument check. *Journal of Colloid and Interface Science* **2007**, *315*, 248-254.

(72) Voinova, M. V.; Rodahl, M.; Jonson, M.; Kasemo, B.: Viscoelastic acoustic response of layered polymer films at fluid-solid interfaces: continuum mechanics approach. *Physica Scripta* **1999**, *59*, 391-396.

(73) Vogt, B. D.; Lin, E. K.; Wu, W-l.; White, C. C.: Effect of film thickness on the validity of the Sauerbrey equation for hydrated polyelectrolyte films. *The Journal of Physical Chemistry B* **2004**, *108*, 12685-12690.

(74) Voinova, M.; Jonson, M.; Kasemo, B.: Internal and interfacial friction in the dynamics of soft/solid interfaces. *arXiv preprint cond-mat/9906415* **1999**.

(75) Ohlsson, G.; Langhammer, C.; Zoric, I.; Kasemo, B.: A nanocell for quartz crystal microbalance and quartz crystal microbalance with dissipation-monitoring sensing. *Review of Scientific Instruments* **2009**, *80*, 083905.

(76) Seddon, K. R.; Stark, A.; Torres, M.-J.: Viscosity and density of 1-alkyl-3-methylimidazolium ionic liquids. In *ACS Symposium Series*; ACS Publications; Washington, DC, **2002**; 819; pp 34-49.

(77) Potyrailo, R. A.; Surman, C.; Nagraj, N.; Burns, A.: Materials and transducers toward selective wireless gas sensing. *Chemical Reviews* **2011**, *111*, 7315-7354.

(78) Szczurek, A.; Maciejewska, M.: Gas sensor array with broad applicability. *Sensor Array, In Tech, Rijeka* **2012**, 81-108.

(79) Gardner, J. W.; Bartlett, P. N.: A brief history of electronic noses. *Sensors and Actuators B: Chemical* **1994**, *18*, 210-211.

(80) Persaud, K.; Dodd, G.: Analysis of discrimination mechanisms in the mammalian olfactory system using a model nose. *Nature* **1982**, *299*, 352-355.

(81) Holloway, A.; Nabok, A.; Thompson, M.; Ray, A.; Crowther, D.; Siddiqi, J.: New method of vapour discrimination using the thickness shear mode (TSM) resonator. *Sensors* **2003**, *3*, 187-191.

(82) Holloway, A.; Nabok, A.; Thompson, M.; Ray, A.; Wilkop, T.: Impedance analysis of the thickness shear mode resonator for organic vapour sensing. *Sensors and Actuators B: Chemical* **2004**, *99*, 355-360.

(83) Wang, X.; Ding, B.; Sun, M.; Yu, J.; Sun, G.: Nanofibrous polyethyleneimine membranes as sensitive coatings for quartz crystal microbalance-based formaldehyde sensors. *Sensors and Actuators B: Chemical* **2010**, *144*, 11-17.

(84) Bougharouat, A.; Bellel, A.; Sahli, S.; Ségui, Y.; Raynaud, P.: Plasma polymerization of TEOS for QCM-based VOC vapor sensing. *The European Physical Journal Applied Physics* **2011**, *56*, 24017.

(85) Fu, Y.; Finklea, H. O.: Quartz crystal microbalance sensor for organic vapor detection based on molecularly imprinted polymers. *Analytical Chemistry* **2003**, *75*, 5387-5393.

(86) Matsuguchi, M.; Uno, T.: Molecular imprinting strategy for solvent molecules and its application for QCM-based VOC vapor sensing. *Sensors and Actuators B: Chemical* **2006**, *113*, 94-99.

(87) Bunte, G.; Hürttlen, J.; Pontius, H.; Hartlieb, K.; Krause, H.: Gas phase detection of explosives such as 2,4,6-trinitrotoluene by molecularly imprinted polymers. *Analytica Chimica Acta* **2007**, *591*, 49-56.

(88) Koshets, I.; Kazantseva, Z.; Shirshov, Y. M.; Cherenok, S.; Kalchenko, V.: Calixarene films as sensitive coatings for QCM-based gas sensors. *Sensors and Actuators B: Chemical* **2005**, *106*, 177-181.

(89) Penza, M.; Cassano, G.; Aversa, P.; Antolini, F.; Cusano, A.; Cutolo, A.; Giordano, M.; Nicolais, L.: Alcohol detection using carbon nanotubes acoustic and optical sensors. *Applied Physics Letters* **2004**, *85*, 2379-2381.

(90) Montmeat, P.; Madonia, S.; Pasquinet, E.; Hairault, L.; Gros, C. P.; Barbe, J.-M.; Guilard, R.: Metalloporphyrins as sensing material for quartz-crystal microbalance nitroaromatics sensors. *Sensors Journal, IEEE* **2005**, *5*, 610-615.

(91) Yang, D.: Nanocomposite films for gas sensing. *Advances in Nanocomposites-Synthesis, Characterization and Industrial Applications, InTech* **2011**, 857-882.

(92) Schlupp, M.; Weil, T.; Berresheim, A. J.; Wiesler, U. M.; Bargon, J.; Müllen, K.: Polyphenylene dendrimers as sensitive and selective sensor layers. *Angewandte Chemie International Edition* **2001**, *40*, 4011-4015.

(93) Panigrahi, S.; Sankaran, S.; Mallik, S.; Gaddam, B.; Hanson, A. A.: Olfactory receptor-based polypeptide sensor for acetic acid VOC detection. *Materials Science and Engineering: C* **2012**, *32*, 1307-1313.

(94) Sankaran, S.; Panigrahi, S.; Mallik, S.: Odorant binding protein based biomimetic sensors for detection of alcohols associated with *Salmonella* contamination in packaged beef. *Biosensors and Bioelectronics* **2011**, *26*, 3103-3109.

(95) Latif, U.; Rohrer, A.; Lieberzeit, P. A.; Dickert, F. L.: QCM gas phase detection with ceramic materials—VOCs and oil vapors. *Analytical and Bioanalytical Chemistry* **2011**, *400*, 2457-2462.

(96) Liang, C.; Yuan, C.-Y.; Warmack, R. J.; Barnes, C. E.; Dai, S.: Ionic liquids: a new class of sensing materials for detection of organic vapors based on the use of a quartz crystal microbalance. *Analytical Chemistry* **2002**, *74*, 2172-2176.

(97) Goubaidoulline, I.; Vidrich, G.; Johannsmann, D.: Organic vapor sensing with ionic liquids entrapped in alumina nanopores on quartz crystal resonators. *Analytical Chemistry* **2005**, *77*, 615-619.

(98) Jin, X.; Yu, L.; Garcia, D.; Ren, R. X.; Zeng, X.: Ionic liquid high-temperature gas sensor array. *Analytical Chemistry* **2006**, *78*, 6980-6989.

(99) Xu, X.; Cang, H.; Li, C.; Zhao, Z. K.; Li, H.: Quartz crystal microbalance sensor array for the detection of volatile organic compounds. *Talanta* **2009**, *78*, 711-716.

(100) Xu, X.; Li, C.; Pei, K.; Zhao, K.; Zhao, Z. K.; Li, H.: Ionic liquids used as QCM coating materials for the detection of alcohols. *Sensors and Actuators B: Chemical* **2008**, *134*, 258-265.

(101) Toniolo, R.; Pizzariello, A.; Dossi, N.; Lorenzon, S.; Abollino, O.; Bontempelli, G.: Room temperature ionic liquids as useful overlayers for estimating food quality from their odor analysis by quartz crystal microbalance measurements. *Analytical Chemistry* **2013**, *85*, 7241-7247.

(102) Seyama, M.; Iwasaki, Y.; Tate, A.; Sugimoto, I.: Room-temperature ionic-liquid-incorporated plasma-deposited thin films for discriminative alcohol-vapor sensing. *Chemistry of Materials* **2006**, *18*, 2656-2662.

(103) Schäfer, T.; Di Francesco, F.; Fuoco, R.: Ionic liquids as selective depositions on quartz crystal microbalances for artificial olfactory systems—a feasibility study. *Microchemical Journal* **2007**, *85*, 52-56.

(104) Jin, X.; Yu, L.; Zeng, X.: Enhancing the sensitivity of ionic liquid sensors for methane detection with polyaniline template. *Sensors and Actuators B: Chemical* **2008**, *133*, 526-532.

(105) Ji, Q.; Honma, I.; Paek, S. M.; Akada, M.; Hill, J. P.; Vinu, A.; Ariga, K.: Layer-by-layer films of graphene and ionic liquids for highly selective gas sensing. *Angewandte Chemie* **2010**, *122*, 9931-9933.

(106) Rehman, A.; Hamilton, A.; Chung, A.; Baker, G. A.; Wang, Z.; Zeng, X.: Differential solute gas response in ionic-liquid-based QCM arrays: elucidating design factors

responsible for discriminative explosive gas sensing. *Analytical Chemistry* **2011**, *83*, 7823-7833.

(107) Regmi, B. P.; Monk, J.; El-Zahab, B.; Das, S.; Hung, F. R.; Hayes, D. J.; Warner, I. M.: A novel composite film for detection and molecular weight determination of organic vapors. *Journal of Materials Chemistry* **2012**, *22*, 13732-13741.

(108) Regmi, B.P.; Speller, N.C.; Anderson, M. J.; Brutus, J. O.; Merid, Y.; Das, S.; El-Zahab, B.; Hayes, D.J.; Murray, K. K.; Warner, I. M.: Molecular weight sensing properties of ionic liquid-polymer composite films: theory and experiment. *Journal of Materials Chemistry C* **2014**, *2*, 4867-4878.

(109) Yu, L.; Jin, X.; Zeng, X.: Methane interactions with polyaniline/butylmethylimidazolium camphorsulfonate ionic liquid composite. *Langmuir* **2008**, *24*, 11631-11636.

(110) Tseng, M-C.; Chu, Y-H.: Chemoselective gas sensing ionic liquids. *Chemical Communications* **2010**, *46*, 2983-2985.

(111) Liu, Y-L.; Tseng, M-C.; Chu, Y-H.:.Sensing ionic liquids for chemoselective detection of acyclic and cyclic ketone gases. *Chemical Communications* **2013**, *49*, 2560-2562.

(112) Tseng, M-C.; Chu, Y-H.: Reaction-based azide gas sensing with tailored ionic liquids measured by quartz crystal microbalance. *Analytical Chemistry* **2014**, *86*, 1949-1952.

(113) Brennecke, J. F.; Maginn, E. J.: Ionic liquids: innovative fluids for chemical processing. *AIChE Journal* **2001**, *47*, 2384-2389.

(114) Malvaldi, M.; Chiappe, C.: From molten salts to ionic liquids: effect of ion asymmetry and charge distribution. *Journal of Physics: Condensed Matter* **2008**, *20*, 035108.

(115) Holbrey, J.; Seddon, K.: Ionic liquids. *Clean Products and Processes* **1999**, *1*, 223-236.

(116) Kulkarni, P. S.; Branco, L. C.; Crespo, J. G.; Nunes, M. C.; Raymundo, A.; Afonso, C. A.: Comparison of physicochemical properties of new ionic liquids based on imidazolium, quaternary ammonium, and guanidinium cations. *Chemistry-A European Journal* **2007**, *13*, 8478-8488.

(117) Tesfai, A.; El-Zahab, B.; Kelley, A. T.; Li, M.; Garno, J. C.; Baker, G. A.; Warner, I. M.: Magnetic and nonmagnetic nanoparticles from a group of uniform materials based on organic salts. *ACS Nano* **2009**, *3*, 3244-3250.

(118) Galpothdeniya, W. I. S.; McCarter, K. S.; De Rooy, S. L.; Regmi, B. P.; Das, S.; Hasan, F.; Tagge, A.; Warner, I. M.: Ionic liquid-based optoelectronic sensor arrays for chemical detection. *RSC Advances* **2014**, *4*, 7225-7234.

(119) Magut, P. K.; Das, S.; Fernand, V. E.; Losso, J.; McDonough, K.; Naylor, B. M.; Aggarwal, S.; Warner, I. M.: Tunable cytotoxicity of Rhodamine 6G via anion variations. *Journal of the American Chemical Society* **2013**, *135*, 15873-15879.

(120) de Rooy, S. L.; El-Zahab, B.; Li, M.; Das, S.; Broering, E.; Chandler, L.; Warner, I. M.: Fluorescent one-dimensional nanostructures from a group of uniform materials based on organic salts. *Chemical Communications* **2011**, *47*, 8916-8918.

(121) Bwambok, D. K.; El-Zahab, B.; Challa, S. K.; Li, M.; Chandler, L.; Baker, G. A.; Warner, I. M.: Near-infrared fluorescent nanoGUMBOS for biomedical imaging. *ACS Nano* **2009**, *3*, 3854-3860.

(122) Siraj, N.; Hasan, F.; Das, S.; Kiruri, L. W.; Steege Gall, K.; Baker, G. A.; Warner, I. M.: Carbazole-derived GUMBOS: solid state fluorescent analogs of ionic liquids for potential applications in organic-based blue light-emitting diodes. *The Journal of Physical Chemistry C* **2014**, *118*, 2312-2320.

(123) Jordan, A. N.; Das, S.; Siraj, N.; de Rooy, S. L.; Li, M.; El-Zahab, B.; Chandler, L.; Baker, G. A.; Warner, I. M.: Anion-controlled morphologies and spectral features of cyanine-based nanoGUMBOS–an improved photosensitizer. *Nanoscale* **2012**, *4*, 5031-5038.

CHAPTER 2 A NOVEL COMPOSITE FILM FOR DETECTION AND MOLECULAR WEIGHT DETERMINATION OF ORGANIC VAPORS*

2.1 Introduction

The development and evaluation of novel sensing materials for detection and quantification of volatile organic compounds (VOCs) is an active area of research. Such VOC sensors are increasingly important because they find extensive use in environmental monitoring, health care, agriculture, food safety, defense, and homeland security applications.[1-9] The most common gas sensor systems comprise an active sensing material immobilized onto the surface of a suitable transducer device. The sensing layer selectively and reversibly sorbs the analytes of interest, and the transducer subsequently converts the binding event into an electronic signal. Among possible transducers, we note that acoustic wave devices,[2-4] chemicapacitors,[5,6] and chemiresistors,[7-9] are attractive choices for analyzing a broad range of chemical vapors**.**

Sensing materials are critical components of sensing devices, and play a key role in the design and successful implementation of a chemical sensor. A wide range of sensing materials including, carbon nanotubes,[6,8,10] conducting polymers,[7,11,12] dendrimers,[1,13] metal oxide nanomaterials,[14,15] various nanocomposites,[16,17] and room temperature ionic liquids (RTILs),[18,19] among others, have been employed for preparation of chemosensitive coatings. Sensors constructed from such materials are found to be highly sensitive for detection of various gaseous analytes. A vast majority of these gas sensors are based on measurement of single-parameter

---

*This chapter previously appeared as Bishnu P. Regmi, Joshua Monk, Bilal El-Zahab, Susmita Das, Franscisco R. Hung, Daniel J. Hayes, and Isiah M. Warner. A novel composite film for detection and molecular weight determination of organic vapors. *Journal of Materials Chemistry* **2012**, *22*, 13732-13741. It is reproduced by permission of The Royal Society of Chemistry. http://pubs.rsc.org/en/content/articlelanding/2012/jm/c2jm31623d/unauth#!divAbstract

response. However, the response of a sensor depends on both the concentration and chemical characteristics of an analyte. Hence, a single sensor is not able to discriminate between analytes unless the concentrations or the partial pressures of the analytes are known. As an alternative to single-parameter-response measurement, Snow and Perkins[10] have recently explored the unique properties of single-walled carbon nanotube (SWNT) to simultaneously measure conductance and capacitance of an SWNT network in the presence of chemical vapors. In that study, the authors demonstrated that the ratio of conductance response to capacitance response is a concentration-independent parameter dependent on the characteristics of the vapor. In fact, the ratio was found to depend on the charge transfer property and polarizability of the analytes. This method holds considerable promise for identifying unknown vapors if combined with other analytical approaches. However, a major disadvantage to this approach is that many vapors and gases produce weak conductance response in SWNTs.[20]

In this chapter, I report on the development and unique gas-sensing properties of a thin composite film immobilized onto the surface of a quartz crystal microbalance (QCM) substrate. The materials employed for preparation of our composite sensing film is comprised of cellulose acetate (CA) and a representative compound from a Group of Uniform Materials Based on Organic Salts (GUMBOS). GUMBOS are solid phase organic salts with melting points between 25 and 250 °C.[21] The model GUMBOS used in this study was 1-n-butyl-2,3-dimethylimidazolium hexafluorophosphate ($[BM_2Im][PF_6]$) with a melting point of 43 °C and a glass transition temperature of -58 °C.[22] The film was prepared through co-deposition of $[BM_2Im][PF_6]$ and CA on the surface of the QCM substrate. The resonance frequency shift (Δf) and the motional resistance shift (ΔR) of the QCM sensor in the presence of various organic vapors were simultaneously measured. The sensor exhibited a rapid and reversible response to all

analytes tested. Notably, it is demonstrated that the ratio $\Delta f/\Delta R$, under low to moderate vapor absorptions, is constant for a particular vapor, and varies directly with the molecular weight of the absorbed chemical species.

Molecular dynamics (MD) simulations were performed to help rationalize the experimental results. Evaluation of data from MD simulations indicates weak interactions between analyte and sensing film, and that these interactions are primarily due to the analyte-[BM_2Im] and analyte-[PF_6] interactions. Since these interactions are weak, the same number of molecules of different analytes may produce similar free volume changes, and consequently similar changes in *R*. The analyte-CA interactions are negligibly small, which suggests that CA only improves the mechanical properties of the composite film.

2.2 Theory of QCM Measurement

The QCM is a highly sensitive piezoelectric transducer with an operating principle based on alteration of the characteristics of acoustic shear waves propagating through a medium. The QCM comprises a thin slice of AT-cut quartz wafer that is sandwiched between two electrodes. When an oscillating electric voltage is applied perpendicular to the surface of the quartz resonator, an acoustic shear wave is produced that propagates across the thickness of the crystal. As the sorbent coating interacts with the target analytes, its mass and mechanical properties are altered, which in turn leads to a phase shift and attenuation of the shear waves. The phase shift leads to a change in resonance frequency, Δf, that depends on the mass change occurring at the interface. The relation between Δf and the added mass per unit area, Δm, is expressed by the Sauerbrey equation:[23]

$$\Delta f = - C_f \Delta m \qquad (2.1),$$

where C_f is a constant that depends on the intrinsic properties of the quartz. The attenuation of the shear wave is due to dissipation of energy during oscillation. This attenuation can be estimated by measuring an electrical property known as the motional resistance, *R*, of the QCM. Thin and rigid films display less dissipation, and hence result in a small increase in *R*, while thick and viscoelastic films exhibit high dissipation and a correspondingly large increase in *R*.[24] It is useful to note that Δf and ΔR are usually obtained simultaneously in a QCM measurement.

2.3 Experimental Section

2.3.1 Materials

1-n-Butyl-2,3-dimethylimidazolium trifluoromethanesulfonate ([BM_2Im][OTf]), 1-n-butyl-3-methylpyridinium hexafluorophosphate ([BMPyr][PF_6]), and [BM_2Im][PF_6] were obtained from Ionic Liquids Technologies, Inc. as crystalline solids. Cellulose acetate (molecular weight 30000 Da), 1-ethyl-2,3-dimethylimidazolium hexafluorophosphate ([EM_2Im][PF_6]) (as crystalline solid), anhydrous heptane, anhydrous acetonitrile, anhydrous chloroform, anhydrous carbon tetrachloride, and anhydrous toluene were obtained from Sigma-Aldrich. Acetone, n-propanol, and anhydrous methanol were obtained from Mallinckrodt Chemicals; absolute ethanol from Pharmco. All chemicals were used as received.

The QCM200 controller and associated crystals were purchased from Stanford Research Systems, Inc., Sunnyvale, CA. The crystals used were 5-MHz AT-cut chromium/gold polished crystals of 1" diameter. Gold-coated silicon wafers were obtained from Sigma-Aldrich. The polytetrafluoroethylene (PTFE) containers used in these experiments were obtained from SPI Supplies/ Structure Probe, Inc. United States.

2.3.2 Preparation of Stock Solutions

Stock solutions of $[BM_2Im][PF_6]$ (1 mg/mL) and cellulose acetate (0.5 mg/mL) in acetone were prepared in 20-ml borosilicate glass scintillation vials. Particulate matter was removed by successive filtration using a glass syringe with a stainless steel filter holder and a Whatman 0.45 μm PTFE/GMF syringe filter.

2.3.3 Cleaning of Gold Surface

The QCM crystal (or gold-coated silicon wafer) was rinsed with water and ultrasonicated in acetone for 5 minutes; and dried using nitrogen gas. The crystal was then immersed in fresh piranha solution (3:1 concentrated sulfuric acid and 30% hydrogen peroxide) for 10 minutes, washed with copious amounts of water, rinsed with acetone, and dried under a stream of nitrogen. The crystal was further dried by placing in an oven at 100 °C, and allowed to cool to room temperature. Cleaned crystals were used immediately for preparation of coatings.

2.3.4 Film Preparation

Coatings were prepared using a solvent precipitation method.[25] To 2 mL of a solution containing various concentrations of $[BM_2Im][PF_6]$, was added 6 mL of anhydrous heptane dropwise while stirring. (In the case of the composite, the mass proportion of $[BM_2Im][PF_6]$ and cellulose acetate in the solution was also varied. The optimal mass $[BM_2Im][PF_6]$-to-CA mass ratio was found to be 7.5:1). The mixture was then transferred to a 25-mL PTFE beaker and a cleaned quartz crystal (or gold-coated silicon) immersed into the mixture and allowed to incubate for six hours. The crystal was ultrasonicated for one minute, while holding it vertically in a fresh pool of heptane to remove any loosely adhered material. The coated crystal was stored in a desiccator for a minimum of 24 hours before mounting it in the crystal holder.

2.3.5 Scanning Electron Microscopy (SEM) Analysis

The film was imaged using a JEOL JSM-6610 scanning electron microscope in high vacuum mode.

2.3.6 Laser Scanning Confocal Microscopy (LSCM) Analysis

The heights of the particles were analyzed using a Leica TCS SP2 laser scanning confocal microscope in the reflection mode with a 488-nm laser.

2.3.7 Powder X-ray Diffraction (XRD) Analysis

Powder XRD data of the films deposited on the gold–coated silicon substrate or glass substrate were collected using a Bruker/Siemens D5000 automated powder X-ray diffractometer utilizing Cu Kα radiation and a scintillation point detector. The operating conditions were set at 40 kV and 30 mA, and the data were recorded over a 2θ range from 2° up to 70° with an interval 0.02° at 1 second per step.

2.3.8 Fourier Transform Infrared (FTIR) Analysis

IR spectra of the films were recorded on a Bruker Tensor 27 spectrometer equipped with a PIKE MIRacle single-bounce attenuated total reflectance (ATR) cell. Spectra were collected over the 3600-530 cm^{-1} region with 256 scans with a resolution of 4 cm^{-1}. FTIR data were analyzed using OPUS 6.5 software.

2.3.9 Electron Probe Microanalysis (EPMA)

EPMA of the films was performed with JEOL Superprobe 733, equipped with wavelength dispersive spectrometer (WDS), using an accelerating voltage of 15 kV, probe current of 10 nA, and a beam diameter of 30 microns. Nine different spots in each film and a blank substrate were analyzed.

2.3.10 QCM Data Acquisition

The QCM sensor was exposed to various VOC vapors by using a custom-made non-flow system. A schematic diagram of the experimental setup is shown in Figure 2.1. The volume of the chamber, excluding the volume of crystal holder, was 4.14 L. The volume of the fan and filter paper was disregarded. As noted, the glass chamber contained an inlet and an outlet for argon; and a rubber septum for sample introduction. Ultrapure argon was intermittently blown through the container until stable frequency and motional resistance were obtained. After achieving equilibrium, the argon inlet and outlet were closed; and a known volume of liquid organic sample was injected into the closed container using a Hamilton microsyringe. The rate of

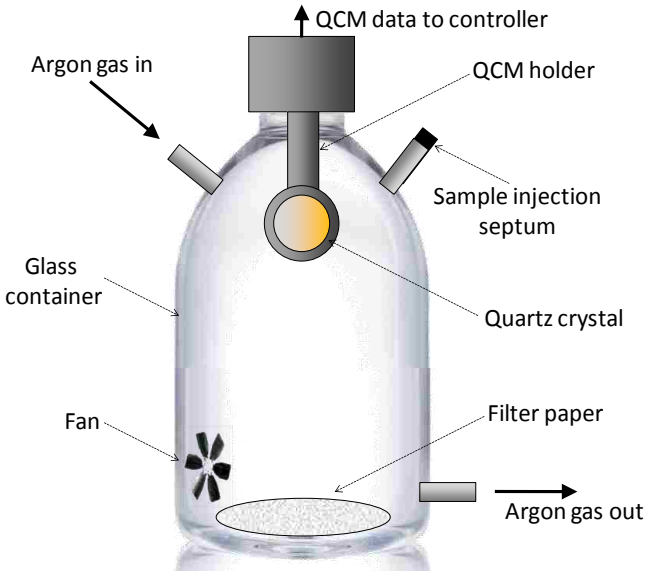

Figure 2.1 Schematic of experimental setup

evaporation was enhanced by dropping the sample onto filter paper, and the vapor was homogenized using a small fan. The frequency and resistance shifts upon introduction of analyte vapor were simultaneously measured using a QCM200 system. The instrument uses a method to nullify static capacitance, C_o, and hence true values of resonance frequency and motional

resistance can be obtained.[26] The concentration of analyte was successively increased to produce a response curve. The introduction of analyte into the chamber produces an increase in overall pressure inside the container, but this pressure change was found to have a negligible effect on both frequency and motional resistance. All experiments were performed in a temperature-controlled room at 22 °C. Temperature fluctuations during experiments were measured to be within ±0.2 °C. Sample vapors were removed by blowing a gentle stream of ultrapure argon gas through the container until the baselines were recovered.

2.3.11 MD Simulations

Classical MD simulations were performed with the GROMACS MD package[27] in the NPT ensemble. The isotropic pressure coupling with a time constant of 0.2 ps was controlled by the Berendsen barostat and the improved velocity-rescaling algorithm recently proposed by Parrinello et al.[28,29] was used to mimic weak thermal coupling with a coupling constant of 0.05 ps. In all our simulations, the Lennard-Jones interactions were cut at 1.2 nm, and the long-range Coulomb interactions were handled by the particle-mesh Ewald (PME)[30] method with a cutoff of 1.0 nm and a grid spacing of 0.1 nm. Periodic boundaries were applied in all directions. In all simulations, H-bond lengths were constrained with the LINCS algorithm.[31]

The system considered in these simulations consists of 500 ($[BM_2Im][PF_6]$) pairs with 18 oligomers of CA, so that a mass ratio of 7.5:1 (similar to experiments) was obtained. One single molecule of analyte was then added to the simulation box. Six different analytes used in the experiments were considered in different simulations: acetone, acetonitrile, chloroform, ethanol, methanol, and toluene. All parameters used for modeling were selected from force fields available in the literature. Intramolecular parameters (bond lengths, valence angles, and torsional profiles) and intermolecular parameters (Lennard-Jones terms and electrostatic charges) were

chosen from the OPLS-AA force field[32] for $[BM_2Im]^+$, $[PF_6]^-$, CA, and the six analytes. Coulomb interactions were represented by partial charges placed on the atomic sites as defined by Lopes and Padua[33,34] and Jorgensen.[32]

Simulations were performed at 350 K, such that $[BM_2Im][PF_6]$ was in the liquid phase. By running at such a high temperature, all molecules in the system had more thermal mobility allowing the sampling of properties of interest using shorter simulations. We also ran two simulations for 4 ns at 295 K (the experimental temperature), and found minimal changes in the trends of the properties of interest. The simulations were run at 350 K for 2 ns for equilibration and the properties of interest were collected during another 2 ns. A representative simulation snapshot for $[BM_2Im][PF_6]$-CA and toluene is shown in Figure A4a, in Appendix A. To determine the electrostatic and van der Waals energies in GROMACS, energy groups were defined including the ions of $[BM_2Im]^+$ and $[PF_6]^-$, the single VOC, and the CA oligomers; as well as a single, randomly–chosen ion/molecule of $[BM_2Im^*]^+$, $[PF_6^*]^-$, and CA. The total interaction energy of any given molecule of VOC with the other species present in the system (all the $[BM_2Im]^+$ and $[PF_6]^-$ ions; and all oligomers of CA) were computed in the simulations. This total interaction energy was compared against the total interaction energies experienced by one $[BM_2Im]^+$ cation, one $[PF_6]^-$ anion and one CA oligomer in the system.

2.4 Results and Discussion

2.4.1 Preparation and Characterization of the Sensing Films

Films were prepared using a 'solvent precipitation method', where the materials that form the films are first dissolved in a binary liquid mixture composed of a volatile solvent and a less volatile non-solvent. The non-solvent does not dissolve the film-forming constituents, but is itself miscible with the solvent. In our study, acetone was used as the solvent and heptane was

used as the non-solvent. Preferential evaporation of acetone left a thin film deposited onto the substrate. Both $[BM_2Im][PF_6]$ and $[BM_2Im][PF_6]$-CA composite films were prepared and studied, with the former being used primarily for comparison. In the case of the composite, the mass proportion of $[BM_2Im][PF_6]$ and CA in the solution was maintained at a ratio of 7.5:1, which we found to be a preferred ratio.

Figures 2.2(a-c) provide SEM micrographs of the films deposited on the gold surface. It is evident from these figures that these films are discontinuous, and composed of isolated microdroplets with variable size distribution. The shapes of the droplets are observed to be different for pure $[BM_2Im][PF_6]$ as compared to those of the composite film. The droplets were found to be a physically stable solid. A decrease in frequency and an increase in motional resistance observed upon exposure of the films to organic vapors during QCM measurements (discussed below) support this contention. In the case of liquid films, under such high loading conditions, the absorption of organic vapor results in a positive frequency shift due to a decrease in viscosity and density of the liquid.[18,35] In addition, a drop in viscosity and density of the liquid is likely to produce a decrease in motional resistance,[36,37] which is contrary to our observations. The heights of these solid droplets were estimated using LSCM and was found to increase with size (or radius) of the droplets. The maximum height of $[BM_2Im][PF_6]$ droplets under intermediate loading conditions (Figure 2.2a) was found to be 2.6 μm. The maximum height of $[BM_2Im][PF_6]$-CA droplets under similar loading conditions (Figure 2.2b) was found to be 2.8 μm. Examination of Figure 2.2c shows that the droplets (maximum height here is 3.2 μm) grow in size as the amount of coating material increases. Powder XRD measurements of the films deposited on gold-silicon do not reveal additional peak(s) beyond those of the substrate (Figures

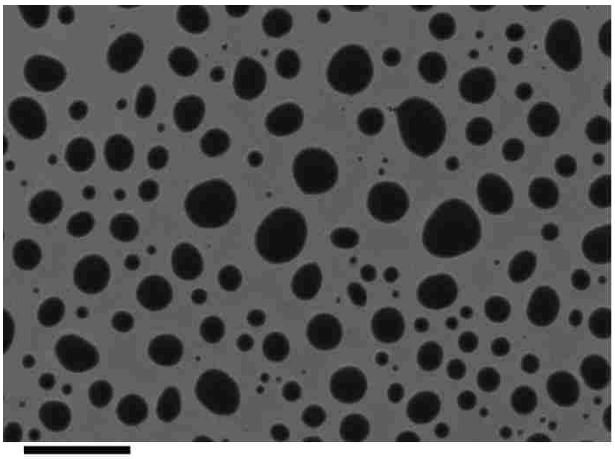

(a)

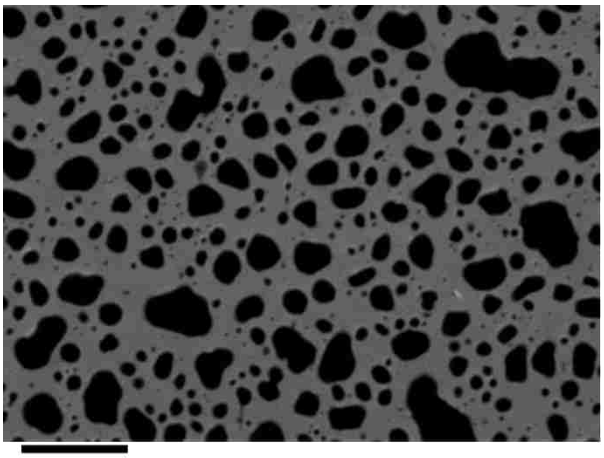

(b)

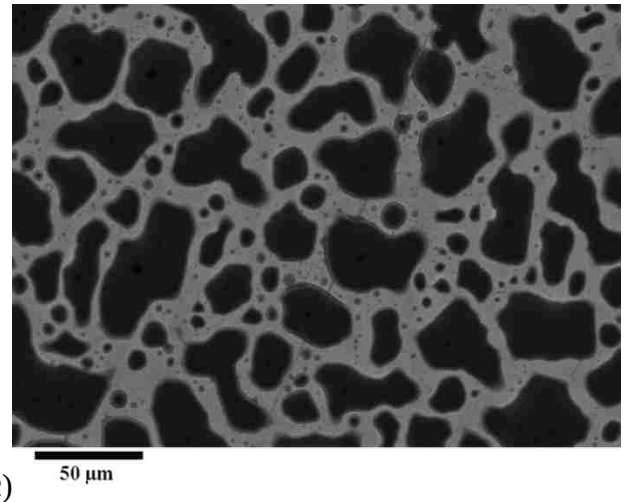

(c)

Figure 2.2 SEM micrographs of approximately a) 73 µg/cm^2 [BM_2Im][PF_6], b) 83 µg/cm^2 [BM_2Im][PF_6]/CA, and c) 214 µg/cm^2 [BM_2Im][PF_6]/CA films on gold surface.

A1 and A2, in Appendix A), which suggest that both the $[BM_2Im][PF_6]$ and the $[BM_2Im][PF_6]$/CA films are amorphous. In order to confirm that there is no coincidental overlap between diffraction peaks of the films and those of the underlying gold-silicon substrate, similar films were prepared using an amorphous glass substrate. No additional peaks indicating crystallized regions were observed (Figure A3, in Appendix A), confirming the amorphous properties of these films.

Attenuated total reflectance Fourier transform infrared (ATR-FTIR) spectra of $[BM_2Im][PF_6]$, CA, and $[BM_2Im][PF_6]$-CA films are shown in Figure 2.3a. CA can be identified though its strong absorption peaks at 1743-1744 cm^{-1}(C=O stretch), 1370 cm^{-1}(C-H bending), 1233 cm^{-1} (C-O stretch in acetyl), and 1051 cm^{-1} (C-O stretch in pyranose ring).[38] $[BM_2Im][PF_6]$ absorption peaks are observed at 3188 cm^{-1} and 3156 cm^{-1} (C-H stretching in imidazolium ring); 2968 cm^{-1}, 2945 cm^{-1} and 2881 cm^{-1} (CH_3 stretching); 1592 cm^{-1} (C=C stretching); 1469 cm^{-1} (CH_3 bending); 833 cm^{-1} (P-F stretching); and 558 cm^{-1} (F-P-F bending).[39,40] Absorption peaks from both $[BM_2Im][PF_6]$ and CA were observed in the IR spectrum of the composite film. However, the intensity of the broad band centered on 3500 cm^{-1} (hydroxyl region) is decreased, and the C=O stretching band is blue shifted by 9-10 cm^{-1} in the composite film (Figure 2.3b). These observations suggest a disruption of hydrogen bonding between CA molecules, and a change in the environment of carbonyl functional groups.[41] The IR patterns of $[BM_2Im][PF_6]$ in the pure and composite films were not notably different.

The ratio of $[BM_2Im][PF_6]$ to CA in the composite film was measured using electron probe microanalysis with wavelength dispersive spectroscopy (EPMA-WDS). The ratios of phosphorus to oxygen (P:O) were analyzed at nine different 30-μm spots. Based on the total P:O

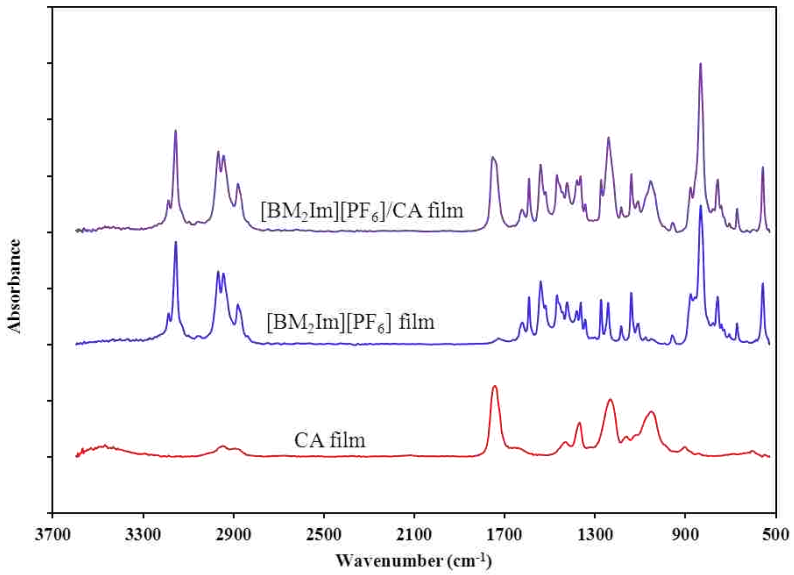

(a)

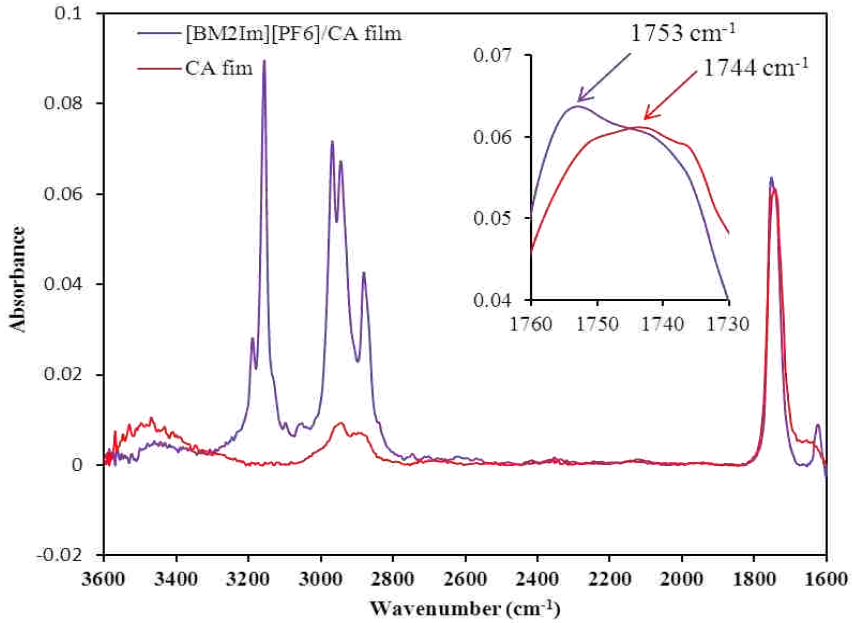

(b)

Figure 2.3 ATR-FTIR spectra. a) CA, $[BM_2Im][PF_6]$, $[BM_2Im][PF_6]$/CA films. b) CA and $[BM_2Im][PF_6]$-CA films illustrating the changes in hydroxyl and carbonyl bands of CA. Inset shows the magnified plot of 1760-1730 cm^{-1} region.

ratio, the mass ratio of $[BM_2Im][PF_6]$ to CA was estimated to be 7.8:1. A small oxygen signal was observed in both the $[BM_2Im][PF_6]$ film and the blank substrate (gold-coated silicon). Only

the excess oxygen present in the composite film as compared to the $[BM_2Im][PF_6]$ film was attributed to cellulose acetate. Variations in P:O ratios were observed, indicating a heterogeneous distribution of $[BM_2Im][PF_6]$ and CA.

2.4.2 Chemical Sensing Properties of the Films

The chemical-sensing properties of these films were evaluated using a QCM transducer. Figure 2.4a shows Δf as a function of acetonitrile vapor concentrations for three different films: the first prepared using $[BM_2Im][PF_6]$ only, the second prepared using $[BM_2Im][PF_6]$ and cellulose acetate at a mass ratio of 7.5:1, and the third prepared using cellulose acetate only. The approximate mass loads calculated using the Sauerbrey equation were 139 $\mu g/cm^2$ for $[BM_2Im][PF_6]$, 176 $\mu g/cm^2$ for $[BM_2Im][PF_6]$-CA, and 3 $\mu g/cm^2$ for the CA films. It is evident from this figure that for the $[BM_2Im][PF_6]$ film, Δf is substantially smaller in magnitude; moreover, the magnitude decreases as the concentration of vapor increases. In other words, above a certain vapor concentration, the frequency increases with an increase in vapor concentration. By contrast, the $[BM_2Im][PF_6]$-CA film shows excellent linearity over a very wide range of concentrations. Attempts to coat only CA using a similar procedure resulted in a comparatively low mass loading, which produced negligible frequency response to acetonitrile vapors. Note that the response would be very low, even if it is linearly normalized to the amount of cellulose acetate in the composite.

Figure 2.4b is a plot of ΔR as a function of acetonitrile concentration for $[BM_2Im][PF_6]$ and $[BM_2Im][PF_6]$-CA films. Both films show an increase in ΔR as a function of acetonitrile concentration. However, as shown in Figure 2.4c the ratio $\Delta R/\Delta f$ is much higher for the $[BM_2Im][PF_6]$ film than the ratio for the $[BM_2Im][PF_6]$-CA film. This observation implies that the $[BM_2Im][PF_6]$-CA film is substantially more rigid than the $[BM_2Im][PF_6]$ film. Evaluation

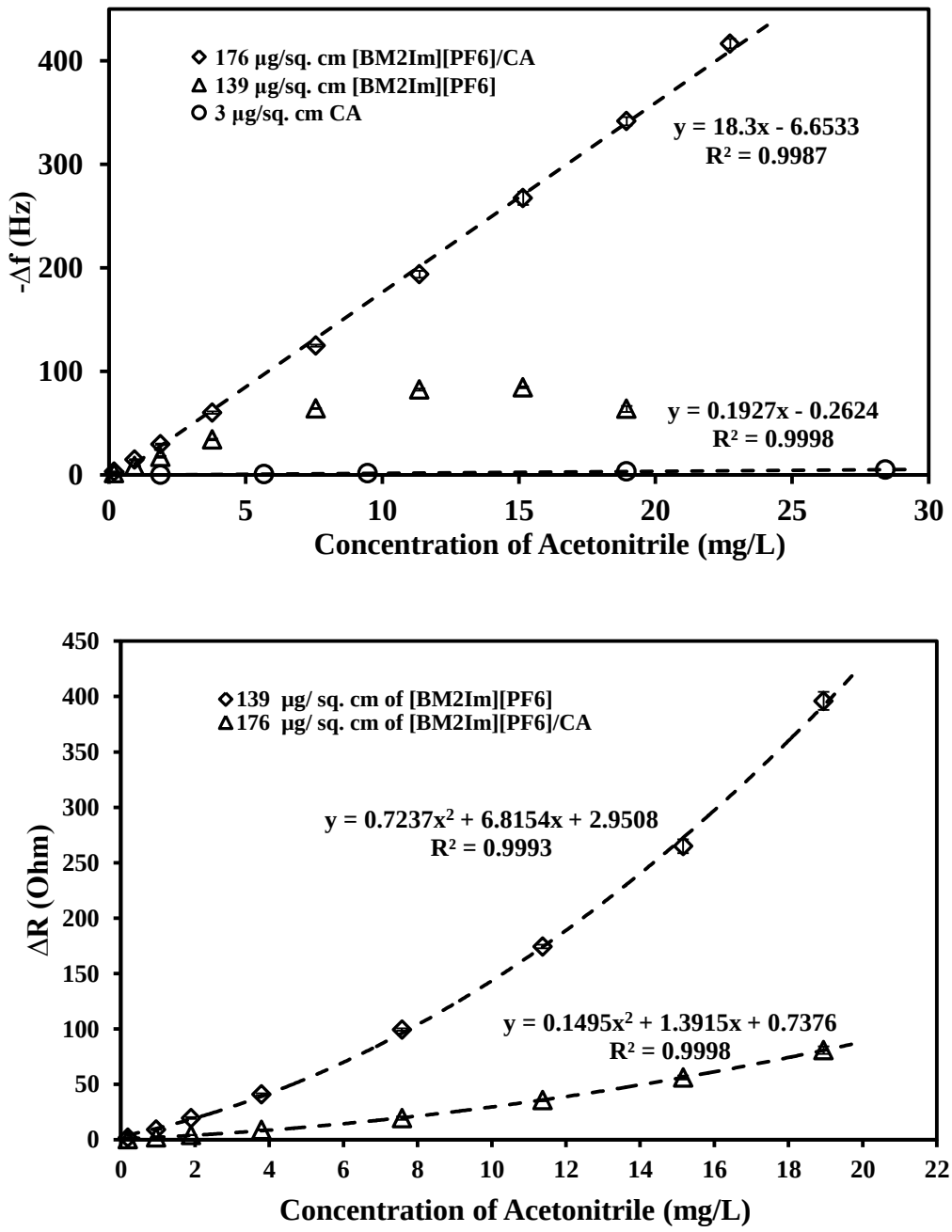

Figure 2.4 a) Frequency change as a function acetonitrile concentration for $[BM_2Im][PF_6]$-CA, $[BM_2Im][PF_6]$, and CA films. b) Motional resistance shift as a function acetonitrile concentrations for $[BM_2Im][PF_6]$ and $[BM_2Im][PF_6]$-CA films, c) Motional resistance shift versus frequency change for $BM_2Im][PF_6]$ and $[BM_2Im][PF_6]$-CA films on exposure to varying concentrations of acetonitrile. Legend in each figure shows the amount of film material on the QCR surface.

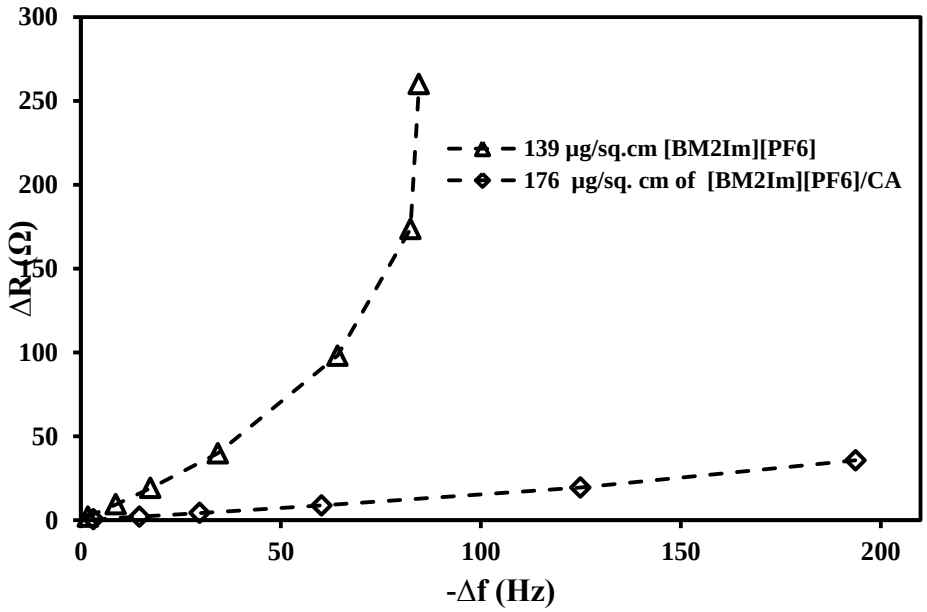

Figure 2.4 c) Continued.

using MD simulations shows that acetonitrile exhibits negligible electrostatic and van der Waals interactions with CA. By contrast, stronger interactions are observed between acetonitrile and $[BM_2Im]^+$ or $[PF_6]^-$ ions (Figure A4b inset, in Appendix A). Similar trends were also observed for other analytes (data not shown). In aggregate, these observations indicate that the sorption characteristics of the composite film are due to $[BM_2Im][PF_6]$, while CA plays a key role in improving the mechanical stiffness of the material. In fact, this increase in rigidity can be qualitatively rationalized using the simple 'rule-of-mixtures', which has often been employed to estimate mechanical response of composite material from the properties and quantities of individual constituents. Based on our initial observations, we concluded that the $[BM_2Im][PF_6]$-CA film is preferred for QCM-based vapor sensing, and hence the composite film was studied in detail, as outlined below.

The sensitivity of our sensor was found to increase linearly with the amount of sensing material deposited on the QCM electrode (Figures A5 and A6, in Appendix A). The linear

relationships between Δf and vapor concentration; and between sensitivity and amount of sensing material indicate that the mass transfer process at the interface is predominantly the bulk absorption of vapors by the coating material. The mass of the sensing material deposited on the resonator can be conveniently controlled by changing the concentrations of $[BM_2Im][PF_6]$ and CA during film preparation. The maximum amount loaded was approximately 214 µg of the sensing material per cm^2 of the electrode surface. While it should be possible to increase the mass loading using the same coating procedure, higher mass loadings exhibited slow response, and thus were not studied in detail. In marked contrast to our observations with GUMBOS-CA, it has been reported that Δf, in response to vapors, either plateaus[42] or becomes positive[43] with RTILs when the thickness of the coating exceeds ~200 nm, corresponding to a mass load of ~20-25 $\mu g/cm^2$.

Our composite material provided excellent linearity, and varying sensitivity to different organic vapors (Figure A7, in Appendix A). Moreover, high sensitivity, low detection limit, high repeatability, and a wide linear range (Table A1, in Appendix A) were obtained. Indeed, the detection limit improvement was 46-fold for acetonitrile, 8.9-fold for methanol, and 8.1-fold for toluene as compared to those typically reported in the literature for an RTIL-based QCM sensor.[19] Use of MD simulations predicted that the order of analyte-sorbent interaction energies for six analytes initially tested was: acetonitrile > toluene > acetone > ethanol > methanol > chloroform (Figure A4b, in Appendix A). We note that this ordering closely correlated with the ordering of the experimental slopes (i.e. Hz.L/mg) observed in Figure A7, in Appendix A. Examination of Figure 2.5 shows a stable baseline and complete regeneration after repeated exposure to chloroform vapors. All other compounds investigated in this study showed similar behavior. Interestingly, our composite material exhibited very rapid response; the time to reach

equilibrium is estimated to be less than one minute (Figure A8, in Appendix A). However, the actual time is probably substantially less since the measured time also includes the time for filling the sample chamber. The regeneration time is apparently somewhat higher. Still this time also depends on how rapidly the analyte vapor is cleared from the chamber. Relative standard deviations for repeated measurements of both Δf and ΔR were typically less than 4% (error bars are shown in Figures 2.4a-b). No significant differences in signals were observed on repeating the experiments several days later. Since temperature variations induce changes in the viscoelastic properties of the films, a strict control of temperature is required to ensure reproducible measurements.

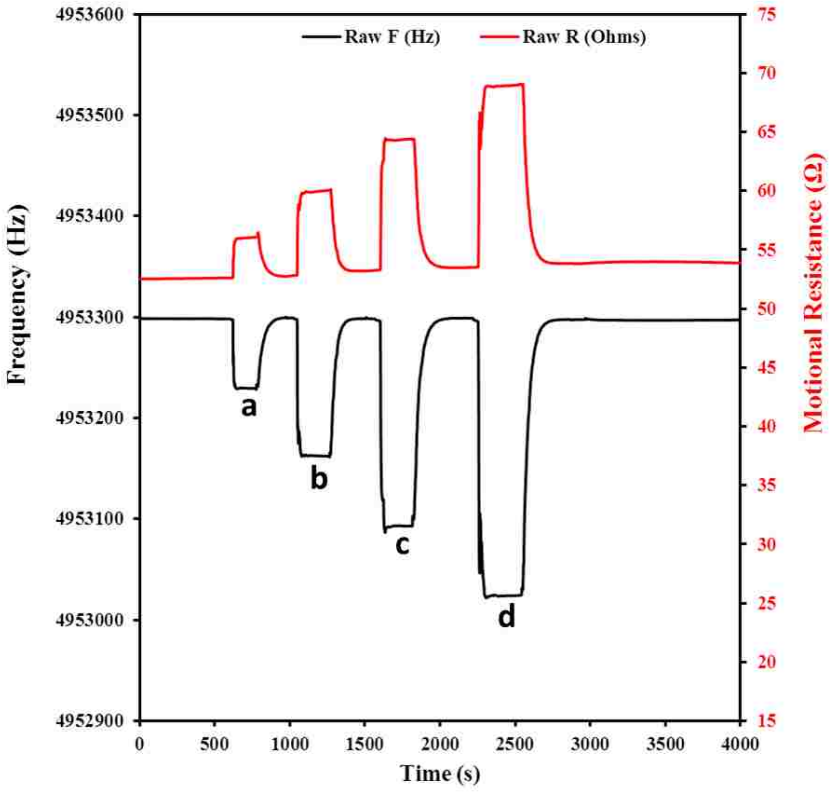

Figure 2.5 Frequency and resistance responses of the QCM sensor to 17.8 mg/L (**a**), 35.6 mg/L (**b**), 53.4 mg/L (**c**), and 71.3 mg/L (**d**) of chloroform vapors. In each case, the liquid sample was injected into the chamber and allowed to vaporize; after equilibrium, the vapor was removed by flushing with UHP argon. The amount of coating material on QCR is 207 µg/cm^2.

Here, we demonstrate a very unique and interesting property of our composite material. The Δf and ΔR of the QCM were simultaneously monitored upon exposure to a number of common VOCs: methanol, acetonitrile, ethanol, acetone, 1-propanol, toluene, chloroform, and carbon tetrachloride. We note that analytes investigated include both polar and non-polar compounds. Figure 2.6a is a display of plots of Δf versus ΔR for all analytes, and it is evident that all plots are linear over a wide range of vapor concentrations. The data presented in Figures 2.6(a-b) were obtained under intermediate loading of the composite material: 83 μg of composite film per cm^2 of electrode area. The analyte concentration ranges are i) 1.93-77.0 mg/L for tetrachloromethane, ii) 0.720-28.8 mg/L for chloroform, iii) 0.209-8.36 mg/L for toluene, iv) 0.194-11.7 mg/L for 1-propanol, v) 0.191-11.5 mg/L for acetone, vi) 0.382-22.9 mg/L for ethanol, vii) 0.190-4.75 mg/L for acetonitrile, and viii) 0.574-23.0 mg/L for methanol.

Figure 2.6b is a plot of $\Delta f/\Delta R$ against molecular weights of analytes. These data points were obtained by taking the ratio of Δf to ΔR at 6-8 different vapor concentrations within the ranges specified above. Interestingly, this plot demonstrates excellent linearity between $\Delta f/\Delta R$ and the molecular weights, as evident from the high correlation coefficient (r^2>0.99). A slight deviation from linearity was consistently observed for acetone (the fourth point in Figure 2.6b), possibly due to the presence of impurities. The relationship between $\Delta f/\Delta R$ and molecular weight (MW) of the absorbed species can therefore be expressed by use of the following equation:

$$\Delta f/\Delta R = k \text{ x MW} + C \qquad (2.2),$$

where k is a proportionality constant. For our system, the value of k was found to depend on the amount of sensing material deposited on the QCR; the relative proportions of GUMBOS and

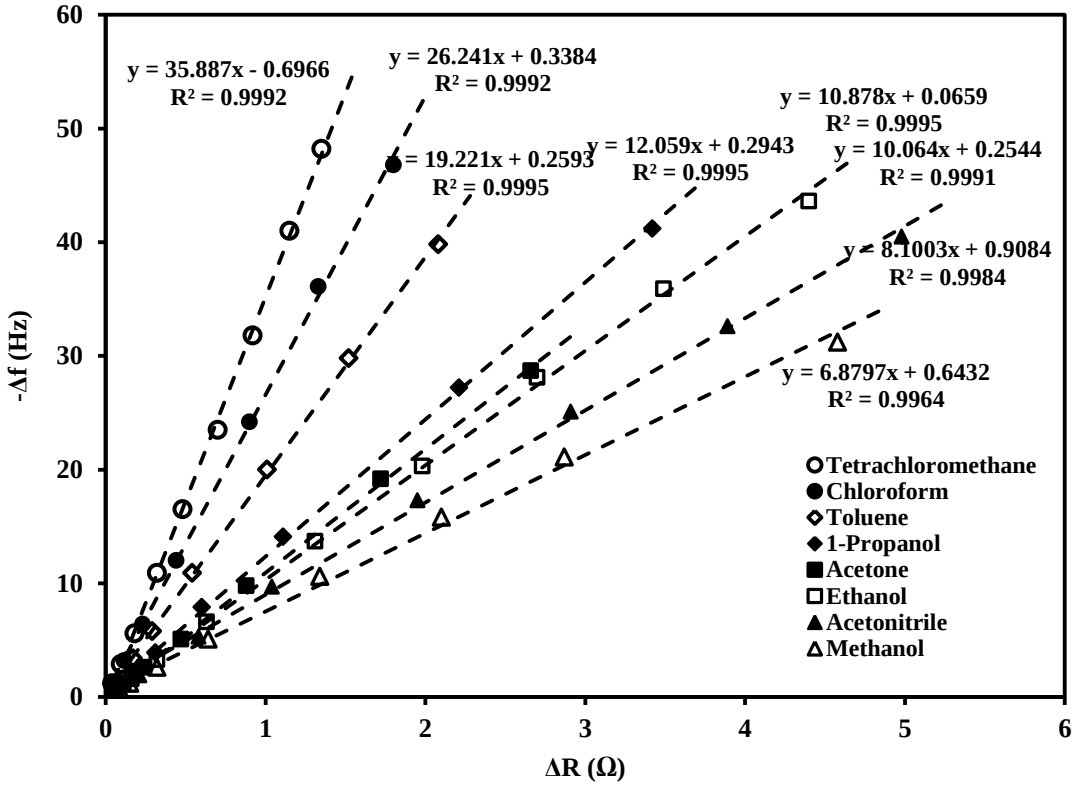

(a)

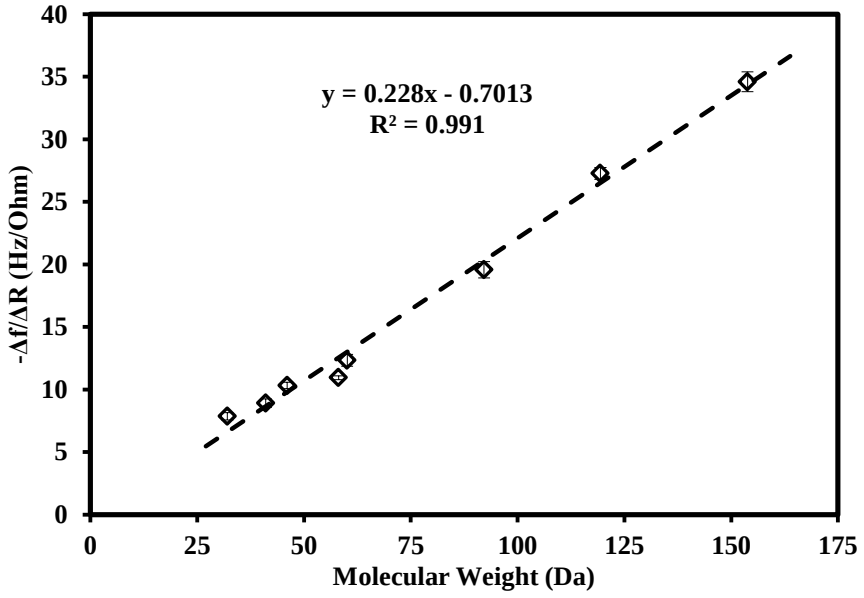

(b)

Figure 2.6 a) Plots of Δ*f* vs Δ*R* for various VOCs. Mass of coating material is 83 μg/cm^2. Analyte concentration ranges: 1.93-77.0 mg/L for tetrachloromethane, 0.720-28.8 mg/L for chloroform, 0.209-8.36 mg/L for toluene, 0.194-11.7 mg/L for 1-propanol, 0.191-11.5 mg/L for acetone, 0.382-22.9 mg/L for ethanol, 0.190-4.75 mg/L for acetonitrile, and 0.574-23.0 mg/L for methanol. b) Variation of Δ*f*/Δ*R* as a function molecular weight of analytes. Error bars represent the standard deviations (n = 6-8).

CA; and the GUMBOS employed (see below). The intercept, C, is small and practically insignificant (when C is set to zero, r^2 becomes 0.9898). In previous studies, Holloway et al.[44] used calyx[4]resorcinarene-coated QCM sensor, and measured Δf and ΔR to distinguish between hexane and toluene vapors. While the authors demonstrated distinctly different parameters for hexane and toluene, they did not report any correlation between $\Delta f/\Delta R$ and the physico-chemical properties of the analytes. To the best of our knowledge, the linear dependences of Δf to ΔR, and $\Delta f/\Delta R$ to the molecular weights of analytes are unique to our material. The simultaneous measurement of Δf and ΔR therefore offers a simple way to estimate molecular weights, and discriminate vapor molecules regardless of their concentrations. Note that the measurement of either Δf or ΔR alone would not provide the molecular identity since the response depends on both the concentration and characteristics of analyte.

2.4.3 Theoretical Basis for Material Behavior

In this section, we rationalize the observed sensing behavior of our material using the concepts of free volume and viscoelasticity. According to free-volume theory,[45] the unoccupied space (free volume) in solids and liquids constitutes the 'interstitial' free volume and the 'hole' free volume (holes or vacancies). Another basic assumption of this theory is that the interstitial free volume is uniformly distributed, while holes or vacancies are discontinuously distributed throughout the material. It is this 'hole' free volume that is primarily responsible for molecular transport. Although this theory has been generally applied to polymers, Dlubek et al.[46] recently demonstrated the presence of subnanometer-size holes in the solid and liquid states of ILs using positron annihilation lifetime spectroscopy (PALS). These holes are comparable to the sizes of the constituent ions, and the estimated 'hole' density is 2.0×10^{20} g^{-1}. The solubility and diffusion of gases in ILs have been explained using the concept of 'free volume' or 'void space' available

in these materials.[47-49] The rapid response and recovery times observed for our sensing material can be attributed to the presence of free volumes that facilitate the rapid diffusion of analyte molecules within our films.

Another consideration for our system is the viscoelastic behavior of ionic materials. Makino et al.[50] recently demonstrated that alkyl imidazolium-based ILs having long enough side chains (≥ C4) exhibit viscoelastic properties. For viscoelastic materials, the shear modulus (G) is a complex quantity [51]: $G = G' + jG''$, where G' is shear storage modulus of the film, G'' shear loss modulus of the film, and j is $(-1)^{1/2}$. A review of the literature indicates that motional resistance depends upon the following film parameters: shear modulus, thickness, mass density,[52] and the particle surface coverage.[53] The viscoelastic properties of polymer films have been extensively studied, and substantial changes in G' and G'' have been observed during vapor absorption.[54] Hence, the shear modulus is assumed to be the more important parameter determining the changes in motional resistance. It is also recognized that gas/vapor absorption induces a detectable swelling in ionic liquids.[55] In fact, the increase in R observed during vapor absorption can be attributed to a decrease in shear modulus as a result of film swelling. As mentioned earlier, our data show that frequency shifts are directly proportional to the vapor phase concentration of the analytes (Figure A7, in Appendix A). Based on simple thermodynamic arguments, the concentration of vapor in the sorbent phase, C_s, is related to the concentration of vapor in the vapor phase, C_v, through the partition coefficient, K:

$$K = C_s/C_v \qquad (2.3)$$

Equation 2.3, together with the data in Figure A7, implies that Δf is directly proportional to the mass of vapor absorbed into the film. This conclusion is clearly consistent with the Sauerbrey

equation. Equation 2.2 then implies that any motional resistance increase is directly proportional to the number of molecules of analyte absorbed, and that it is largely independent of the chemical properties of the molecules**.** Examination of Figure 2.7 shows that ΔR varies linearly with the number of moles of analyte absorbed. (In fact, Figure 2.7 and Figure 2.6a are two different forms of the same information.)

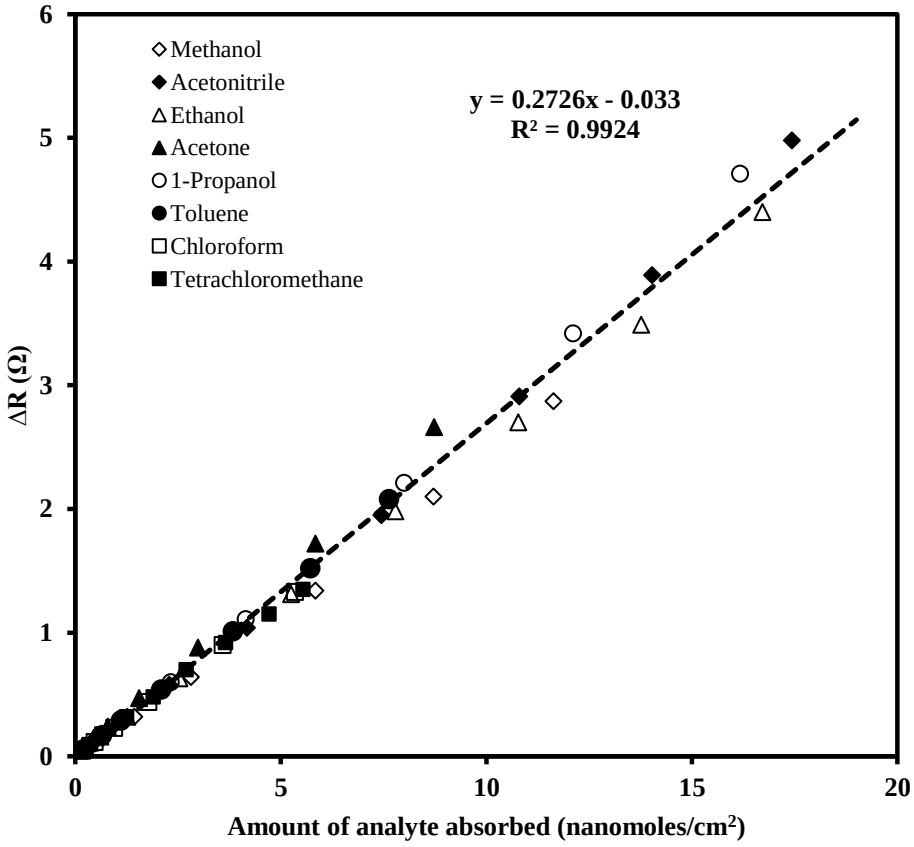

Figure 2.7 Variation of ΔR with the moles of analytes absorbed. The dashed line represents the linear fit. Amount of vapor absorbed is calculated using Sauerbrey equation.

While more rigorous theoretical and experimental studies are needed and underway to fully rationalize the observed mole-dependent increase in motional resistance, we present here a

simple theoretical analysis that, at least qualitatively, accounts for our experimental observations. We assume that any motional resistance increase is due to changes in mass density, thickness, and shear modulus of the film, since these are the parameters that change during vapor absorption. Since the amount of vapor absorbed is relatively low (the estimated maximum mass fraction of analyte in our experiments is approximately 0.01), the density of the sorbent-analyte system remains essentially the same for all analytes, given an equal number of absorbed molecules. Examination of data from our MD simulations suggest that the total interaction energy experienced by any given molecule of analyte with other species present in the system ($[BM_2Im]^+$, $[PF_6]^-$ and CA), is much lower than the total interaction energy experienced by one random cation, anion, or oligomer of CA in the same system (Figure A4b, in Appendix A). Since an analyte is present in low concentration and does not interact strongly with the sorbent phase, it is possible that the vapor molecules behave more-or-less as an ideal gas within the free volume of the sorbent matrix. Consequently, the same number of molecules of analyte should produce similar thickness and free volume changes, and should be more-or-less independent of the chemical identity of the analyte. To a good approximation, the motional resistance increase depends only on the number of molecules that are absorbed.

Preliminary vapor sensing studies were also performed using three other GUMBOS: $[BM_2Im][OTf]$, $[BMPyr][PF_6]$, and $[EM_2Im][PF_6]$. $[BM_2Im][OTf]$-CA and $[BMPyr][PF_6]$-CA showed similar behavior to that of $[BM_2Im][PF_6]$-CA. By contrast, $[EM_2Im][PF_6]$ or $[EM_2Im][PF_6]$-CA exhibited decreased sensitivity, very slow response, and negligible motional resistance shift. These observations support our contention that free volume and viscoelasticity play an extremely important role in determining the unique response characteristics of our sensing materials. $[EM_2Im][PF_6]$ does not show appreciable viscoelastic behavior, and possesses

less free volume due to a decrease in the length of the alkyl side chain. Since important structural differences exist between GUMBOS and polymers, these two classes of material should exhibit very different motional resistance response.

2.5 Conclusions

In summary, we have prepared and characterized a composite film comprising $[BM_2Im][PF_6]$ and CA; and investigated its vapor sensing characteristics using a QCM transducer. The material not only exhibited performance characteristics superior to other materials, but also provided unique viscoelastic behavior. A remarkable correlation between $\Delta f/\Delta R$ of the sensor and molecular weight of the absorbed chemical species was observed. Films with similar sensing properties were also developed using CA and other suitable GUMBOS. In like manner, it is possible to develop new composite materials with desirable viscoelastic properties using GUMBOS and other suitable polymers. These novel sensing materials should facilitate easy detection, discrimination, and molecular weight determination of gaseous analytes. Since these materials hold considerable promise for constructing reliable chemical sensors, further development is essential to realize their full potential. More rigorous theoretical and experimental studies are currently underway to fully understand the observed mole-dependent increase in motional resistance. Such investigations also include assessing the free volume of the materials upon exposure to various VOCs.

2.6 References

(1) Schlupp, M.; Weil, T.; Berresheim, A. J.; Wiesler, U. M.; Bargon, J.; Mullen, K.: Polyphenylene dendrimers as sensitive and selective sensor layers. *Angewandte Chemie-International Edition* **2001**, *40*, 4011-4015.

(2) Di Natale, C.; Macagnano, A.; Martinelli, E.; Paolesse, R.; D'Arcangelo, G.; Roscioni, C.; Finazzi-Agro, A.; D'Amico, A.: Lung cancer identification by the analysis of breath

by means of an array of non-selective gas sensors. *Biosensors and Bioelectronics* **2003**, *18*, 1209-1218.

(3) Penza, M.; Antolini, F.; Vittori-Antisari, M.: Carbon nanotubes-based surface acoustic waves oscillating sensor for vapour detection. *Thin Solid Films* **2005**, *472*, 246-252.

(4) Si, P.; Mortensen, J.; Kornolov, A.; Denborg, J.; Moller, P. J.: Polymer coated quartz crystal microbalance sensors for detection of volatile organic compounds in gas mixtures. *Analytica Chimica Acta* **2007**, *597*, 223-230.

(5) Patel, S. V.; Mlsna, T. E.; Fruhberger, B.; Klaassen, E.; Cemalovic, S.; Baselt, D. R.: Chemicapacitive microsensors for volatile organic compound detection. *Sensors and Actuators B: Chemical* **2003**, *96*, 541-553.

(6) Snow, E. S.; Perkins, F. K.; Houser, E. J.; Badescu, S. C.; Reinecke, T. L.: Chemical detection with a single-walled carbon nanotube capacitor. *Science* **2005**, *307*, 1942-1945.

(7) Li, B.; Sauve, G.; Iovu, M. C.; Jeffries-El, M.; Zhang, R.; Cooper, J.; Santhanam, S.; Schultz, L.; Revelli, J. C.; Kusne, A. G.; Kowalewski, T.; Snyder, J. L.; Weiss, L. E.; Fedder, G. K.; McCullough, R. D.; Lambeth, D. N.: Volatile organic compound detection using nanostructured copolymers. *Nano Letters* **2006**, *6*, 1598-1602.

(8) Wang, F.; Swager, T. M.: Diverse Chemiresistors based upon covalently modified multiwalled carbon nanotubes. *The Journal of the American Chemical Society* **2011**, *133*, 11181-11193.

(9) Read, D. H.; Martin, J. E.: Field-structured chemiresistors. *Advanced Functional Materials* **2010**, *20*, 1577-1584.

(10) Snow, E. S.; Perkins, F. K.: Capacitance and conductance of single-walled carbon nanotubes in the presence of chemical vapors. *Nano Letters* **2005**, *5*, 2414-2417.

(11) Janata, J.; Josowicz, M.: Conducting polymers in electronic chemical sensors. *Nature Materials* **2003**, *2*, 19-24.

(12) Freund, M. S.; Lewis, N. S.: A chemically diverse conducting polymer-based "electronic nose". *Proceedings of the National Academy of Sciences of the United States of America* **1995**, *92*, 2652-2656.

(13) Lubczyk, D.; Siering, C.; Lorgen, J.; Shifrina, Z. B.; Mullen, M.; Waldvogel, S. R.: Simple and sensitive online detection of triacetone triperoxide explosive. *Sensors and Actuators B: Chemical* **2010**, *143*, 561-566.

(14) Shen, G.; Chen, P. C.; Ryu, K.; Zhou, C.: Devices and chemical sensing applications of metal oxide nanowires. *Journal of Materials Chemistry* **2009**, *19*, 828-839.

(15) Sysoev, V. V.; Strelcov, E.; Sommer, M.; Bruns, M.; Kiselev, I.; Habicht, W.; Kar, S.; Gregoratti, L.; Kiskinova, M.; Kolmakov, A.: Single-nanobelt electronic nose: engineering and tests of the simplest analytical element. *ACS Nano* **2010**, *4*, 4487-4494.

(16) Krasteva, N.; Fogel, Y.; Bauer, R. E.; Mullen, K.; Joseph, Y.; Matsuzawa, N.; Yasuda, A.; Vossmeyer, T.: Vapor sorption and electrical response of Au-nanoparticle-dendrimer composites. *Advanced Functional Materials* **2007**, *17*, 881-888.

(17) Penza, M.; Tagliente, M. A.; Aversa, P.; Cassano, G.: Organic-vapor detection using carbon-nanotubes nanocomposite microacoustic sensors. *Chemical Physics Letters* **2005**, *409*, 349-354.

(18) Liang, C. D.; Yuan, C. Y.; Warmack, R. J.; Barnes, C. E.; Dai, S.: Ionic liquids: A new class of sensing materials for detection of organic vapors based on the use of a quartz crystal microbalance. *Analytical Chemistry* **2002**, *74*, 2172-2176.

(19) Goubaidoulline, I.; Vidrich, G.; Johannsmann, D.: Organic vapor sensing with ionic liquids entrapped in alumina nanopores on quartz crystal resonators. *Analytical Chemistry* **2005**, *77*, 615-619.

(20) Snow, E. S.; Perkins, F. K.; Robinson, J. A.: Chemical vapor detection using single-walled carbon nanotubes. *Chemical Society Reviews* **2006**, *35*, 790-798.

(21) Tesfai, A.; El-Zahab, B.; Kelley, A. T.; Li, M.; Garno, J. C.; Baker, G. A.; Warner, I. M.: Magnetic and nonmagnetic nanoparticles from a group of uniform materials based on organic salts. *ACS Nano* **2009**, *3*, 3244-3250.

(22) Fredlake, C. P.; Crosthwaite, J. M.; Hert, D. G.; Aki, S.; Brennecke, J. F.: Thermophysical properties of imidazolium-based ionic liquids. *Journal of Chemical & Engineering Data* **2004**, *49*, 954-964.

(23) Sauerbrey, G.: The use of quartz oscillators for weighing thin layers and for microweighing. *Zeitschrift Fur Physik* **1959**, *155*, 206-222.

(24) Smith, A. L.; Mulligan, R. B.; Shirazi, H. M.: Determining the effects of vapor sorption in polymers with the quartz crystal microbalance/heat conduction calorimeter. *Journal of Polymer Science Part B: Polymer Physics* **2004**, *42*, 3893-3906.

(25) Kahle, C. F.: Microporous organic thin films by the solvent precipitation method: A review of formulation techniques and their commercial applications. *Industrial & Engineering Chemistry Research* **2001**, *40*, 33-36.

(26) Sorrell, C. D.; Lyon, L. A.: Bimodal swelling responses in microgel thin films. *The Journal of Physical Chemistry B* **2007**, *111*, 4060-4066.

(27) Hess, B.; Kutzner, C.; van der Spoel, D.; Lindahl, E.: GROMACS 4: Algorithms for highly efficient, load-balanced, and scalable molecular simulation. *Journal of Chemical Theory and Computation* **2008**, *4*, 435-447.

(28) Bussi, G.; Donadio, D.; Parrinello, M.: Canonical sampling through velocity rescaling. *The Journal of Chemical Physics* **2007**, *126*, 014101.

(29) Bussi, G.; Zykova-Timan, T.; Parrinello, M.: Isothermal-isobaric molecular dynamics using stochastic velocity rescaling. *The Journal of Chemical Physics* **2009**, *130*, 074101.

(30) Darden, T.; York, D.; Pedersen, L.: Particle mesh ewald - an n.log(n) method for Ewald sums in large systems. *The Journal of Chemical Physics* **1993**, *98*, 10089-10092.

(31) Hess, B.; Bekker, H.; Berendsen, H. J. C.; Fraaije, J.: LINCS: A linear constraint solver for molecular simulations. *Journal of Computational Chemistry* **1997**, *18*, 1463-1472.

(32) Jorgensen, W. L.; Maxwell, D. S.; Tiradorives, J.: Development and testing of the opls all-atom force-field on conformational energetics and properties of organic liquids. *Journal of the American Chemical Society* **1996**, *118*, 11225-11236.

(33) Lopes, J. N. C.; Deschamps, J.; Padua, A. A. H.: Modeling ionic liquids using a systematic all-atom force field. *The Journal of Physical Chemistry B* **2004**, *108*, 2038-2047.

(34) Lopes, J. N. C.; Padua, A. A. H.; Shimizu, K.: Molecular force field for ionic liquids IV: Trialkylimidazolium and alkoxycarbonyl-imidazolium cations; alkylsulfonate and alkylsulfate anions. *The Journal of Physical Chemistry B* **2008**, *112*, 5039-5046.

(35) Schafer, T.; Di Francesco, F.; Fuoco, R.: Ionic liquids as selective depositions on quartz crystal microbalances for artificial olfactory systems—a feasibility study. *Microchemical Journal* **2007**, *85*, 52-56.

(36) Shen, D. Z.; Li, X. Y.; Kang, Q.; Zhang, H. T.; Qi, Y.: Monitor adsorption of acetone vapor to a room temperature ionic liquid 1-octyl-3-methylimidazolium bromide by a langasite crystal resonator. *Analytica Chimica Acta* **2006**, *566*, 19-28.

(37) Muramatsu, H.; Tamiya, E.; Karube, I.: Computation of equivalent-circuit parameters of quartz crystals in contact with liquids and study of liquid properties. *Analytical Chemistry* **1988**, *60*, 2142-2146.

(38) Ilharco, L. M.; de Barros, R. B.: Aggregation of pseudoisocyanine iodide in cellulose acetate films: structural characterization by FTIR. *Langmuir* **2000**, *16*, 9331-9337.

(39) Katsyuba, S. A.; Zvereva, E. E.; Vidis, A.; Dyson, P. J.: Application of density functional theory and vibrational spectroscopy toward the rational design of ionic liquids. *The Journal of Physical Chemistry A* **2007**, *111*, 352-370.

(40) Wang, J. Y.; Chu, H. B.; Li, Y.: Why single-walled carbon nanotubes can be dispersed in imidazolium-based ionic liquids. *ACS Nano* **2008**, *2*, 2540-2546.

(41) Puleo, A. C.; Paul, D. R.; Kelley, S. S.: The effect of degree of acetylation on gas sorption and transport behavior in cellulose-acetate. *Journal of Membrane Science* **1989**, *47*, 301-332.

(42) Jin, X. X.; Yu, L.; Garcia, D.; Ren, R. X.; Zeng, X. Q.: Ionic liquid high-temperature gas sensor array. *Analytical Chemistry* **2006**, *78*, 6980-6989.

(43) Xu, X. M.; Cang, H. W.; Li, C. Z.; Zhao, Z. B. K.; Li, H. Y.: Quartz crystal microbalance sensor array for the detection of volatile organic compounds. *Talanta* **2009**, *78*, 711-716.

(44) Holloway, A. F.; Nabok, A.; Thompson, M.; Ray, A. K.; Crowther, D.; Siddiqi, J.: New method of vapour discrimination using the thickness shear mode (TSM) resonator. *Sensors* **2003**, *3*, 187-191.

(45) Vrentas, J. S.; Duda, J. L.: Diffusion in polymer-solvent systems.1. Re-examination of free-volume theory. *Jouranl of Polymer Science Part B: Polymer Physcis.* **1977**, *15*, 403-416.

(46) Dlubek, G.; Yu, Y.; Krause-Rehberg, R.; Beichel, W.; Bulut, S.; Pogodina, N.; Krossing, I.; Friedrich, C.: Free volume in imidazolium triflimide ($[C_3MIM][NTf_2]$) ionic liquid from positron lifetime: amorphous, crystalline, and liquid states.*The Journal of Chemical Physics* **2010**, *133*, 124502.

(47) Blanchard, L. A.; Gu, Z. Y.; Brennecke, J. F.: High-pressure phase behavior of ionic liquid/CO2 systems. *The Journal of Physical Chemistry B* **2001**, *105*, 2437-2444.

(48) Ferguson, L.; Scovazzo, P.: Solubility, diffusivity, and permeability of gases in phosphonium-based room temperature ionic liquids: Data and correlations. *Industrial & Engineering Chemistry Research* **2007**, *46*, 1369-1374.

(49) Condemarin, R.; Scovazzo, P.: Gas permeabilities, solubilities, diffusivities, and diffusivity correlations for ammonium-based room temperature ionic liquids with comparison to imidazolium and phosphonium RTIL data. *Chemical Engineering Journal* **2009**, *147*, 51-57.

(50) Makino, W.; Kishikawa, R.; Mizoshiri, M.; Takeda, S.; Yao, M.: Viscoelastic properties of room temperature ionic liquids. *The Journal of Chemical Physics* **2008**, *129*, 104510.

(51) Martin, S. J.; Frye, G. C.; Senturia, S. D.: Dynamics and response of polymer-coated surface-acoustic-wave devices–effect of viscoelastic properties and film resonance. *Analytical Chemistry* **1994**, *66*, 2201-2219.

(52) Smith, A. L.; Ashcraft, J. N.; Hammond, P. T.: Sorption isotherms, sorption enthalpies, diffusion coefficients and permeabilities of water in a multilayer PEO/PAA polymer film using the quartz crystal microbalance/heat conduction calorimeter. *Thermochimica. Acta* **2006**, *450*, 118-125.

(53) Tellechea, E.; Johannsmann, D.; Steinmetz, N. F.; Richter, R. P.; Reviakine, I.: Model-independent analysis of QCM Data on colloidal particle adsorption. *Langmuir* **2009**, *25*, 5177-5184.

(54) Katz, A.; Ward, M. D.: Probing solvent dynamics in concentrated polymer films with a high-frequency shear mode quartz resonator. *Journal of Applied Physics* **1996**, *80*, 4153-4163.

(55) Sakellarios, N. I.; Kazarian, S. G.: In situ IR spectroscopic study of the CO_2-induced swelling of ionic liquid media. In i*onic liquids IIIA: fundamentals, progress, challenges, and opportunities, properties and structure*; Editors Rogers, R. D., Seddon, K. R.; American Chemical Society; Washington, DC, **2005**; Vol. 901, pp. 89-101.

CHAPTER 3 MOLECULAR WEIGHT SENSING PROPERTIES OF IONIC LIQUID-POLYMER COMPOSITE FILMS: THEORY AND EXPERIMENT[**]

3.1 Introduction

At present, there has been a rapid increase in interest in the development of high performance sensors for volatile organic compounds (VOCs) owing to the ever expanding need to monitor a wide array of chemical vapors in different environments. Specifically, VOC vapor sensors have proven to be very useful for 1) analysis of exhaled breath in evaluating medical conditions and environmental exposure to volatile toxins, 2) detection and discrimination of bacterial pathogens in medicine and industry, 3) examination of quality of food and beverages, and 4) assessment of environmental pollution.[1-6] In this regard, several research groups are involved in developing improved sensing devices for detection and discrimination of pure as well as complex mixtures of VOCs. The vast majority of these studies have employed the concept of sensor arrays.[7-17] In a sensor system, sensing materials are important components that play a key role in successful design and implementation of the sensor. Therefore, there is a recent upsurge of interest in the design and synthesis of improved sensing materials to couple with a variety of physical transducers. In this regard, the best combination of a sensing material and transducer is often sought to obtain optimal sensing performance.

Among a number of sensing technologies, sensors built on the use of acoustic wave-based transducers are favored for detection and discrimination of chemical vapors because such

---

[**]This chapter previously appeared as Bishnu P. Regmi, Nicholas C. Speller, Michael John Anderson, Jean Olivier Brutus, Yonathan Merid, Susmita Das, Bilal El-Zahab, Daniel J. Hayes, Kermit K. Murray, and Isiah M. Warner. Molecular weight sensing properties of ionic liquid-polymer composite films: theory and experiment. *Journal of Materials Chemistry C* **2014**, *2*, 4867-4878. It is reproduced by permission of The Royal Society of Chemistry. http://pubs.rsc.org/en/content/articlelanding/2014/tc/c3tc32528h/unauth#!divAbstract

devices are often sensitive, compact, and amenable to creation of sensor arrays. In an acoustic wave sensor, a piezoelectric substrate is excited using an AC voltage to generate an acoustic wave that subsequently interacts with the surrounding medium, thereby probing its properties. Among different classes of acoustic wave devices, the thickness shear mode (TSM) resonator, better known as a quartz crystal microbalance (QCM), has been demonstrated to be a sensitive analytical tool for detection of chemical and biological species, as well as for probing interfacial properties and phenomena.

The use of a QCM device for chemical sensing entails immobilization of a thin film of sensing materials on the surface of the quartz crystal resonator (QCR), and the successful use of a QCM sensor relies on the performance of these materials. In this regard, ionic liquids (ILs) have emerged as promising sensing materials for QCM-based detection of a wide variety of organic vapors.[10,18-20] ILs are organic salts with melting points below 100 °C. ILs that are liquid at room temperature are commonly known as room temperature ionic liquids (RTILs), whereas those that are solid at room temperature are referred to as frozen ionic liquids. In our studies, we define frozen ionic liquids and related organic salts with melting points up to 250 °C collectively as a group of uniform materials based on organic salts (GUMBOS). High thermal stability, non-volatility, tunable physicochemical properties, chemical stability, and ease of synthesis make ILs and GUMBOS ideal candidates for gas sensing applications. In addition, these materials provide rapid and reversible response to various VOCs. More importantly, ILs and GUMBOS promote viscoelastic properties in composites which allow measurement of two QCM responses, thereby providing greater analytical information for vapor sensing studies.

We have recently reported results of vapor sensing using a QCM sensor prepared by depositing a thin film of a composite material comprising a binary mixture of GUMBOS and

cellulose acetate (CA).[20] An interesting relationship between the ratio $\Delta f/\Delta R$ (where Δf refers to frequency change and ΔR refers to motional resistance change) and the molecular weight of the absorbed analytes was discovered. While this observation was very useful, the data were not sufficient to fully explain the unique vapor sensing characteristics of these films. It must be emphasized that a fundamental understanding of the material characteristics is essential to realizing the full potential of these materials.

In the present study, I have systematically investigated a number of IL-polymer combinations to fully evaluate the superior vapor sensing capabilities of this class of materials. A series of heterogeneous thin films comprising binary blends of an IL and polymer were immobilized on the QCR surface, and the reponse of the sensor toward a wide array of organic vapors over an extended concentration range was monitored. Solid phase (i.e. GUMBOS) as well as liquid phase ILs with a range of viscosities were investigated. Two different polymers—cellulose acetate (CA) and polymethylmethacrylate (PMMA)—were utilized to prepare these composite films. In addition, two types of interface electronics, one based on the use of an oscillator circuit and another based on a ring-down approach, were used to measure the QCM responses. Based on these new observations over an extended concentration range of analytes, a quadratic equation for estimation of the molecular weight of organic vapors is proposed. Additionally, the frequency (f) and dissipation (D) at multiple harmonics, as measured by use of a quartz crystal microbalance with dissipation monitoring (QCM-D), were fitted to different materials models. Excellent agreement between the experimental data and theoretical values predicted by use of the Maxwell viscoelastic model was observed. In light of these observations, we propose a theoretical model to explain our previous as well as current observations relating QCM parameters with the molecular weight of absorbed volatile analytes. Assessment of our

overall data suggests that the observed molecular weight relationship for this class of materials has a sound theoretical basis. Overall, these materials exhibit truly unique sensing characteristics, which make the QCM sensor an even more promising tool with capabilities for detection, discrimination, and molecular weight determination of a wide range of chemical vapors.

3.2 Theory of QCM

The QCR comprises a thin plate of AT-cut quartz crystal coated on each face with thin metallic electrodes. Owing to the piezoelectric properties of quartz, application of an AC voltage across the quartz crystal causes oscillations in the thickness shear mode with resonance frequencies in the megahertz (MHz) range. This shear wave experiences a frequency shift and attenuation as it is transmitted through the sensing film immobilized on the electrode surface. The mass and mechanical properties of the coating, which determine the acoustic load at the interface, are perturbed as an analyte interacts with the coating material resulting in alteration of the propagation characteristics (phase and amplitude) of the shear waves. The resonance behavior of the QCM is described by two essential parameters, and in this regard three different types of interface electronics have been commonly employed to measure these quantities. A simple way to accomplish QCM measurements is by use of an oscillator circuit which gives frequency shift (Δf) and motional resistance shift (ΔR) as output parameters.[21,22] However, oscillator circuits are limited to only one harmonic, which makes it difficult to interpret the acquired data. Another kind of interface electronics used to acquire QCM parameters employs an impedance analyzer, and this provides frequency shift (Δf) and bandwidth shift ($\Delta \Gamma$) at different harmonics.[22-24] A relatively new approach to QCM measurements introduced by Kasemo and coworkers,[25,26] is a ring-down-based technique, and this allows measurement of frequency shift

(Δf) and dissipation factor shift (ΔD) over a range of odd harmonics. In fact, the QCM-D instrumentation is based on this ring-down approach.

Motional resistance (R), bandwidth (Γ), and dissipation factor (D) are equivalent parameters; all of them represent energy loss during oscillation, and are therefore related as follows:[25-27]

$$D = \frac{E_{dissipated}}{2\pi E_{stored}} \quad (3.1), \qquad D = \frac{2\Gamma}{f} \quad (3.2), \quad \text{and} \quad D = \frac{R}{2\pi f L} \quad (3.3)$$

where f is the resonance frequency, L is the motional inductance of the Butterworth-van Dyke equivalent circuit of QCR, $E_{dissipated}$ is the energy lost per oscillation cycle, and E_{stored} is the total energy stored in the system.

It is well documented that the resonance frequency of a QCR system decreases when the surface of the crystal is loaded with a mass. For a thin and rigid film uniformly coated on the surface, the relationship between resonance frequency shift (Δf) and the mass adsorbed can be expressed by the well-known Sauerbrey equation as follows:[28]

$$\Delta f = -\frac{n}{C}\Delta m = -\frac{n}{C}\rho_f t_f \quad (3.4)$$

where Δm is mass per unit area of the film, ρ_f is the density of the film, t_f is the thickness of the film, n is the harmonic number which can only be an odd integer, and C is the mass sensitivity or Sauerbrey constant which depends on the fundamental resonance frequency and properties of the quartz (C = 17.7 ng.cm^{-2}.Hz^{-1} for a 5 MHz AT-cut quartz crystal). If the film is thin and rigid, it has the properties of an ideal mass layer and the change in dissipation factor is zero. However, the films used in many QCM-based applications are viscoelastic, and hence dissipate energy

during oscillations. For such films, the frequency change is a function of both mass and viscoelastic properties of the coating material. The rheological behavior of viscoelastic materials can be characterized by a complex shear modulus (G^*), and thus $G^* = G' + iG''$, where G' (or μ) is the elastic shear modulus and G'' is the loss modulus. Several mathematical models have been proposed for simulation of the viscoelastic properties of materials. Two commonly used models in this regard are the Maxwell model, in which a spring and dashpot are connected in series, and the Kelvin-Voigt model, in which the spring and dashpot are arranged in parallel.

The frequency and dissipation changes of a QCR coated with a thin layer of Maxwell viscoelastic material, which is consistent with the present study, is given as follows:[29]

$$\Delta f \approx -\frac{t_f \rho_f \omega}{2\pi \rho_q t_q}\left(1 + \frac{{t_f}^2 \rho_f \omega^2}{3\mu}\right) \quad (3.5), \quad \text{and}$$

$$\Delta D \approx \frac{2{t_f}^3 {\rho_f}^2 \omega}{3\rho_q t_q \eta} \quad (3.6),$$

where ρ_q is the density of the quartz, t_q is the thickness of the quartz, ω is the angular frequency, μ is the elastic shear modulus of the film, and η is the viscosity of the film. The first term in equation 3.5 is in fact the Sauerbrey mass, while the second term represents the viscoelastic correction to the Sauerbrey mass. It is evident from equations 3.5 and 3.6 that the mass correction depends on the elasticity of the film, while the dissipation depends only on the viscosity of the film. Similar equations have been derived for Kelvin-Voigt materials where the mass correction, as well as dissipation factor, is found to depend on both the elasticity and viscosity of the film.[29,30] Despite the fact that these two parameters can be simultaneously obtained in QCM measurements, the vast majority of previous studies have focused only on measuring Δf as a function of analyte concentration. However, it is clear that monitoring both

parameters in QCM studies is much more informative for many applications. It should be noted that not all sensing materials provide this two-parameter response, and hence the selection of suitable sensing materials is important.

3.3 Experimental Section

3.3.1 Materials

Four ILs 1-butyl-2,3-dimethylimidazolium hexafluorophosphate ($[BM_2Im][PF_6]$), 1-hexyl-3-methylimidazolium hexafluorophosphate ($[HMIm][PF_6]$), 1-hexyl-3-methylpyridinium hexafluorophosphate ($[HMPyr][PF_6]$), and 1-hexyl-3-methylpyridinium bis(trifluoromethane)sulfonimide ([HMPyr][TFSI]); and two polymers cellulose acetate (CA) and poly(methyl methacrylate) (PMMA) were used to prepare coatings for the present studies. The compound $[BM_2Im][PF_6]$ was obtained from Ionic Liquids Technologies, Inc. (Tuscaloosa, AL, USA) as a crystalline solid and $[HMIm][PF_6]$ was obtained from TCI America, Inc. (Portland, OR, USA) as a liquid. PMMA (molecular weight ~500,000 Da) was obtained from Polysciences, Inc. (Warrington, PA, USA). CA (average molecular weight ~30,000 Da), anhydrous heptane, anhydrous acetonitrile, anhydrous chloroform, anhydrous toluene, anhydrous methanol, anhydrous ethyl acetate, anhydrous 1-propanol, anhydrous 2-propanol, anhydrous 1-butanol, p-xylene, 3-picoline, 1-bromohexane, lithium *N*,*N*-bis-(trifluoromethane)sulfonimide (LiTFSI), potassium hexafluorophosphate (KPF_6) were obtained from Sigma-Aldrich (St. Louis, MO, USA). Acetone and dichloromethane were obtained from Avantor Performance Materials, Inc. (Center Valley, PA, USA). Absolute ethanol was obtained from Pharmco Products, Inc. (Brookfield, CT, USA). All chemicals were used as received without further purification.

Two different QCM instruments, one based on an oscillator circuit (QCM200) and the other based on an impulse excitation technique (QCM-D), were used in the studies presented

here. Crystals with a fundamental resonance frequency of 5 MHz were used in both instruments. The QCM200 system and optically polished chromium/gold AT-cut quartz crystals with a diameter of 1" were purchased from Stanford Research Systems, Inc. (Sunnyvale, CA, USA). The QCM-D E4 system and optically polished gold-coated AT-cut quartz crystals with a diameter of 14 mm were obtained from Q-Sense AB (Gothenburg, Sweden). Mass flow controllers (Model 5850E) and instrument control and read out equipment (Model 5878) were obtained from Brooks Instrument, LLC (Hatfield, PA, USA). The polytetrafluoroethylene (PTFE) containers were purchased from SPI Supplies/ Structure Probe, Inc. (West Chester, PA, USA).

3.3.2 Synthesis of Ionic Liquids

The compounds [HMPyr][PF_6] and [HMPyr][TFSI] were synthesized using a two-step procedure.[31] Briefly, equimolar amounts of 3-picoline and 1-bromohexane were refluxed at 65 °C for 40 hours. The resulting product was washed several times with ethyl acetate and finally rotovaped to obtain a viscous light yellow liquid [HMPyr][Br]. Then, [HMPyr][Br] was dissolved in water and a slight excess of aqueous KPF_6 was added and stirred overnight at room temperature to obtain [HMPyr][PF_6]. The product was washed several times with water and freeze-dried to remove water in order to obtain a highly viscous light yellow liquid. [HMPyr][TFSI] was prepared similarly by reacting [HMPyr][Br] with LiTFSI. The product was found to be a colorless liquid of low viscosity.

3.3.3 Preparation of Stock Solutions

Stock solutions of 1 mg/mL ionic liquids were prepared in acetone. A stock solution of 0.5 mg/mL cellulose acetate was prepared in acetone, and a stock solution of 1 mg/mL PMMA was prepared in dichloromethane.

3.3.4 Cleaning of Quartz Crystals

The quartz crystal was rinsed with distilled water followed by acetone and finally with dichloromethane. The crystal was carefully dried using flowing nitrogen, and then immersed in fresh piranha solution (3:1 concentrated sulfuric acid and 30% hydrogen peroxide) until no bubbles were seen (usually 5-10 minutes), followed by rinsing with copious amounts of distilled water. The crystal was further rinsed with acetone and then dichloromethane followed by drying under a stream of nitrogen. The crystal was placed in an oven at 100 °C until it was completely dry, and subsequently allowed to cool to room temperature before film deposition.

3.3.5 Thin Film Preparation and Characterization

Thin films were deposited on the surface of the QCR using a solvent precipitation method that has been previously described.[20] Freshly prepared stock solutions were used for all coatings. To prepare an IL-only coating, a 600 µL stock solution of IL was diluted with acetone to a final volume of 2 mL, followed by addition of 6 mL of anhydrous heptane to the solution while stirring. The entire solution was placed in a 25 mL PTFE beaker, and a freshly cleaned crystal was dipped into the solution (the Q-Sense sensor crystal is smaller in diameter, and hence it was placed on top of the SRS quartz crystal) and left undisturbed for 6 hours. All ILs used in this study are soluble in acetone but insoluble in heptane. Acetone is more volatile and evaporates more rapidly, ultimately depositing a thin film on the substrate. To prepare IL-CA films, 160-200 µL of CA solution was added to 600 µL of IL solution and the mixture diluted with acetone to a final volume of 2 mL, while the subsequent steps were the same as defined above. For preparation of the IL-PMMA film, 80-100 µL of PMMA solution (in dichloromethane) was added to 600 µL of IL solution and the mixture diluted with acetone to a final volume of 2 mL, and all subsequent steps were as defined above. Both cellulose acetate and PMMA are insoluble

in heptane, and hence each is co-deposited with the IL. After incubation, residual heptane was drained and the crystal was ultrasonicated in a vertical position within a fresh pool of heptane for approximately 1 minute. The lower surface of the crystal was wiped using solvent-soaked cotton, and left to dry in a desiccator for at least 24 hours. The films were imaged using atomic force microscopy (AFM+, Anasys Instruments, Santa Barbara, CA) in tapping mode. An area of 80x80 μm^2 was scanned with 0.5 Hz scan rate using N-type tapping mode tips (AppNano, Mountain View, CA, ACCESS-NC, resonant frequency: *ca* 250 kHz) with a tip radius of 6 nm and nominal spring constant of 78 $N.m^{-1}$.

3.3.6 Vapor Sensing Studies

Two types of vapor delivery systems, static and dynamic, were used during vapor sensing studies. For measurements using the QCM200, a static system was used, while a flow system was used for QCM-D measurements. The experimental arrangement for the static system is reported in our previous publication.[20] All experiments were performed at 22 °C. A schematic diagram of the experimental setup with the flow-type system is shown in Figure B1, in Appendix B. Again, all experiments were conducted at 22 °C. Each analyte vapor was generated by bubbling ultrapure argon through the liquid sample in a sealed container and the vapor was diluted with an additional stream of argon. The diluted vapor was then allowed to flow through a 1-meter-long tube to ensure complete mixing before reaching the sensor chamber. The flow rates of each of the two streams of argon were changed using two mass flow controllers (MFC1 and MFC2), while the total flow rate was adjusted to 100 sccm. The QCM-D E4 system was fitted with a flow module, and data acquired using the QSoft401 software.

3.4 Results and Discussion

3.4.1 Chemosensitive Film Preparation and Characterization

All sensing films used in these studies were prepared using the solvent precipitation method as previously described.[20] These films were characterized by optical microscopy (OM), scanning electron microscopy (SEM), and atomic force microscopy (AFM). Representative AFM images of two of the several films are shown in Figures 3.1a-d. Figure 3.1a is the AFM topographic image of approximately 90 $\mu g.cm^{-2}$ of $[BM_2Im][PF_6]$-PMMA, and Figure 3.1b is the height profile following the blue line indicated in Figure 3.1a. Similarly, Figure 3.1c is the AFM topographic image of approximately the same amount of $[BM_2Im][PF_6]$-CA, and Figure 3.1d is the height profile corresponding to the blue line indicated in Figure 3.1c. From these images, it is evident that the coatings comprise isolated microdroplets of varying size with heights reaching 2.7 μm. Coating-to-coating mass variations were found to be less than 10 percent. The heights measured by AFM and the heights measured by laser scanning confocal microscopy, as reported in our earlier publication,[20] are in very good agreement. All other films were characterized using OM and SEM, and all had similar isolated microdropets of varying dimensions (data not shown).

3.4.2 Vapor Sensing Studies Using QCM

All QCM sensors were exposed to a variety of organic vapors as pure analytes, and changes in frequency and motional resistance were monitored simultaneously. Plots of the magnitude of Δf versus the concentration of VOC for a QCM sensor coated with $[HMPyr][PF_6]$ are shown in Figure B2, in Appendix B. For each analyte, the best fit for the data is a second-degree polynomial with a downward curvature. Similarly, a plot of ΔR against concentration of analytes is also a polynomial curve, but with upward curvature (Figure B3, in Appendix B). The plots of Δf versus ΔR for different analytes (only six analytes are shown for clarity) are displayed

in Figure 3.2. It is evident that each analyte shows a unique polynomial relationship between Δf and ΔR with a coefficient of determination (R^2) of unity or very close to unity. Therefore, simultaneous measurements of Δf and ΔR for a single QCM sensor enable an excellent discrimination of chemical vapors irrespective of their concentration. On the other hand, a

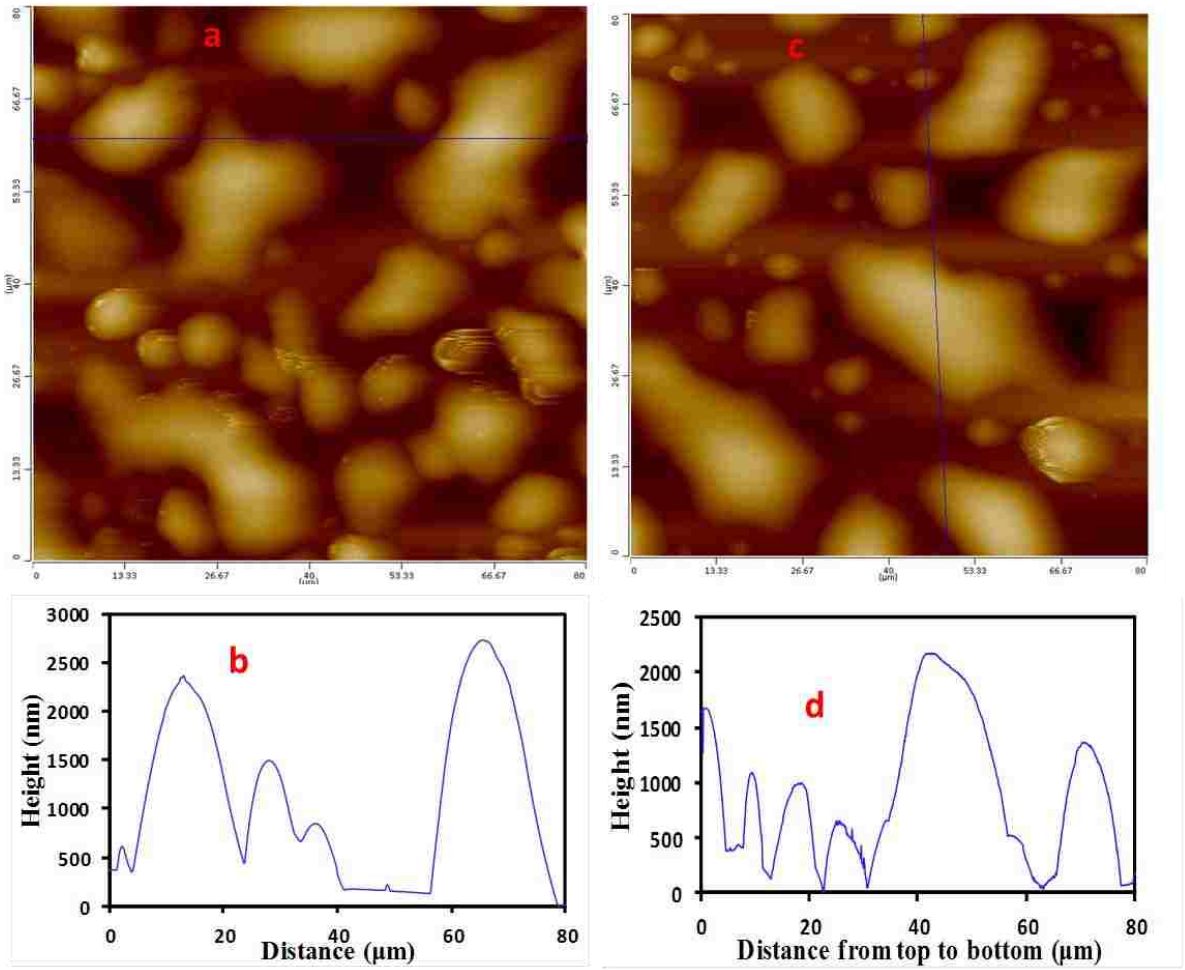

Figure 3.1 (a) AFM topographic image of $[BM_2IM][PF_6]$-PMMA film. (b) Height profile corresponding to the horizontal blue line drawn in topographic image a. (c) AFM topographic image of $[BM_2IM][PF_6]$-CA film. (d) Height profile corresponding to the vertical blue line drawn in the image c. Amount of film material in each case is approximately 90 µg.cm^{-2}.

conventional QCM sensor, which is based on measurement of Δf alone, requires multiple sensors in order to achieve the same level of discrimination. In fact, a sensor based on two-parameter

response, as demonstrated here, provides more information in array-based vapor sensing, thereby greatly enhancing vapor discrimination.

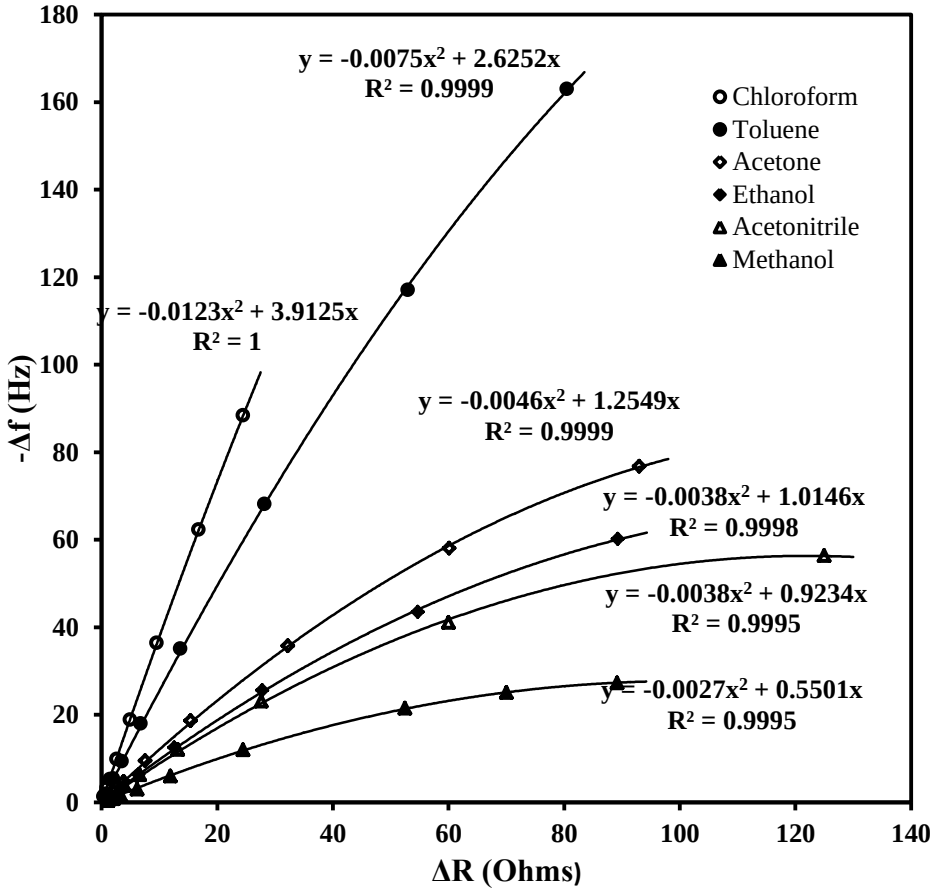

Figure 3.2 Frequency shift versus motional resistance shift during vapor absorption by a QCM sensor coated with [HMPyr][PF_6].

An obvious question arises regarding a comparison of the above data involving pure ILs to binary mixtures similar to those obtained in our previous study. Thus, we evaluated the vapor sensing characteristics of a QCM coated with binary blends of [HMPyr][PF_6] and polymers. Two polymers including CA and PMMA were used for this study. Some notable differences in the sensing performance of the composite films as compared to that of the pure ionic liquid films were observed. Specifically, the slope of Δf versus concentration for composite films is found to increase for each analyte as compared to that of pure IL films, and these plots are primarily linear

(Figures B4 and B6, in Appendix B). In contrast, the slope of the ΔR versus concentration plot for each composite film decreases as compared to that of the pure ionic liquid film (Figures B5 and B7, in Appendix B). The relative values of the slopes of the Δf versus concentration plots for different analytes are quite different for pure IL films as compared to those of composite films (Figures B2, B4, and B6, in Appendix B). However, the relative values of the slopes for the two composite films are essentially the same (Figures B4 and B6, in Appendix B). It is noted that the relative slopes of ΔR versus concentration plots remain similar for all three films (Figures B3, B5, and B7, in Appendix B). In short, all these observations imply that the ionic liquid is largely responsible for vapor absorption, whereas PMMA or CA modulates the viscoelastic properties of the ionic liquid.

A plot of Δf versus ΔR for the composite films, similar to the pure IL film, follows a second-degree polynomial for each analyte (Figure 3.3). More importantly, when the Δf-ΔR plots for each vapor are divided by the molecular weight (MW) of the respective vapor, all curves merge into a single second-degree polynomial curve, and this is true only for the composite-coated QCM sensors. Figure 3.4 is such a Δf/MW versus ΔR plot for a [HMPyr][PF_6]-PMMA coating exposed to nine different analytes—methanol, acetonitrile, ethanol, acetone, 2-propanol, nitromethane, dichloromethane, toluene, and chloroform—over an extended range of vapor concentrations. This plot has a R^2 of 0.998, which is a very remarkable correlation. Similar results were obtained for the [HMPyr][PF_6]-CA coated sensor (Figure B8, in Appendix B). It is important to note that IL-PMMA film displayed better correlation as compared to IL-CA film. This could possibly be due to better mechanical stability of the IL-PMMA films; additional studies are needed to fully understand this observation.

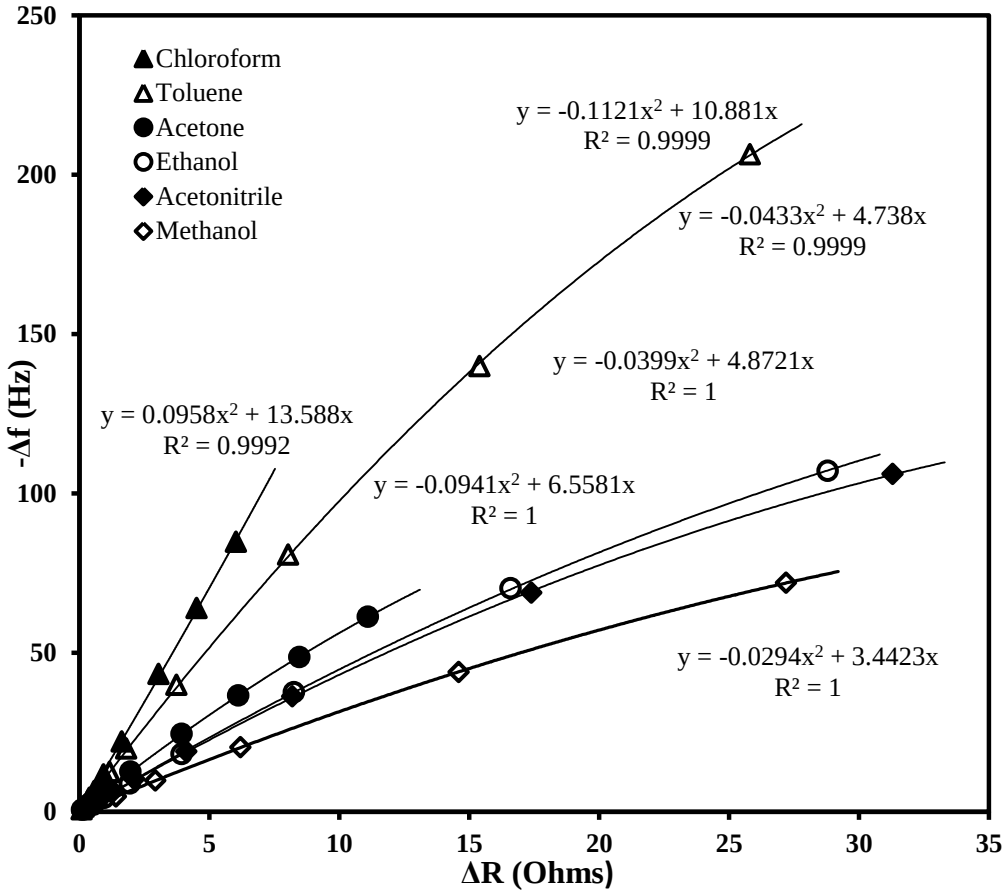

Figure 3.3 Frequency shift versus motional resistance shift due to vapor absorption by a QCM sensor coated with [HMPyr][PF_6]-PMMA.

To illustrate further, we investigated the vapor sensing characteristics of composite films prepared using other ionic liquids. The response of a [HMIm][PF_6]-PMMA coated sensor to 11 different analyte vapors (p-xylene and ethyl acetate in addition to the above-mentioned analytes) is shown in Figure 3.5; and the response of the [BM_2Im][PF_6]-PMMA coated sensor to six different analytes is shown in Figure 3.6. It is clear that the composite films prepared from all three ILs show similar behavior. The relationship between QCM parameters and molecular weight is not evident in the pure IL films (Figure B9, in Appendix B). Hence, simultaneous measurements of Δf and ΔR for IL-polymer composite-coated QCM sensors during vapor

exposure can be used to determine the approximate molecular weight of an unknown vapor with the following equation:

$$\mathrm{MW} = \frac{-\Delta f}{\mathrm{k}'\Delta R^2 + \mathrm{k}\Delta R} \qquad (3.7)$$

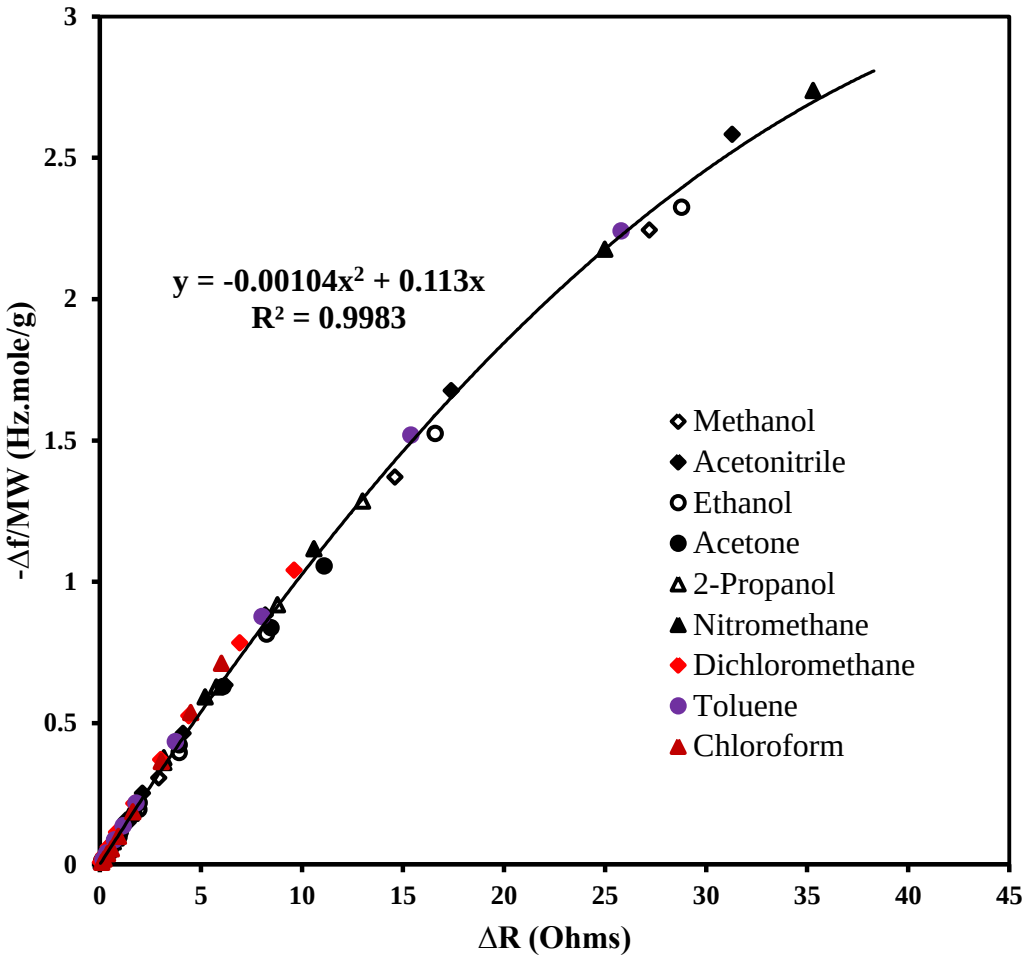

Figure 3.4 Plot of the ratio of frequency shift to molecular weight against motional resistance shift of a QCM sensor coated with [HMPyr][PF_6]-PMMA for nine different organic vapors. Concentration ranges of the vapors are 0.574 to 45.9 mg L^{-1} for methanol, 0.114 to 11.4 mg L^{-1} for acetonitrile 0.382 to 38.2 mg L^{-1} for ethanol, 0.191 to 19.1 mg L^{-1} for acetone, 0.190 to 26.6 mg L^{-1} for 2-propanol, 0.138 to 6.88 mg L^{-1} for nitromethane, 0.321 to 64.2 mg L^{-1} for dichloromethane, 0.125 to 20.9 mg L^{-1} for toluene, and 0.216 to 29.0 mg L^{-1} for chloroform.

In this equation, k' and k are constants that are coating dependent. For instance, for the data from the [HMPyr][PF_6]-PMMA coating displayed in Figure 3.4, k' is -0.00104 and k is 0.113. For all

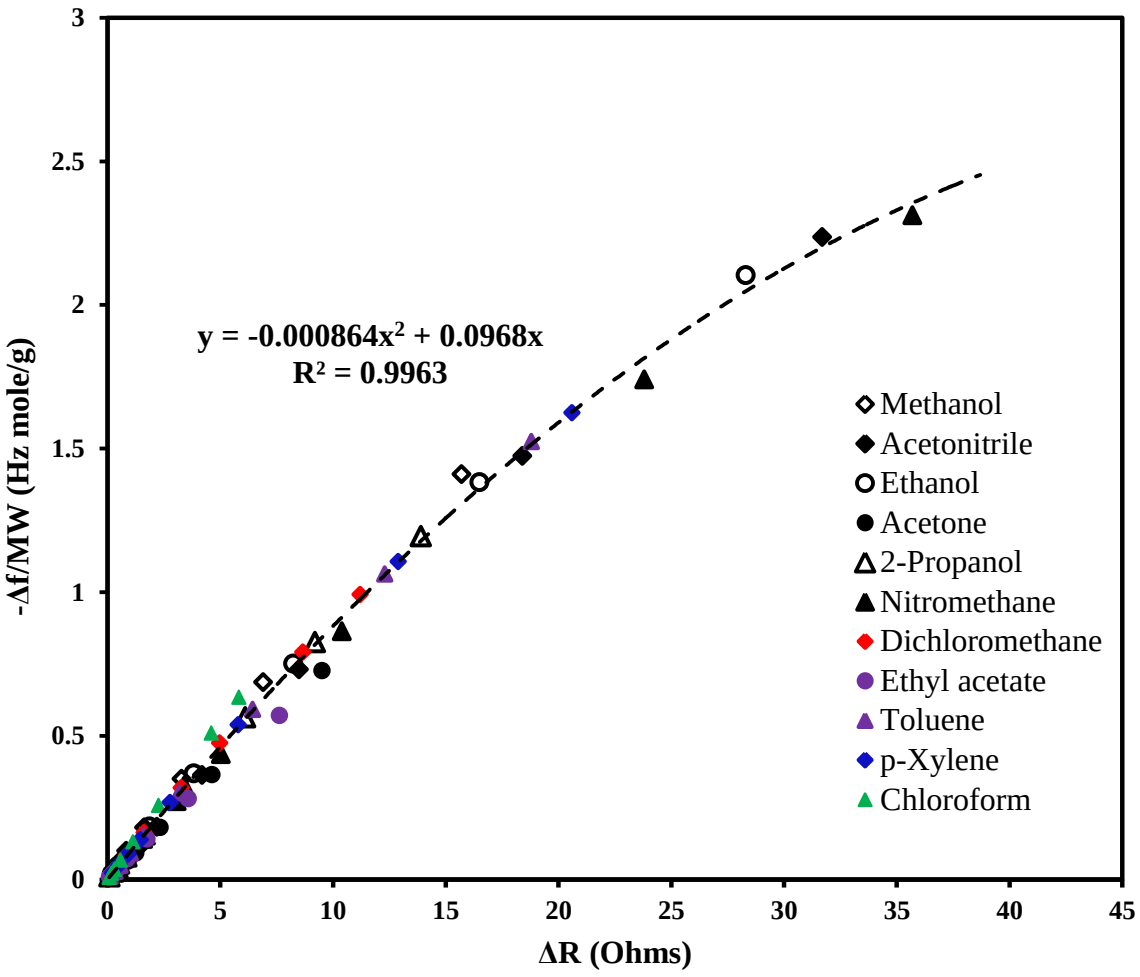

Figure 3.5 Plot of the ratio of frequency shift to molecular weight against motional resistance shift of a QCM sensor coated with [HMIm][PF_6]-PMMA for 11 different organic vapors. Concentration ranges of the vapors are 0.574 to 30.6 mg.L^{-1} for methanol, 0.114 to 11.4 mg.L^{-1} for acetonitrile 0.382 to 38.2 mg.L^{-1} for ethanol, 0.229 to 15.3 mg.L^{-1} for acetone, 0.190 to 26.6 mg.L^{-1} for 2-propanol, 0.138 to 6.88 mg.L^{-1} for nitromethane, 0.643 to 80.3 mg.L^{-1} for dichloromethane, 0.218 to 17.4 mg.L^{-1} for ethyl acetate, 0.125 to 20.9 mg.L^{-1} for toluene, 0.125 to 12.5 mg.L^{-1} for p-xylene, and 0.360 to 36.0 mg.L^{-1} for chloroform.

coatings in our study, k' is much smaller than k. Hence, under low vapor absorptions (low values of ΔR), Equation 3.7 reduces to

$$\frac{\Delta f}{\Delta R} = -\mathrm{kMW} \qquad (3.8),$$

which is consistent with the observations reported in our previous report.[20] In our earlier studies, $[BM_2Im][PF_6]$-CA composite was used as the coating material. It is important to note that $[BM_2Im][PF_6]$ is in the solid state at room temperature, and thus our previous studies were limited to solid phase ILs only. The present study confirms that highly viscous liquid phase ILs also show sensing characteristics similar to the solid phase ILs.

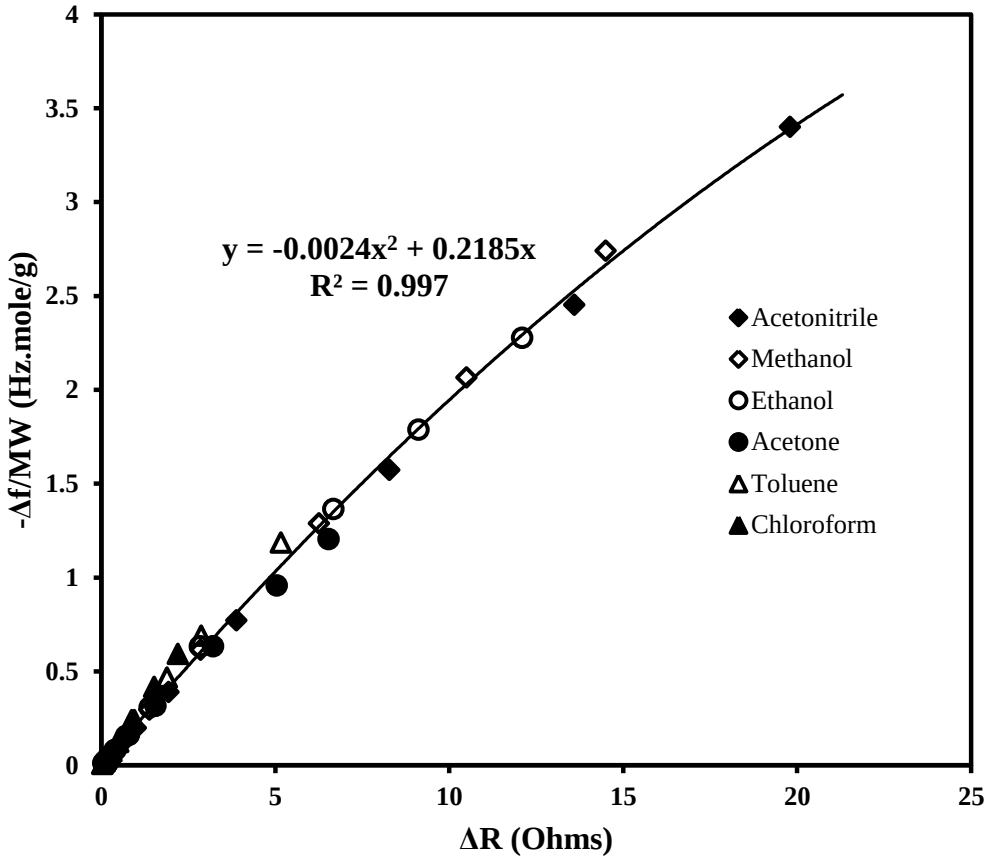

Figure 3.6 Plot of the ratio of frequency shift to molecular weight against motional resistance shift of a QCM sensor coated with $[BM_2Im][PF_6]$-PMMA for six different organic vapors. Concentration ranges of the vapors are 0.574 to 57.4 $mg.L^{-1}$ for methanol, 0.114 to 15.2 $mg.L^{-1}$ for acetonitrile 0.382 to 45.8 $mg.L^{-1}$ for ethanol, 0.267 to 28.6 $mg.L^{-1}$ for acetone, 0.125 to 20.9 $mg.L^{-1}$ for toluene, and 0.360 to 36.0 $mg.L^{-1}$ for chloroform.

The sensor displayed a frequency noise of ~0.2 Hz, motional resistance noise of ~10 mΩ, and minimal drifts of both these parameters. The repeatability of the sensor response was evaluated by repeatedly exposing the sensors to various concentrations of acetonitrile and then

evaluating the $\frac{\Delta f}{\Delta R}$ ratio. These sensors showed excellent repeatability with relative standard deviations (RSDs) for three replicate measurements between 1 and 4% (see Figure B10 in Appendix B).

As pointed out above, an important parameter that greatly influences the sensor responses is the viscosity of the IL. Therefore, we decided to study the effects of changing the viscosity of the IL on the sensing performance of the sensor. It has been shown that TFSI anion-based ILs are much less viscous than PF_6 anion-based ILs.[32,33] Hence, [HMPyr][TFSI] was selected as a representative low viscosity IL for our studies. A film of [HMPyr][TFSI] exhibited slightly lower Δf (almost 20 percent lower), but much higher ΔR (more than five times) as compared to similarly prepared [HMPyr][PF_6] film. The [HMPyr][TFSI]-coated sensor upon exposure to different organic vapors produced a positive Δf as well as a positive ΔR. A plot of Δf versus ΔR was found to be linear with slopes dependent on the vapors (Figure B11, in Appendix B); however, a correlation with the molecular weight was not apparent. In addition, binary blends of this IL with polymers did not improve the relationship of QCM parameters with molecular weight. Based on these observations, we conclude that ILs with higher viscosities (or solid phase equivalents, i.e. GUMBOS) are essential materials for achieving a direct correlation between molecular weight of measured analytes and changes in QCM parameters.

3.4.3 QCM-D Studies and the Theoretical Basis for Molecular Weight Estimation

In order to further elucidate the unique sensing behavior of these types of materials, additional studies were conducted using a QCM-D. For these QCM-D studies, a flow-type system was used to generate the analyte vapors where a stream of ultra-pure argon was bubbled through a liquid sample, and the vapors generated were subsequently diluted with another stream

of argon to produce vapor of a desired concentration. Assuming the primary gas stream contains the saturated vapor of the analyte, the minimum concentration obtained was 1.0% of the saturation vapor pressure. Plots of Δf versus ΔD for the first harmonic of a [HMPyr][PF_6]-PMMA coated QCM-D sensor after exposure to eight different vapors are shown in Figure 3.7a. Similar to the Δf versus ΔR plots, all Δf-ΔD plots are second-degree polynomials, and each exhibits an R^2 close to unity. A plot of Δf-to-MW ratio versus ΔD is shown in Figure 3.7b. The relationship for molecular weight with Δf and ΔD is observed to be very remarkable. Some analytes have slight deviations at high vapor concentrations. It is noted that the correlation of molecular weight with QCM-D parameters is even better with compounds belonging to the same class. For instance, the response for the five alcohols is shown in Figure 3.8a. As expected, 1-propanol and 2-propanol were found to be indistinguishable (Figure 3. 8b). Plots of Δf versus ΔD for the third and fifth harmonics were also found to be second-degree polynomials (see Figures B12 and B13, in Appendix B). However, much larger deviations from the molecular weight relationship were observed. The frequency noise for the first harmonic was less than 0.1 Hz and dissipation noise was less than 0.02×10^{-6}. The response time was less than 20 seconds, while the recovery time was approximately 5 seconds. The repeatability of the sensor was assessed by repeating the measurements three times for methanol and ethanol vapors (see Figure. B14, in Appendix B). The RSD for both analytes was between 0.1 to 1%. The much higher repeatability of the QCM-D is attributed to better temperature control. We believe that a similar RSD is achievable for other analytes. Such high precision measurements are particularly important in differentiation of closely related analytes or mixtures.

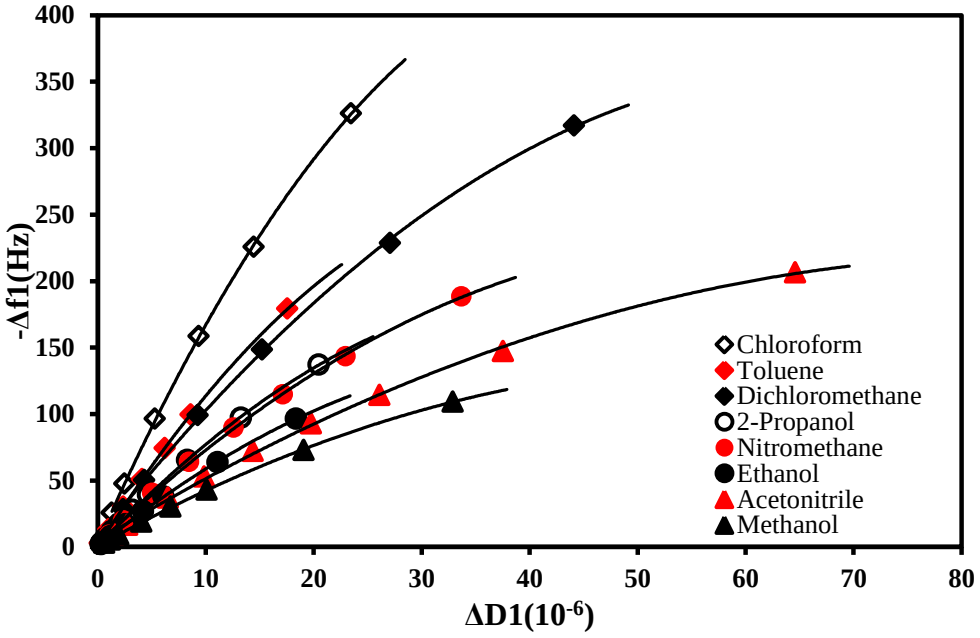

(a)

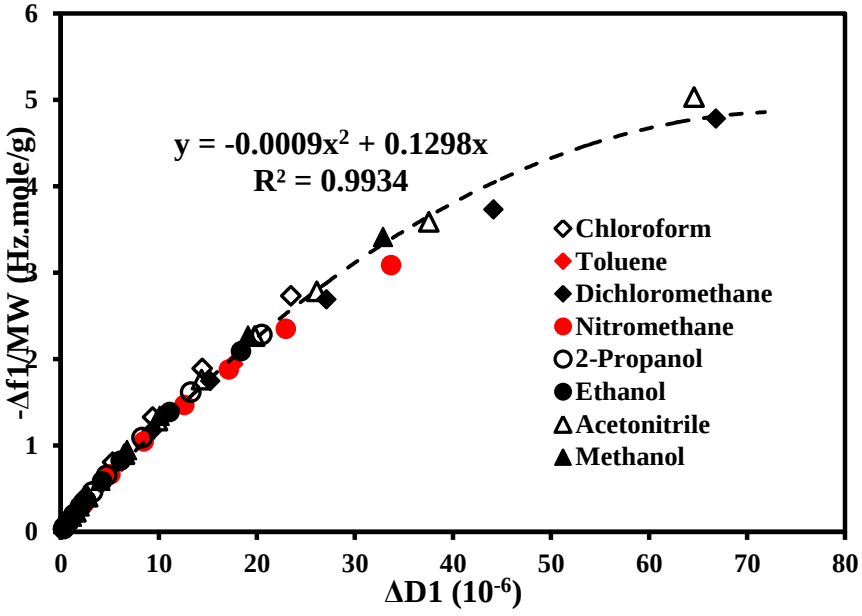

(b)

Figure 3.7 (a) Frequency shift versus dissipation shift plots for the first harmonic of a QCM-D sensor coated with [HMPyr][PF_6]-PMMA during absorption of eight different organic vapors. Each analyte shows a second-degree polynomial curve with the coefficient of determination (R^2) nearly 1 (R^2 not shown in the graph). Concentration ranges of the vapors are 1.5 to 40% for methanol, 1 to 20% for acetonitrile, 1.5 to 40% for ethanol, 1 to 50% for 2-propanol, 1 to 15% for nitromethane, 1 to 15% for dichloromethane, 1 to 30% for toluene, and 1 to 15% for chloroform. Percentage refers to the percentage of saturated vapor concentration (b) Plot of the frequency shift-to-molecular weight ratio versus dissipation shift for the data from Figure 3.7a.

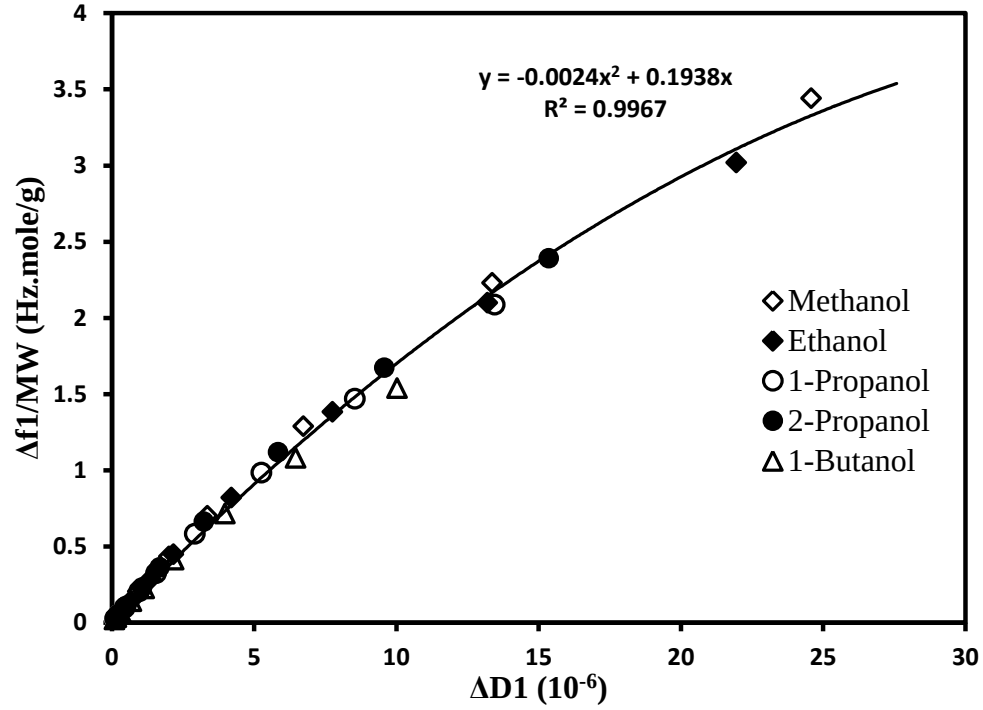

(a)

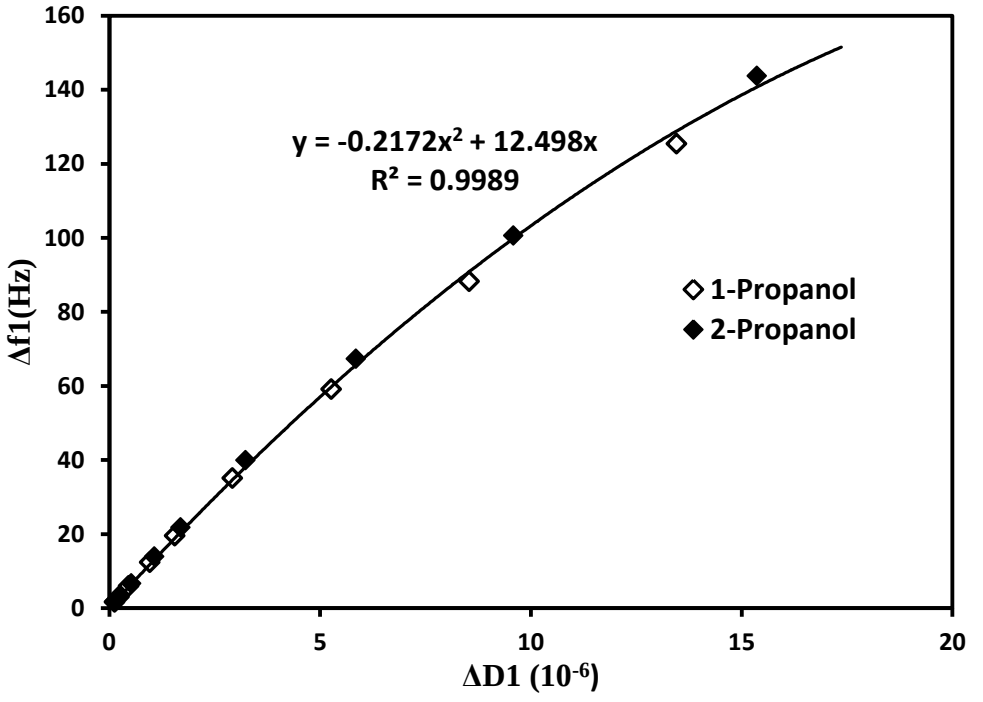

(b)

Figure 3.8 (a) Frequency shift-to-molecular weight ratio versus dissipation shift plot for the first harmonic of a QCM-D sensor coated with [HMPyr][PF_6]-PMMA during absorption of five different alcohols. Concentration ranges of the vapors are 1.5 to 40% for methanol, 1 to 50% for all other alcohols and (b) plots of the frequency shift versus dissipation shift for n-propanol and isopropanol.

Our QCM-D data were modeled using QTools software 3.0.17.560 provided by the manufacturer (Q-Sense AB). The Δf and ΔD values of the first, third, and fifth harmonics (higher harmonics were not obtained) were used to model the data both before and during vapor uptake by the sensing films. The modeling of QCM-D data, acquired at different harmonics, to extract mass and other parameters of the film has been described in detail by several authors,[34-36] and similar procedures were applied to modeling our data. The film was treated as a single layer, and the density of the film was assumed to be 1300 $kg.m^{-3}$ and also assumed to remain unchanged during vapor absorption.[37] These data were fit to different mathematical models, and the goodness of fit for each model was judged by comparison of the chi-square (χ^2) value, which is defined as $\chi^2 = \sum_{i=1}^{l} [\{y_i(theory) - y_i(experiment)\}/\sigma_i]^2$, where y_i (theory) and y_i(experiment) represent modeled and measured values of Δf or ΔD, respectively, and σ_i represents the associated noise. A smaller χ^2 indicates a better fit to the data set.[35,36] As a first assumption, the film was treated as if it were purely elastic, and hence η was set to zero, while the thickness (t_f) and elasticity (μ) were fit by the model.[34,35] The experimental Δf and ΔD values were not consistent with the fit values (see Figure B15, in Appendix B). The film was then assumed to be purely viscous by setting μ to zero, and fitting t_f and η to the model. The experimental Δf and ΔD values were again not consistent with the fit values, (see Figure B16, in Appendix B) suggesting that a purely viscous model cannot accurately describe the film. Given the fact that neither purely elastic nor purely viscous models could be used to explain our observations, we attempted to fit our data using viscoelastic models. This meant that all three parameters, t_f, η, and μ, were required for a fit to the model. The ranges of the fitting parameters were kept as follows: film viscosity between 0.0005 and 10 $kg.m^{-1}.s^{-1}$, film shear between 10 and $1x10^{10}$ Pa, and film thickness between $1x10^{-10}$ and $1x10^{-5}$ m (or corresponding mass between

$1.3x10^{-7}$ and $1.3x10^{-2}$ $kg.m^{-2}$). Our data were then fit to both the Voigt and Maxwell viscoelastic models. Although we saw some improvements as compared to purely viscous or purely elastic models, the experimental Δf and ΔD values do not agree well with the fit values (see Figures. B17 and B18, in Appendix B). It must be stressed here that while fitting the data with the viscoelastic models, η and μ were assumed to be frequency independent. However, as pointed out by Reviakine, Johannsmann, and Richter,[23] this assumption cannot be justified for most of the viscoelastic materials. In fact, it has been recently demonstrated that the viscoelastic properties of ILs are frequency dependent.[38] In order to account for the frequency dependence of viscoelastic parameters, Q-Sense has introduced a new modeling option known as "extended viscoelastic model", which has been included in the QTools software. The frequency dependence of viscoelastic properties of the film was assumed to follow a power law, and hence the relationships $\mu_{n=}\mu_0\left(\frac{f_n}{f_o}\right)^{\alpha'}$ and $\eta_{n=}\eta_0\left(\frac{f_n}{f_o}\right)^{\alpha}$ were used. The range chosen during modeling for α' was between 0 and 2 and for α between -2 and 0. Interestingly, we observed excellent agreement between the fit and experimental values of Δf and ΔD upon using the extended Maxwell viscoelastic model (Figures 3.9a-c). Attempts to fit these data using the extended Voigt viscoelastic model (see Figures B19a-c, in Appendix B) resulted in a several fold increase in χ^2. Hence, we conclude that the best model for describing the sensing response of our composite films is the extended Maxwell viscoelastic model. This inference is quite logical since the Maxwell viscoelastic model is more appropriate for liquids and amorphous solids,[29] and indeed the viscoelastic properties of ILs have previously been described using the Maxwell model.[39]

We should emphasize here that the viscoelastic models used above to analyze the QCM-D data assume a laterally homogeneous film. However, the films in our studies comprise isolated

(a)

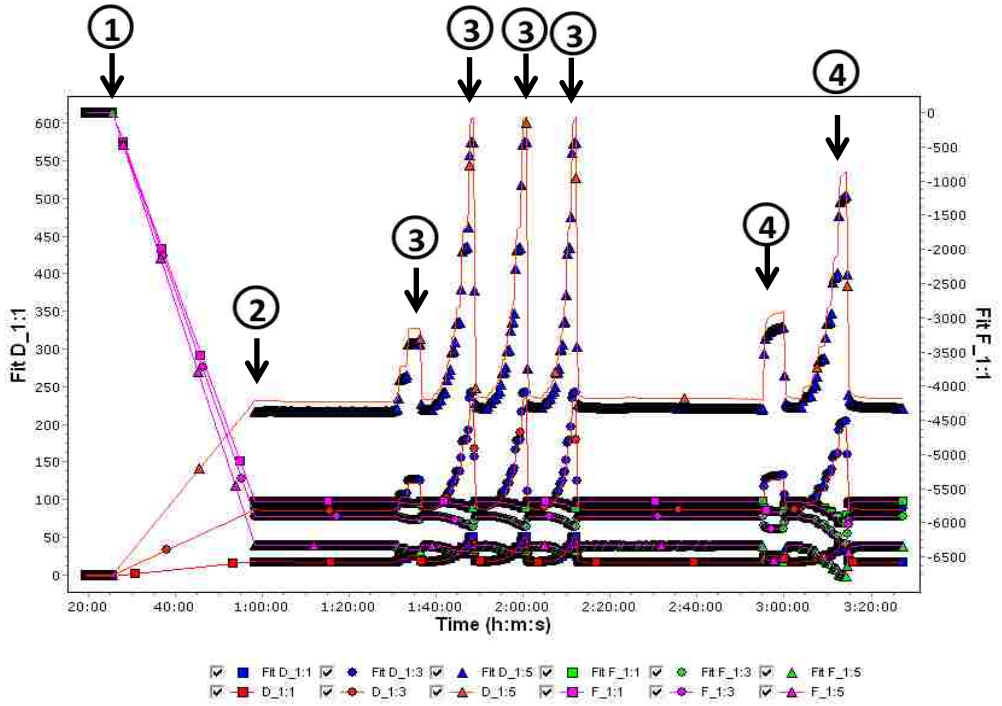

(b)

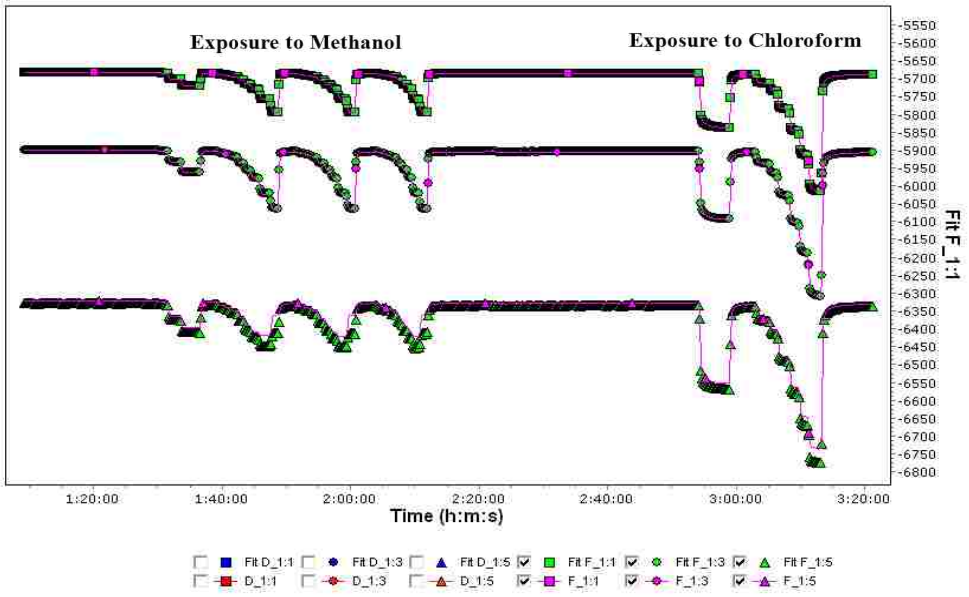

Figure 3.9 **(**a) Representative QCM-D data displaying frequency and dissipation changes for the first, third, and fifth harmonics. Arrows represent: (1) bare quartz crystal, (2) after coating with [HMPyr][PF_6]-PMMA, (3) during exposure to methanol vapors, and (4) during exposure to chloroform vapors. The figure shows both the experimental and fit values of Δf and ΔD. The data were fit using extended Maxwell viscoelastic model. (b) Experimental and fit values of Δf and (c) experimental and fit values of ΔD during exposure to methanol and chloroform shown for clarity.

(c)

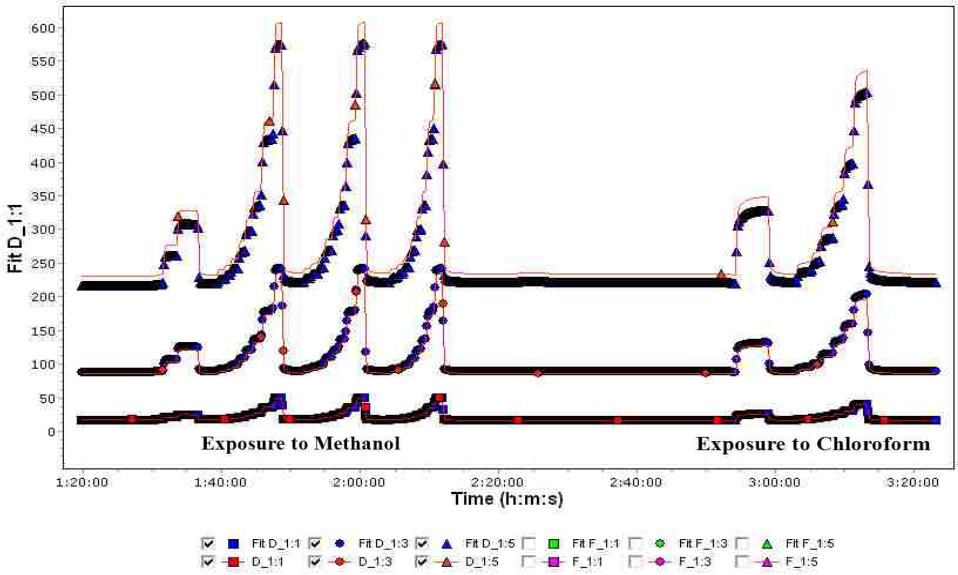

Figure 3.9 (continued)

microdroplets of varying dimensions, and we are not aware of any model that can correctly describe the behavior of such laterally heterogeneous films. We note that it has been previously assumed such laterally heterogeneous films can be appropriately analyzed with models that have been used for laterally homogeneous films.[40-42] While this assumption has been shown to be questionable in liquids, the models based on laterally homogeneous films have been suggested to be applicable for laterally heterogeneous films in air.[23,43-45] Here, we simplify our analyses by assuming the film to be an "effective medium". However, it must be remembered that when analyzing heterogeneous films using models based on homogeneous films, the effective values of μ and η also depend on the heterogeneity of the film. Based on these discussions, we assert that our heterogeneous films are analogous to films of Maxwell viscoelastic fluids. For such films, Δf and ΔD are given by equations 3.5 and 3.6, respectively. However, these equations are for thin film where the thickness of the film (t_f) is much less than the viscous penetration depth

(δ), $\delta = \sqrt{\frac{2\eta}{\rho_f \omega}}$, of the acoustic wave.[29,30,46] For thicker films, an increase or decrease in resonance frequency or dissipation can occur depending on the thickness and viscoelasticity.[30,46] ILs exhibit a wide variation in viscosities; for instance, at ambient pressure and 25 °C the viscosities of [HMIm][PF_6] and [HMIm][TFSI] are 607 and 68 mPa.s, respectively.[47] The densities of [HMIm][PF_6] and [HMIm][TFSI] at 25 °C are 1293 and 1372 kg.m^{-3} respectively.[47] For [HMIm][PF_6] at 25 °C, therefore, the penetration depth of the acoustic shear wave for the first (5MHz), third (15 MHz), and fifth (25 MHz) harmonics will be 5.47, 3.16, and 2.44 μm, respectively. Similarly, the penetration depth for [HMIm][TFSI] will be 1.78, 1.03, and 0.794 μm for the first, third, and fifth harmonics, respectively. The PF_6-based ILs are much more viscous than TFSI-based ILs, and pyridinium-based ILs are found to be more viscous than the equivalent imidazolium-based ILs.[48,49] It is observed that the modeled mass of the film before and during vapor absorption (or the mass of vapor absorbed) is very close to the Sauerbrey mass for the fundamental resonance frequency (Figure B20, in Appendix B). However, substantial deviations can be seen at higher harmonics (Figure B20, in Appendix B). These observations are consistent with the studies reported by Vogt et al.[50] for hydrated polyelectrolyte films. It is further noted that both the elastic shear modulus and viscosity of the film decrease during vapor absorption (Figure B21, in Appendix B); and similar behavior has been reported during addition of water to ILs.[38] The pure IL films could not be correctly modeled. However, a rough estimation is that the effective viscosity of the IL-PMMA may have increased up to six times as compared to that of the pure IL film. This ensures that the thickness of the composite film remains much lower than the decay length of the shear wave. Both PMMA and CA can increase the effective viscosity of the film. However, not all polymers were found to be equally effective; for example,

polystyrene does not appear to modulate the viscoelastic properties of the IL films (data not shown).

After concluding that the sensing film behaves like a Maxwell viscoelastic fluid, we attempted to rationalize the relationship between molecular weight and $\frac{\Delta f}{\Delta D}$ ratio. For a Maxwell viscoelastic material, as shown in equation 3.5, Δf is the sum of two terms; the first term depends on mass, while the second term depends on the elastic modulus and density of the film. Hence, during analyte absorption, the first term varies as a function of mass absorbed independent of the analyte, whereas the second term, which comes as a small correction, may depend to some extent on the type of analyte absorbed. It is quite interesting to see that Δf is independent of the viscosity change so long as the film remains in the thin-film regime. It is also important to note that ΔD depends on viscosity, but is independent of elastic modulus. However, in the case of Voigt viscoelastic materials, both Δf and ΔD depend on the elasticity as well as viscosity of the film.[29,30] Upon rearranging equation 3.6, we obtain $\Delta D \approx \left(\frac{2\omega}{3\rho_q t_q}\right) \times \left(\frac{{m_f}^3}{\rho_f \eta}\right)$, where m_f is mass per unit area of the film. For a fixed harmonic, the first factor in this equation is constant, and hence ΔD depends on mass, viscosity, and density of the film. During vapor absorption, these three parameters i.e. m_f, ρ_f, and η undergo a change, and the total change in D is the sum of the contributions from the changes in all three parameters. For example, we have observed that deposition of 100.7 µg of composite film per cm^2 causes a dissipation factor change of 18.9 D (where $D=10^{-6}$) at the first harmonic. Absorption of 1.6 $\mu g.cm^{-2}$ of methanol by this film causes an increase in the dissipation factor to 51.9 D (change = 33.0 D). The increase in dissipation due to mass change, if viscosity and density were constant, would be only 0.89 D. Similarly, the change in dissipation due to density change would be much less than that contributed by mass

change. Therefore, we conclude that the dissipation change is almost exclusively due to the viscosity change of the coating material.

We note that there have been extensive theoretical and experimental efforts to understand the viscosities of binary mixtures of ionic liquids and common molecular solvents; and many studies have demonstrated a dramatic decrease in the viscosity of an IL in the presence of molecular species.[51-61] One of the most notable studies to predict viscosity of binary mixtures of IL and molecular solvent is that by Seddon and coworkers.[51] In that study, the authors systematically examined the influence of water and a number of organic solvents with different polarities on the viscosity of room temperature ionic liquids. Interestingly, the viscosity of the binary mixture was found to depend primarily on the mole fraction of the molecular component, irrespective of its polarity or dielectric constant. Hence, the authors proposed a single exponential equation to estimate the viscosity of such mixtures. This finding has been repeatedly confirmed in subsequent studies by many other research groups.[52,54,58] More rigorous rules have also been applied for more accurate predictions of the viscosities of mixtures.[58,61] For example, Wang et al.[58] examined the viscosity of a wide range of IL-molecular solvent systems by combining Eyring's absolute rate theory with activity coefficient models, and the results were compared with those obtained by use of Seddon's equation. The authors concluded that the Seddon equation always achieves satisfactory estimates of the viscosities of mixtures in IL-rich regions. Based on these discussions, we assert that the viscosity change of films in our study depends on the number of moles of vapor absorbed irrespective of their chemical characteristics. Such an assumption clearly explains the mole-dependent change in dissipation observed in our studies. Hence, simultaneous measurements of Δf and ΔD or ΔR of an IL or GUMBOS composite coated QCM sensor during vapor absorption provides a reasonable approximation of

molecular weight of the vapor. Our findings should provide a sound foundation for further studies with respect to the discrimination of vapors based on molecular weights using these composite films.

3.5 Conclusions

The vapor-sensing applications of a number of IL or GUMBOS-polymer composite films were studied with a QCM/QCM-D transducer. As many as 13 analytes were tested, and the data clearly demonstrate that an IL or GUMBOS-based QCM sensor offers an outstanding capability for estimating the molecular weight of organic vapor analytes. Viscoelastic modeling of the QCM-D data suggests that our composite films follow the Maxwell viscoelastic model. Based on this observation, a theoretical explanation for the observed relationship between the molecular weight of analytes and the QCM parameters is proposed. These types of materials when combined with QCM show considerable promise for discrimination of vapors based on their molecular weights. Further work is warranted to develop a sensor for more accurate prediction of molecular weights of vapors. Future work will focus on evaluation of viscosities of an extended range of IL-organic solvent mixtures and comparison of these data with the QCM observations. In addition, further understanding of the viscoelastic behavior of such films should be the focus of future studies.

3.6 Notes and References

(1) Bourgeois, W.; Romain, A. C.; Nicolas, J.; Stuetz, R. M.: The use of sensor arrays for environmental monitoring: interests and limitations. *Journal of Environmental Monitoring* **2003**, *5*, 852-860.

(2) Turner, A. P. F.; Magan, N.: Electronic noses and disease diagnostics. *Nature Reviews Microbiology* **2004**, *2*, 161-166.

(3) Machado, R. F.; Laskowski, D.; Deffenderfer, O.; Burch, T.; Zheng, S.; Mazzone, P. J.; Mekhail, T.; Jennings, C.; Stoller, J. K.; Pyle, J.; Duncan, J.; Dweik, R. A.; Erzurum, S. C.: Detection of lung cancer by sensor array analyses of exhaled breath. *American Journal of Respiratory and Critical Care Medicine* **2005**, *171*, 1286-1291.

(4) Roeck, F.; Barsan, N.; Weimar, U.: Electronic nose: current status and future trends. *Chemical Reviews* **2008**, *108*, 705-725.

(5) Carey, J. R.; Susick, K. S.; Hulkower, K. I.; Imlay, J. A.; Imlay, K. R. C.; Ingison, C. K.; Ponder, J. B.; Sen, A.; Wittrig, A. E.: Rapid identification of bacteria with a disposable colorimetric sensing array. *Journal of the Americal Chemical Society* **2011**, *133*, 7571-7576.

(6) Badjagbo, K.: Potential of breath analysis: from environmental exposure assessment to medical diagnosis. *WebmedCentral ENVIRONMENTAL MEDICINE* **2012**, *3*(3), WMC003174.

(7) Walt, D. R.; Dickinson, T.; White, J.; Kauer, J.; Johnson, S.; Engelhardt, H.; Sutter, J.; Jurs, P.: Optical sensor arrays for odor recognition. *Biosensors & Bioelectronics* **1998**, *13*, 697-699.

(8) Ho, C. K.; Lindgren, E. R.; Rawlinson, K. S.; McGrath, L. K.; Wright, J. L.: Development of a surface acoustic wave sensor for in-situ monitoring of volatile organic compounds. *Sensors* **2003**, *3*, 236-247.

(9) Suslick, K. S.; Rakow, N. A.; Sen, A.: Colorimetric sensor arrays for molecular recognition. *Tetrahedron* **2004**, *60*, 11133-11138.

(10) Jin, X.; Yu, L.; Garcia, D.; Ren, R. X.; Zeng, X.: Ionic liquid high-temperature gas sensor array. *Analytical Chemistry* **2006**, *78*, 6980-6989.

(11) Jin, C. G.; Kurzawski, P.; Hierlemann, A.; Zellers, E. T.: Evaluation of multitransducer arrays for the determination of organic vapor mixtures. *Analytical Chemistry* **2008**, *80*, 227-236.

(12) Scholten, K.; Bohrer, F. I.; Dattoli, E.; Lu, W.; Zellers, E. T.: Organic vapor discrimination with chemiresistor arrays of temperature modulated tin-oxide nanowires and thiolate-monolayer-protected gold nanoparticles. *Nanotechnology* **2011**, *22*.

(13) Garcia-Berrios, E.; Gao, T.; Theriot, J. C.; Woodka, M. D.; Brunschwig, B. S.; Lewis, N. S.: Response and discrimination performance of arrays of organothiol-capped Au nanoparticle chemiresistive vapor sensors. *The Journal of Physical Chemistry C* **2011**, *115*, 6208-6217.

(14) Park, S. J.; Kwon, O. S.; Lee, S. H.; Song, H. S.; Park, T. H.; Jang, J.: Ultrasensitive flexible graphene based field-effect transistor (FET)-type bioelectronic nose. *Nano Letters* **2012**, *12*, 5082-5090.

(15) Weiguo Huang ; Jasmine Sinha ; Ming-Ling Yeh ; Josué F. Martínez Hardigree ; Rachel LeCover ; Kalpana Besar ; Ana María Rule ; Patrick N. Breysse , a.; Katz, H. E.: Diverse organic field-effect transistor sensor responses from two functionalized naphthalenetetracarboxylic diimides and copper phthalocyanine semiconductors distinguishable over a wide analyte range. *Advanced Functional Materials* **2013,** *23*, 4094-4104.

(16) Kybert, N. J.; Lerner, M. B.; Yodh, J. S.; Preti, G.; Johnson, A. T. C.: Differentiation of complex vapor mixtures using versatile DNA-carbon nanotube chemical sensor arrays. *ACS Nano* **2013**, *7*, 2800-2807.

(17) Alona Bayn; Xinliang Feng; Klaus Müllen, a. H. H.: Field effect transistors based on polycyclic aromatic hydrocarbons for the detection and classification of volatile organic compounds. *ACS Applied Materials & Interfaces* **2013**, *5*, 3431-3440.

(18) Liang, C. D.; Yuan, C. Y.; Warmack, R. J.; Barnes, C. E.; Dai, S.: Ionic liquids: a new class of sensing materials for detection of organic vapors based on the use of a quartz crystal microbalance. *Analytical Chemistry* **2002**, *74*, 2172-2176.

(19) Rehman, A.; Zeng, X.: Ionic liquids as green solvents and electrolytes for robust chemical sensor development. *Accounts of Cheical Research* **2012**, *45*, 1667-1677.

(20) Regmi, B. P.; Monk, J.; El-Zahab, B.; Das, S.; Hung, F. R.; Hayes, D. J.; Warner, I. M.: A novel composite film for detection and molecular weight determination of organic vapors. *Journal of Materials Chemistry* **2012**, *22*, 13732-13741.

(21) Lee, S. W.; Hinsberg, W. D.: Determination of the viscoelastic properties of polymer films using a compensated phase-locked oscillator circuit. *Analytical Chemistry* **2002**, *74*, 125-131.

(22) Schroder, J.; Borngraber, R.; Eichelbaum, F.; Hauptmann, P.: Advanced interface electronics and methods for QCM. *Sensors and Actuators A: Physical* **2002**, *97-98*, 543-547.

(23) Reviakine, I.; Johannsmann, D.; Richter, R. P.: Hearing what you cannot see and visualizing what you hear: interpreting quartz crystal microbalance data from solvated interfaces. *Analytical Chemistry* **2011**, *83*, 8838-8848.

(24) Schroder, J.; Borngraber, R.; Lucklum, R.; Hauptmann, P.: Network analysis based interface electronics for quartz crystal microbalance. *Review of Scientific Instruments* **2001**, *72*, 2750-2755.

(25) Rodahl, M.; Hook, F.; Krozer, A.; Brzezinski, P.; Kasemo, B.: Quartz crystal microbalance setup for frequency and Q-factor measurements in gaseous and liquid environments. *Review of Scientific Instruments* **1995**, *66*, 3924-3930.

(26) Rodahl, M.; Kasemo, B.: A simple setup to simultaneously measure the resonant frequency and the absolute dissipation factor of a quartz crystal microbalance. *Review of Scientific Instruments* **1996**, *67*, 3238-3241.

(27) Johannsmann, D.; Reviakine, I.; Richter, R. P.: Dissipation in films of adsorbed nanospheres studied by quartz crystal microbalance (QCM). *Analytical Chemistry* **2009**, *81*, 8167-8176.

(28) Sauerbrey, G.: The use of quartz oscillators for weighing thin layers and for microweighing. *Zeitschrift Fur Physik* **1959**, *155*, 206-222.

(29) Voinova, M. V., Jonson M., and Kasemo B.: Internal and interfacial friction in the dynamics of soft/solid interfaces. *http://arxiv.org/abs/cond-mat/9906415* **1999**.

(30) Voinova, M. V.; Rodahl, M.; Jonson, M.; Kasemo, B.: Viscoelastic acoustic response of layered polymer films at fluid-solid interfaces: Continuum mechanics approach. *Physica Scripta* **1999**, *59*, 391-396.

(31) Huddleston, J. G.; Visser, A. E.; Reichert, W. M.; Willauer, H. D.; Broker, G. A.; Rogers, R. D.: Characterization and comparison of hydrophilic and hydrophobic room temperature ionic liquids incorporating the imidazolium cation. *Green Chemistry* **2001**, *3*, 156-164.

(32) Jacquemin, J.; Husson, P.; Padua, A. A. H.; Majer, V.: Density and viscosity of several pure and water-saturated ionic liquids. *Green Chemistry* **2006**, *8*, 172-180.

(33) Pensado, A. S.; Comunas, M. J. P.; Fernandez, J.: The pressure-viscosity coefficient of several ionic liquids. *Tribology Letters* **2008**, *31*, 107-118.

(34) Munro, J. C.; Frank, C. W.: Polyacrylamide adsorption from aqueous solutions on gold and silver surfaces monitored by the quartz crystal microbalance. *Macromolecules* **2004**, *37*, 925-938.

(35) Irwin, E. F.; Ho, J. E.; Kane, S. R.; Healy, K. E.: Analysis of interpenetrating polymer networks via quartz crystal microbalance with dissipation monitoring. *Langmuir* **2005**, *21*, 5529-5536.

(36) Eisele, N. B.; Andersson, F. I.; Frey, S.; Richter, R. P.: Viscoelasticity of thin biomolecular films: a case study on nucleoporin phenylalanine-glycine repeats grafted to a histidine-tag capturing QCM-D sensor. *Biomacromolecules* **2012**, *13*, 2322-2332.

(37) Because of the spatial heterogeneity of the film, the effective density of the film will be less than 1300 $kg.m^{-3}$. On rearranging equation 3.6, it can be seen product of viscosity and density in the denominator. As a consequecne, the modeled viscosity will be less than the

effective viscosity, while other things remain unchaged. Strictly speaking, there is a very slight change in density during vapor absorption, but for simplicity the density is assumed to remain constant.

(38) Yamaguchi, T.; Mikawa, K.; Koda, S.: Shear relaxation of water-ionic liquid mixtures. *Bulletin of the Chemical Society of Japan* **2012**, *85*, 701-705.

(39) Makino, W.; Kishikawa, R.; Mizoshiri, M.; Takeda, S.; Yao, M.: Viscoelastic properties of room temperature ionic liquids. *The Journal of Chemical Physics* **2008**, *129*, 104510.

(40) Larsson, C.; Rodahl, M.; Hook, F.: Characterization of DNA immobilization and subsequent hybridization on a 2D arrangement of streptavidin on a biotin-modified lipid bilayer supported on SiO2. *Analytical Chemistry* **2003**, *75*, 5080-5087.

(41) Reviakine, I.; Rossetti, F. F.; Morozov, A. N.; Textor, M.: Investigating the properties of supported vesicular layers on titanium dioxide by quartz crystal microbalance with dissipation measurements. *The Journal of Chemical Physics* **2005**, *122*, 204711.

(42) Patel, A. R.; Frank, C. W.: Quantitative analysis of tethered vesicle assemblies by quartz crystal microbalance with dissipation monitoring: Binding dynamics and bound water content. *Langmuir* **2006**, *22*, 7587-7599.

(43) Rojas, E.; Gallego, M.; Reviakine, I.: Effect of sample heterogeneity on the interpretation of quartz crystal microbalance data: impurity effects. *Analytical Chemistry* **2008**, *80*, 8982-8990.

(44) Johannsmann, D.; Reviakine, I.; Rojas, E.; Gallego, M.: Effect of sample heterogeneity on the interpretation of QCM(-D) data: comparison of combined quartz crystal microbalance/atomic force microscopy measurements with finite element method modeling. *Analytical Chemistry* **2008**, *80*, 8891-8899.

(45) Tellechea, E.; Johannsmann, D.; Steinmetz, N. F.; Richter, R. P.; Reviakine, I.: Model-Independent Analysis of QCM Data on Colloidal Particle Adsorption. *Langmuir* **2009**, *25*, 5177-5184.

(46) McHale, G.; Lucklum, R.; Newton, M. I.; Cowen, J. A.: Influence of viscoelasticity and interfacial slip on acoustic wave sensors. *Journal of Applied Physics* **2000**, *88*, 7304-7312.

(47) Muhammad, A.; Mutalib, M. I. A.; Wilfred, C. D.; Murugesan, T.; Shafeeq, A.: Thermophysical properties of 1-hexyl-3-methyl imidazolium based ionic liquids with tetrafluoroborate, hexafluorophosphate and bis(trifluoromethylsulfonyl)imide anions. *The Journal of Chemical Thermodynamics* **2008**, *40*, 1433-1438.

(48) Crosthwaite, J. M.; Muldoon, M. J.; Dixon, J. K.; Anderson, J. L.; Brennecke, J. F.: Phase transition and decomposition temperatures, heat capacities and viscosities of pyridinium ionic liquids. *The Journal of Chemical Thermodynamics* **2005**, *37*, 559-568.

(49) Gardas, R. L.; Coutinho, J. A. P.: A group contribution method for viscosity estimation of ionic liquids. *Fluid Phase Equilibria* **2008**, *266*, 195-201.

(50) Vogt, B. D.; Lin, E. K.; Wu, W. L.; White, C. C.: Effect of film thickness on the validity of the Sauerbrey equation for hydrated polyelectrolyte films. *The Journal of Physical Chemistry B* **2004**, *108*, 12685-12690.

(51) Seddon, K. R.; Stark, A.; Torres, M. J.: Influence of chloride, water, and organic solvents on the physical properties of ionic liquids. *Pure and Applied Chemistry* **2000**, *72*, 2275-2287.

(52) Wang, J. J.; Tian, Y.; Zhao, Y.; Zhuo, K.: A volumetric and viscosity study for the mixtures of 1-n-butyl-3-methylimidazolium tetrafluoroborate ionic liquid with acetonitrile, dichloromethane, 2-butanone and N,N-dimethylformamide. *Green Chemistry* **2003**, *5*, 618-622.

(53) Comminges, C.; Barhdadi, R.; Laurent, M.; Troupel, M.: Determination of viscosity, ionic conductivity, and diffusion coefficients in some binary systems: ionic liquids plus molecular solvents. *Journal of Chemical & Engineering Data* **2006**, *51*, 680-685.

(54) Zafarani-Moattar, M. T.; Majdan-Cegincara, R.: Viscosity, density, speed of sound, and refractive index of binary mixtures of organic solvent plus ionic liquid, 1-butyl-3-methylimidazolium hexafluorophosphate at 298.15 K. *Journal of Chemical & Engineering Data* **2007**, *52*, 2359-2364.

(55) Li, W.; Zhang, Z.; Han, B.; Hu, S.; Xie, Y.; Yang, G.: Effect of water and organic solvents on the ionic dissociation of ionic liquids. *The Journal of Physical Chemistry B* **2007**, *111*, 6452-6456.

(56) Malham, I. B.; Turmine, M.: Viscosities and refractive indices of binary mixtures of 1-butyl-3-methylimidazolium tetrafluoroborate and 1-butyl-2,3-dimethylimidazolium tetrafluoroborate with water at 298 K. *The Journal of Chemical Thermodynamics* **2008**, *40*, 718-723.

(57) Khupse, N. D.; Kumar, A.: Dramatic change in viscosities of pure ionic liquids upon addition of molecular solvents. *Journal of Solution Chemistry* **2009**, *38*, 589-600.

(58) Wang, Y-g.; Chen, D-x.; OuYang, X-k.: Viscosity calculations for ionic liquid-cosolvent mixtures based on Eyring's absolute rate theory and activity coefficient models. *Journal of Chemical & Engineering Data* **2010**, *55*, 4878-4884.

(59) Canongia Lopes, J. N.; Gomes, M. F. C.; Husson, P.; Padua, A. A. H.; Rebelo, L. P. N.; Sarraute, S.; Tariq, M.: Polarity, viscosity, and ionic conductivity of liquid mixtures containing $[C_4C_1im][Ntf_2]$ and a molecular component. *The Journal of Physical Chemistry B* **2011**, *115*, 6088-6099.

(60) Jouyban, A.; Soleymani, J.; Jafari, F.; Khoubnasabjafari, M.; Acree, W. E.: Mathematical representation of viscosity of ionic liquid plus molecular solvent mixtures at various temperatures using the Jouyban-Acree model. *Journal of Chemical & Engineering Data* **2013**, *58*, 1523-1528.

(61) Tariq, M.; Altamash, T.; Salavera, D.; Coronas, A.; Rebelo, L. P. N.; Canongia Lopes, J. N.: Viscosity mixing rules for binary systems containing one ionic liquid. *ChemPhysChem* **2013**, *14*, 1956-1968.

CHAPTER 4 PHTHALOCYANINE- AND PORPHYRIN-BASED GUMBOS FOR RAPID AND SENSITIVE DETECTION OF ORGANIC VAPORS

4.1 Introduction

Cyclic tetrapyrroles such as phthalocyanines and porphyrins are an interesting class of materials that have attracted considerable attention because of their unique properties and flexible synthesis. These macrocyclic compounds are particularly noted for their high thermal, chemical, and photochemical stabilities and have thus found diverse uses in various fields. Such uses include, but are not limited to, as sensing materials for chemical sensors,[1-4] photosensitizers for dye sensitized solar cells,[5-7] photoconductors,[8,9] light-emitting materials,[10] photosensitizers in photodynamic therapy,[11,12] and many other uses.[13] In particular, these macrocycles and their metal complexes have been shown to interact with a large number of gases and vapors, and hence they have been widely employed as molecular recognition elements for gas-phase detection of a wide range of analytes through implementation of different transduction principles.[1-4] To clarify, the interaction of vapors with these materials perturbs the electrical and optical properties of these macrocyles, and the resulting changes in mass, optical, or electrical properties can be measured by a suitable transducer in order to obtain qualitative and/or quantitative information about the target chemical species. Among previously used transducers, the quartz crystal microbalance (QCM) has been particularly attractive, and in this regard, cyclic tetrapyrroles and their metalloderivatives have been shown to be very promising coating materials for sensitive detection of a wide array of organic vapors.[14-27]

The key component of a sensor system is the sensing material since it determines the selectivity and sensitivity of a chemical sensor. Therefore, much attention has been focused on the design and evaluation of novel or improved sensing materials. Two approaches have been

commonly employed to design sensing materials.[28,29] The conventional approach involves the development of highly selective materials such as molecularly imprinted polymers, zeolites, and cavitands which strongly bind to an analyte of interest.[28] However, the synthesis of a highly selective material for each analyte is challenging, and at the same time this approach is not useful for analyses of complex mixtures.[29] A more modern approach involves development of materials that show broad and partial selectivity toward a wide range of analytes. A group of cross-reactive sensors is then used to obtain a response pattern specific to an analyte or complex mixture. The collection of such sensors is known as a sensor array or electronic nose, and the first electronic nose to discriminate between complex odorant mixtures was reported by Persaud and Dodd in 1982.[30] Phthalocyanine and porphyrin derivatives are ideally suited for sensor array applications because they absorb a large number of chemical species; moreover, the selectivity of these materials can be finely tuned by altering the central metal atom as well as the peripheral substitution pattern.[17,19,22,23] As an illustration, Di Natale et al.[24] have developed an electronic nose comprising eight QCM sensors, each coated with a different metalloporphyrin derivative, and have demonstrated with high accuracy that the breath of lung cancer patients is different from that of healthy individuals. Although cyclic tetrapyrroles have been demonstrated as excellent sensing materials for QCM sensors, some aspects of this class of materials still require further improvement. For example, imperfect adhesion of the film to the transducer surface, low sensitivity, complex deposition procedures, and slow response times are major limitations associated with such materials.[15-20]

The QCM is a common mass-sensitive transducer whose operating principle is based on the converse piezoelectric effect. It comprises a thin circular plate of AT-cut quartz crystal sandwiched between two circular metallic electrodes. Applying an AC voltage across the

electrodes causes the quartz crystal to undergo thickness shear mode (TSM) oscillations with resonance frequencies in the megahertz (MHz) region. The resonance frequency of the crystal is the central parameter that provides important information regarding analytical measurements. The use of the QCM transducer as a sensor, however, requires immobilization of a thin film of suitable sensing material on the surface of the crystal. The frequency and amplitude of the shear wave are then altered as it propagates through the film. Interaction of an anlayte with the coating material causes a change in mass and/or viscoelastic properties of the coating; as a result, further alterations in the wave characteristics will occur. The relationship between the frequency shift (Δf) and the surface mass was first derived by Sauerbrey, which is mathematically expressed as:[31]

$$\Delta f = -\frac{n}{C}\Delta m = -\frac{n}{C}\rho_f t_f \ , \qquad (4.1)$$

where Δm is mass per unit area of the film (in air or vacuum), ρ_f is the density of the film, t_f is the thickness of the film, n is the harmonic number which can only be an odd integer, and C is the mass sensitivity or Sauerbrey constant which depends on the fundamental resonance frequency and properties of the quartz ($C = 17.7\ ng.cm^{-2}.Hz^{-1}$ for a 5 MHz AT-cut quartz crystal). It should be noted that this relationship is applicable only for a small mass which is rigidly and uniformly deposited on the surface. For viscous and viscoelastic films, some modifications to the Sauerbrey equation have been proposed.[32-34] In addition, for such films, the wave also undergoes attenuation which can be estimated by measuring another parameter known as motional resistance (R) or dissipation (D).[33,34]

Herein, we report the synthesis and vapor-sensing characteristics of two representative GUMBOS, one derived from porphyrin and the other derived from phthalocyanine. GUMBOS,

an acronym for a '**g**roup of **u**niform **m**aterials **b**ased on **o**rganic **s**alts', is a collective term that we use to refer to solid phase ionic liquids and related organic salts with melting points up to 250 °C, while ionic liquids (ILs) are defined as organic salts that melt below 100 °C.[35,36] Thus, GUMBOS are solids at room temperature and have a melting point range of 25 to 250 °C. Specifically, copper (II) meso-tetra (4-carboxyphenyl) porphyrin (Cu-TCPP) tetrasodium salt was reacted with trihexyl(tetradecyl)phosphonium chloride ([P66614][Cl]) to produce $[P66614]_4[CuTCPP]$. Similarly, copper phthalocyanine-3,4',4",4"'-tetrasulfonic acid ($CuPcS_4$) tetrasodium salt was reacted with [P66614][Cl] to obtain $[P66614]_4[CuPcS_4]$. Both of these compounds were found to be solids at room temperature. Thin films of these compounds were deposited on the surface of the quartz crystal resonator by dipping the crystal into a solvent/nonsolvent/GUMBOS ternary mixture, and subsequently evaporating the more volatile solvent. The vapor-sensing characteristics of these films were then evaluated by exposing each sensor to 11 different organic vapors over a wide range of concentrations. Each sensor exhibited high sensitivity, rapid response, and partial selectivity toward all vapors. Moreover, the two sensors exhibited cross-reactivity patterns, thereby making these materials promising candidates for array-based vapor sensing applications.

4.2 Experimental Section

4.2.1 Materials

Copper phthalocyanine-3,4',4",4"'-tetrasulfonic acid ($CuPcS_4$) tetrasodium salt, trihexyl(tetradecyl)phosphonium chloride ([P66614][Cl]), lithium *N*,*N*-bis-(trifluoromethane)sulfonimide (LiTFSI), heptane, acetonitrile, chloroform, toluene, methanol, 1-propanol, 2-propanol, 1-butanol, dichloromethane (DCM) and 3-methyl-1-butanol were obtained from Sigma-Aldrich (St. Louis, MO, USA). Copper (II) meso-tetra(4-

carboxyphenyl)porphyrin was obtained from Frontier Scientific, Inc. (Logan, UT, USA). Acetone was obtained from Avantor Performance Materials, Inc. (Center Valley, PA, USA). Absolute ethanol was obtained from Pharmco Products, Inc. (Brookfield, CT, USA). All chemicals were used as received without any further purification.

In these studies, two different types of QCM instruments were employed. A QCM200 system and the associated AT-cut polished chromium/gold quartz crystals were purchased from Stanford Research Systems, Inc. (Sunnyvale, CA, USA). A quartz crystal microbalance with dissipation monitoring (QCM-D) E4 system and the associated gold-coated quartz crystals were obtained from Q-Sense AB (Gothenburg, Sweden). For both the instruments, AT-cut quartz crystals with the fundamental resonance frequency of 5 MHz were used. Mass flow controllers (Model 5850E), along with instrument control and read out equipment (Model 5878) were purchased from Brooks Instrument, LLC (Hatfield, PA, USA), and polytetrafluoroethylene (PTFE) containers were procured from SPI Supplies/Structure Probe, Inc. (West Chester, PA, USA).

4.2.2 Synthesis of GUMBOS and IL

The GUMBOS and IL were synthesized by using metathesis reactions in a binary solvent mixture.[37] Briefly, copper (II) meso-tetra(4-carboxyphenyl)porphyrin (Cu-TCPP) was neutralized using an excess of sodium hydroxide in water to obtain the water soluble tetrasodium salt. The other reactant [P66614][Cl] was dissolved in DCM, and subsequently these two solutions were mixed and stirred for 24-48 hours to obtain $[P66614]_4[CuTCPP]$. Likewise, $[P66614]_4[CuPcS_4]$ was prepared by reacting $CuPcS_4$ and [P66614][Cl]; and [P66614][TFSI] was prepared by reacting [Li][TFSI] and [P66614][Cl]. In all three reactions, the water-soluble reactant was used in slight excess. After completion of reaction, the product was washed several

times with water, and DCM removed by rotary evaporation under reduced pressure. Finally, residual water was removed by freeze drying. Among these three compounds, $[P66614]_4[CuTCPP]$ and $[P66614]_4[CuPcS_4]$ are found to be solid, while [P66614][TFSI] is found to remain in a liquid state, i.e. an IL.

4.2.3 Characterization of GUMBOS

All compounds were characterized using thermal analysis i.e. differential scanning calorimetry (DSC) and thermogravimetric analysis (TGA). The phase transition behaviors of these compounds were investigated using a Q100 differential scanning calorimeter (TA instruments, New Castle, DE). Analyses were performed by heating the sample from -40 to 275 °C at a rate of 10 °C min^{-1}. Thermogravimetric analyses were performed by using a Hi-Res Modulated TGA 2950 instrument (TA instrument) in the high-resolution mode. Samples were heated from room temperature to 600 °C at a heating rate of 10 °C min^{-1}. Melting points were determined using a DigitMelt MPA 160 apparatus obtained from Stanford Research Systems, Inc.

4.2.4 Preparation and Characterization of Sensing Films

Before preparation of a coating, the quartz crystal was cleaned using a piranha solution (3:1 concentrated sulfuric acid and 30% hydrogen peroxide). Both GUMBOS were dissolved in acetone (solvent). Then, 1 ml of freshly prepared 0.6–1.3 mg/ml of GUMBOS solution was added dropwise to 6 ml of anhydrous heptane (non-solvent), under ultrasonication, contained in a 25 ml PTFE beaker, and further ultrasonicated for 20 minutes. A freshly cleaned quartz crystal was dipped into this mixture, and left undisturbed for approximately 5 hours to remove the acetone solvent. After 5 hours, the crystal was removed and ultrasonicated while holding it vertically in a fresh pool of heptane for approximately 1 minute. The lower surface of the crystal

was then wiped using acetone-soaked cotton. The coated crystal was stored in a desiccator for at least 24 hours before performing vapor sensing studies. Films were imaged using a JEOL JSM-6610LV scanning electron microscope operating in a high vacuum mode. Both secondary electron and backscattered electron images were acquired simultaneously.

4.2.5 Vapor Sensing Studies

The QCM200 instrument was used for most of the vapor sensing studies. In these studies, the analyte vapors were generated using a static method. In addition, a few studies were performed using a QCM-D E4 system, where a dynamic method was used to generate analyte vapors. The experimental setups employed in both cases are described in detail in our previous publications.[35,36] Eleven different organic vapors were tested in these studies. All experiments were conducted at 22 °C.

4.3 Results and Discussions

4.3.1 Preparation and Characterization of GUMBOS

Two representative GUMBOS, namely, $[P66614]_4[CuPcS_4]$ and $[P66614]_4$[CuTCPP], were synthesized and used for vapor-sensing studies. These compounds were prepared using ion exchange reactions which are outlined in Figures 4.1a-b**.** Tetrasodium salts of phthalocyanine and porphyrins are soluble in water, but insoluble in DCM. By contrast, [P66614][Cl] is soluble in DCM, but insoluble in water. Therefore the sodium salts of phthalocyanine and porphyrin were dissolved in water, and [P66614][Cl] was dissolved in DCM; and these two solutions were subsequently mixed to obtain the desired products. Both GUMBOS are soluble in DCM, but are insoluble in water; and hence they remained in the DCM layer. While preparing these compounds, the water soluble reactant was used in 10 % excess as compared to the

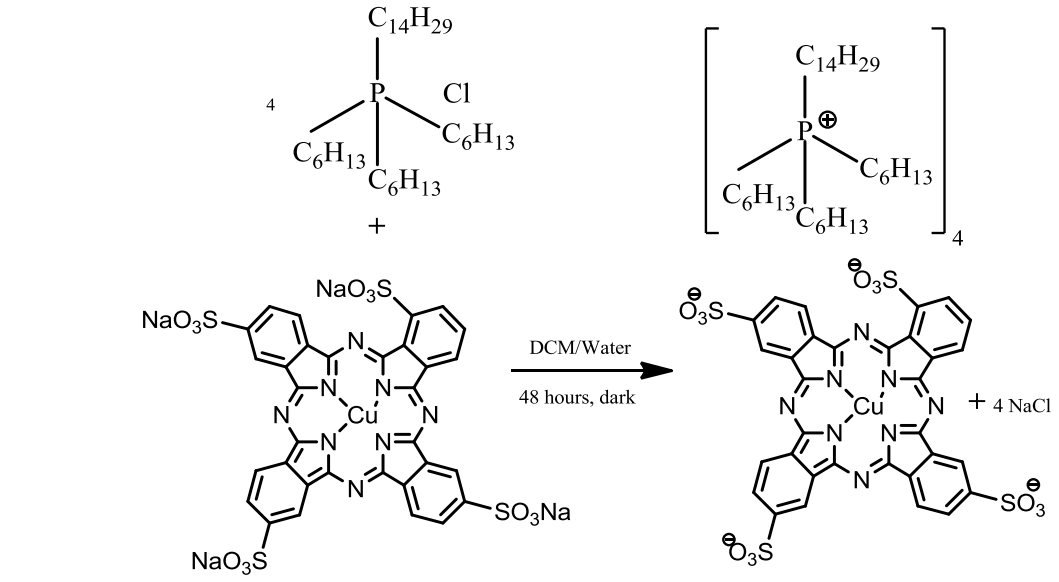

a

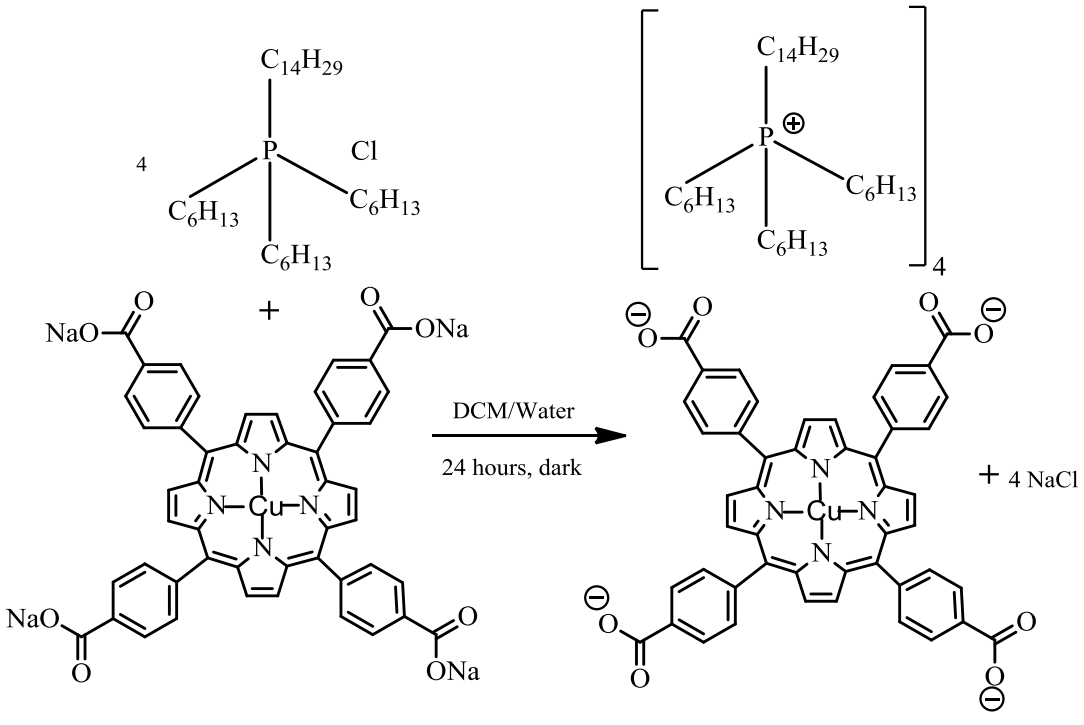

b

Figure 4.1 Ion exchange reactions showing syntheses of $[P66614]_4[CuPcS_4]$ (a) and $[P66614]_4[CuTCPP]$ (b).

stoichiometric ratio of the two reactants. The excess reactant and byproduct (NaCl) were removed by repeated rinsing with water. The products in both cases are found to be solids. The yield was close to 100 percent for phthalocyanine-based GUMBOS and ~90 percent for porphyrin-based GUMBOS.

Thermal properties of our GUMBOS were evaluated using TGA and DSC. The thermogravimetric (TG) curves for these compounds are shown in Figure. 4.2**.** Both of these compounds exhibited high thermal stability. The onset temperature of decomposition for $[P66614]_4[CuTCPP]$ is found to be 349 °C. The compound $[P66614]_4[CuPcS_4]$ was found to decompose in two steps; the onset temperature for the first step is 236 °C, and that for the second step is 418 °C. DSC thermogram of $[P66614]_4[CuTCPP]$ exhibited a single endothermic peak that corresponds to the melting point of the compound (Figure 4.3). The melting point, taken as the onset of melting, is 129 °C. The melting point of $[P66614]_4[CuPcS_4]$ is measured by using a simple melting apparatus, and it was found to be 135 °C. These melting points are considered to be very low as compared to melting points typically observed for porphyrins.[38]

4.3.2 Preparation and Characterization of the Sensing Films

Our GUMBOS films were prepared using a procedure similar to one previously outlined.[35,36] Both GUMBOS used in this study are soluble in acetone, but insoluble in heptane. Hence, these compounds were first dissolved in acetone, and then added dropwise to heptane under sonication, followed with further sonicated for 20 minutes. Afterwards, the quartz crystal was dipped into this mixture and allowed to sit for several hours. Since acetone is more volatile than heptane, preferential evaporation of acetone occurs, leading to deposition of a thin film on the crystal. This procedure for film preparation may be classified as a nonsolvent-induced phase

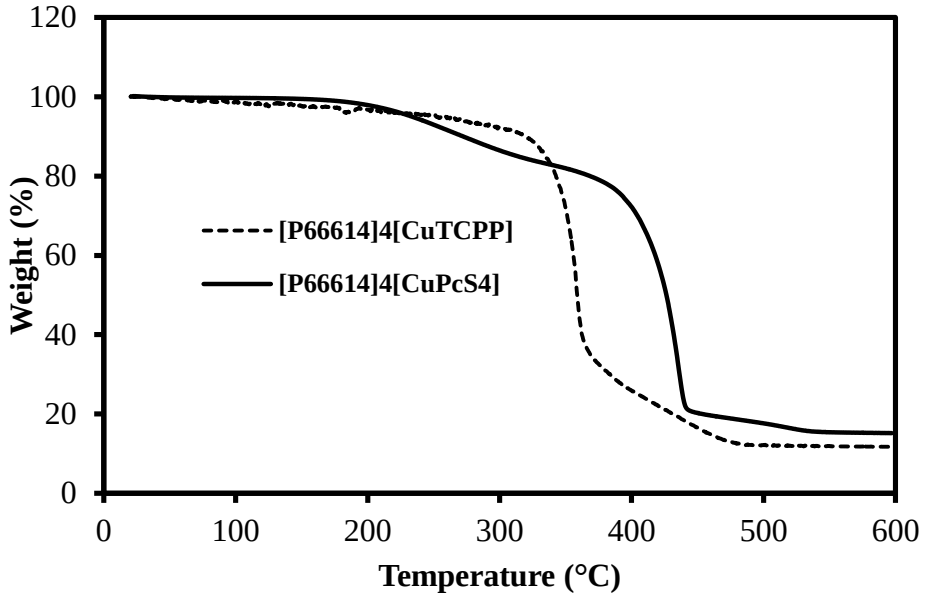

Figure 4.2 Thermogravimetric curves for $[P66614]_4[CuTCPP]$ (broken line) and $[P66614]_4[CuPcS4]$ (solid line).

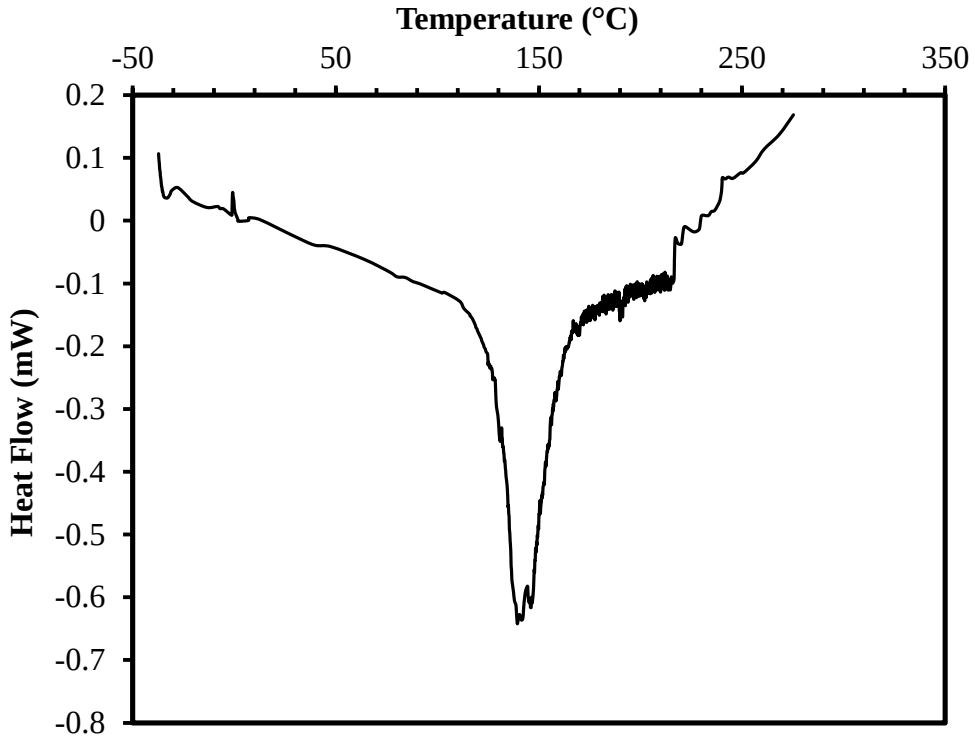

Figure 4.3 Differential scanning calorimetry (DSC) curve for $[P66614]_4[CuTCPP]$. The negative peak corresponds to an endothermic process.

separation (NIPS) or evaporation-induced phase separation (EIPS).[39,40] The resultant film was found to be strongly adhered to the surface since we see no effect when dipped in heptane and ultrasonicated. The amount of film material can be controlled by changing the concentration of the coating material, while keeping the volumes of both solvent and nonsolvent constant. Films obtained were then analyzed using scanning electron microscope (SEM). SEM images are shown in Figures 4.4a-b, which reveal that the surface is almost completely covered with GUMBOS.

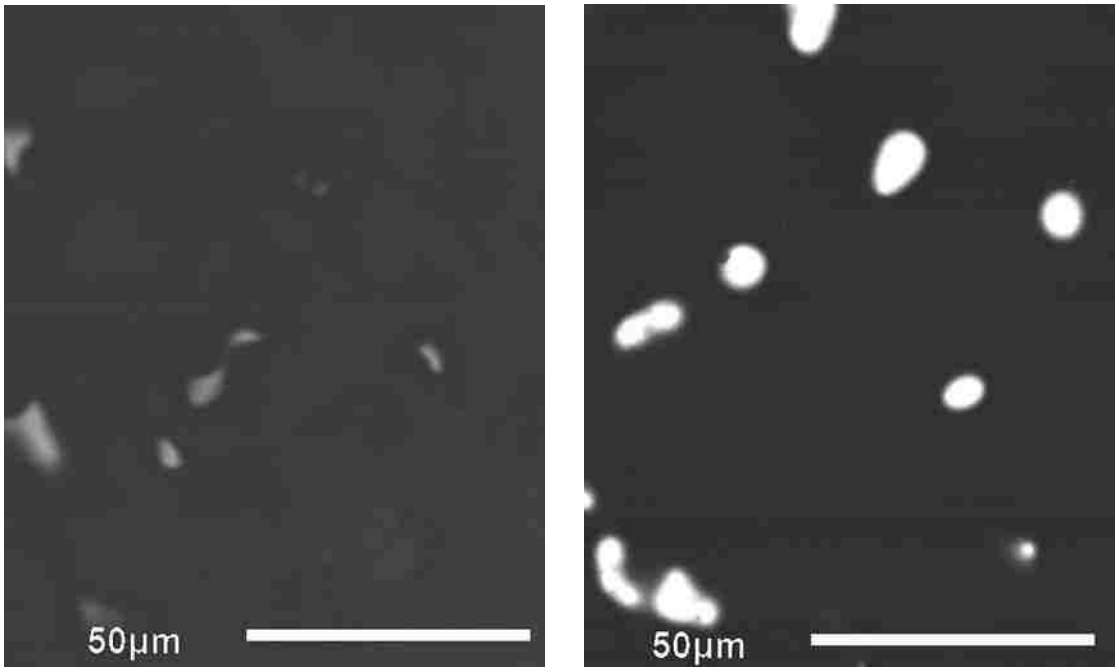

a **b**

Figure 4.4 Backscattered SEM micrographs in COMPO mode. (a)$[P66614]_4[CuPcS_4]$ film and (b) $[P66614]_4$[CuTCPP] film. The coated regions appear black, while the uncoated regions appear bright.

4.3.3 Evaluation of Vapor-Sensing Characteristics of the Films

Vapor-sensing characteristics of these novel materials were evaluated by exposing the QCM sensors to a number of different organic vapors in a closed environment. The details of the experimental setup have been described in a previous manuscript, i.e. chapter 2 of this

dissertation.[35] In the present studies, we selected 11 different organic vapors; and the change in resonance frequency (Δf) of the sensor as a function of vapor concentrations is monitored. The different vapors studied included methanol, ethanol, 1-propanol, 2-propanol, 1-butanol, 3-methyl-1-butanol, acetonitrile, acetone, nitromethane, chloroform, and toluene. The Δf-versus-concentration plots, for a QCM sensor coated with $[P66614]_4$[CuTCPP], upon exposure to these vapors are summarized in Figures 4.5a-b. It is evident from Figure.4.5a that each plot for the alcohol vapors can be best described as a second-degree polynomial with downward curvature. In other words, the sensor exhibits a higher sensitivity at lower concentrations and a lower sensitivity at higher concentrations. This type of behavior is characteristics of a sorption process consisting of both specific and non-specific interactions between the analytes and the sorbent material.[41] The specific interactions are stronger, and are assumed to obey Langmuir-type behavior, while the non-specific interactions are weaker and are believed to obey Henry's law.[41] In fact, previous studies relating vapor sensing using metalloporphyrin-coated QCM have shown roughly similar type of curves.[18-21] Figure 4.5b is the response of the sensor towards five nonalcohol vapors. Among the five vapors tested, toluene and nitromethane showed linear response, while chloroform, acetone, and acetonitrile showed nonlinear response curves.

As noted in Figures 4.5a-b, the coating responds to all organic vapors tested, and is found to be much more sensitive toward alcohol vapors. For example, the sensitivity for methanol is0.167 $Hz.ppm^{-1}$, which represents up to 130-fold improvement in sensitivity as compared to the sensitivity obtained by QCM employing various metalloporphyrins as the coating materials.[19] Note that in the case of alcohols, there is a drastic increase in sensitivity with an increase in molecular weight and boiling point of analytes. The sensitivity for ethanol is 0.529 $Hz.ppm^{-1}$,

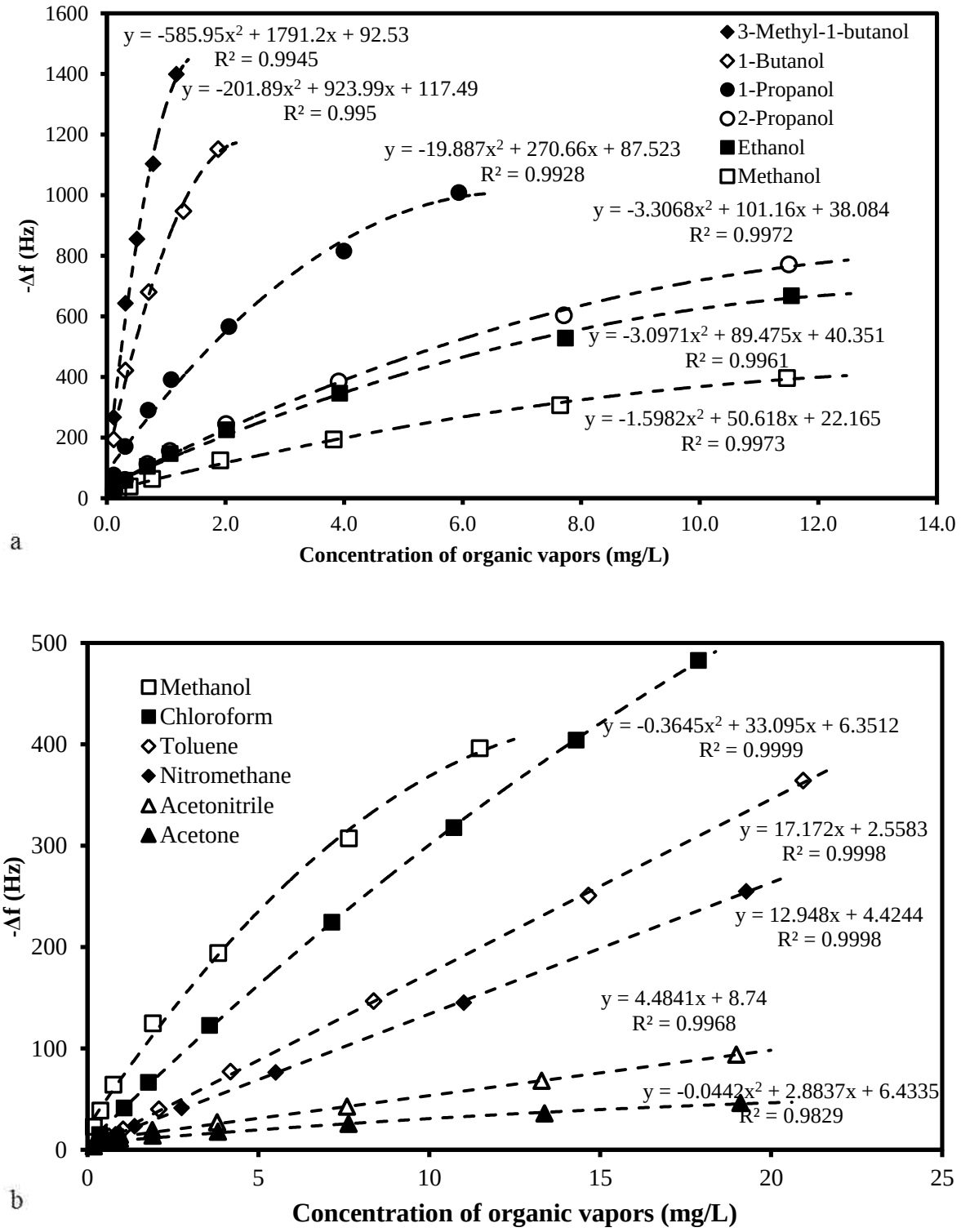

Figure 4.5 (a-b). Plots of frequency change as a function of concentration of different organic vapors for a QCM sensor coated with $[P66614]_4[CuTCPP]$. Amount of film material on the crystal surface is 163 $\mu g.cm^{-2}$. In Figure 4.5b, methanol is shown just for comparison purposes.

which is an up to 320-fold improvement, as compared to previous reports employing various metalloprophyrins as the coating materials.[26] Overall, this coating provides excellent sensitivity as compared to similar systems reported in the literature. The baseline of our sensor was found to be very stable, with a noise of approximately 0.2 Hz. The approximate detection limits and the ranges studied for all analytes are shown in Table 4.1. Among different analytes tested, the coating was found to be most sensitive to 3-methyl-1-butanol with a detection limit of 0.264 $\mu g.L^{-1}$, which corresponds to approximately 70 ppb by volume.

Table 4.1 Summary of concentration ranges investigated and estimated detection limits for all organic vapors for $[P66614]_4[CuTCPP]$-coated QCM sensor.

Organic compound	Range studied (mg/L)	Detection limit (μg/L)
Acetone	0.191–19.1	35.8
Acetonitrile	0.190–19.0	18.7
Nitromethane	0.275–19.3	25.4
Toluene	0.209–20.9	27.3
Chloroform	0.357–17.9	14.3
Methanol	0.191–11.5	5.06
Ethanol	0.114–11.5	2.3
2-Propanol	0.114–11.5	2.39
1-Propanol	0.116–5.94	0.911
1-Butanol	0.117–1.88	0.363
3-Methy-1-butanol	0.117–1.17	0.264

We have also examined the vapor-sensing properties of the $[P66614]_4[CuPcS_4]$-coated QCM sensor. The response curves for all organic vapors are shown in Figures 4.6a-b. As noted in these figures, the Δf-versus-concentration relationships are linear, with $R^2>0.99$ over a wide range of vapor concentrations. The ranges studied and the estimated detection limits for each vapor are listed in Table 4.2. It is important to again note that the two films show cross-reactivity, which is an important requirement for use of these materials as recognition elements

in array-based vapor sensors.[29] Although the response of the sensor coated with porphyrin-based GUMBOS does not strictly vary linearly with the concentration, suitable pattern recognition techniques, e.g. artificial neural network (ANN), can be used to best handle data arising from such sensor array-based systems.[29] In fact, Di Natale and coworkers[21] have analyzed the data from metalloporphyrin-coated QCM sensor array with an ANN technique to evaluate fish storage time .

After determining that these GUMBOS are highly sensitive materials, we sought to examine the constituent ion responsible for vapor absorption. To this end, further vapor-sensing studies were performed using an ionic liquid that contained the same cation, but different anion. Hence, we prepared [P66614][TFSI] using a similar procedure as was used to prepare GUMBOS in our studies. This compound is found to be liquid at room temperature. The IL was dissolved in acetone, and the solution was drop casted on the surface of the quartz crystal resonator. Then, two QCM sensors, one coated with $[P66614]_4$[CuTCPP] and the other coated with [P66614][TFSI], were simultaneously exposed to 10 percent saturated vapor of methanol using a flow system, which has been described in a previous publication, i.e chapter 3 of this dissertation.[36] Changes in the first harmonic frequency for both the sensors upon repeated exposure to methanol vapors are shown in Figures 4.7a-b. As evident from Figures 4.7a-b, the [P66614][TFSI] film exhibits very low response as compared to the $[P66614]_4$[CuTCPP] film. Therefore, we conclude that the QCM response to vapors is almost exclusively due to the counteranion of the GUMBOS. Moreover, Figure 4.7a shows that the sensor exhibits excellent baseline stability, rapid response and recovery times, and excellent repeatability. The response time, t_{90}, taken as the time required to reach 90% of the steady-state value is 30-35 s in the case

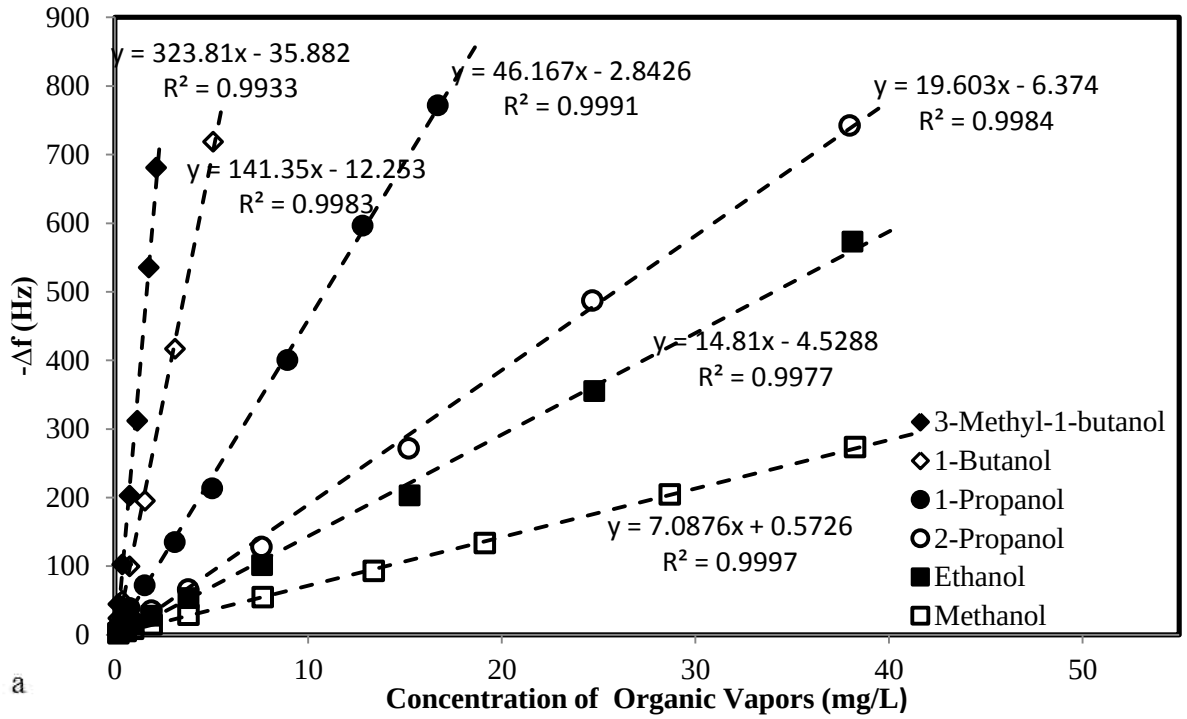

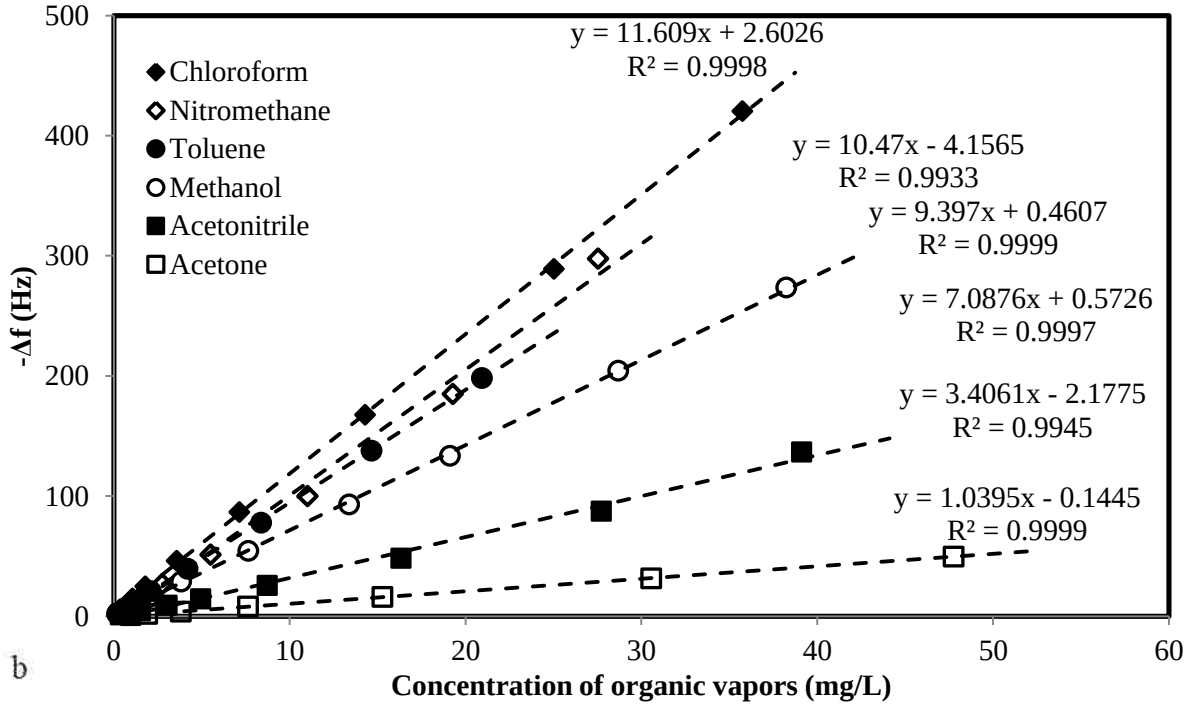

Figure 4.6 (a-b). Plots of frequency change as a function of concentration of different organic vapors for a QCM sensor coated with $[P66614]_4[CuPcS_4]$. Amount of film material on the crystal surface is 136 $\mu g.cm^{-2}$.

of methanol. Interestingly, this time is similar to what is observed for ionic liquids. Similar sensing characteristics are also exhibited by $[P66614]_4[CuPcS_4]$ film (data not shown).

Table 4.2 Summary of concentration ranges investigated and estimated detection limits for all organic vapors for $[P66614]_4[CuPcS_4]$-coated QCM sensor.

Organic compound	Range studied (mg/L)	Detection limit (μg/L)
Acetone	0.955–47.8	636
Acetonitrile	0.380–39.1	228
Methanol	0.191–38.2	64
Toluene	0.209–20.9	55
Nitromethane	0.275–27.5	59
Chloroform	0.357–35.7	43
Ethanol	0.191–38.1	38
2-Propanol	0.190–38.0	34
1-Propanol	0.184–16.7	11
1-Butanol	0.196–5.09	4.9
3-Methy-1-butanol	0.196–2.15	2.7

It is clear that these GUMBOS offer several distinct advantages as possible sensing materials. As mentioned above, the chemical selectivity of porphyrins and phthalocyanines can be easily tuned by changing the central metal atom and/or peripheral substituents. This would allow creation of a number of different compounds exhibiting slightly different selectivity characteristics to be used in gas-sensor arrays. In fact, converting these macrocyclic molecules to ionic liquids or GUMBOS offers additional flexibility in tuning the sensing properties by changing the structures of both the cation and anion. These macrocyclic compounds can also be used in the cationic form. As an illustration, Xu et al.[42] recently synthesized a number of liquid and solid-phase salts using cationic porphyrins. Another advantage of using GUMBOS is that

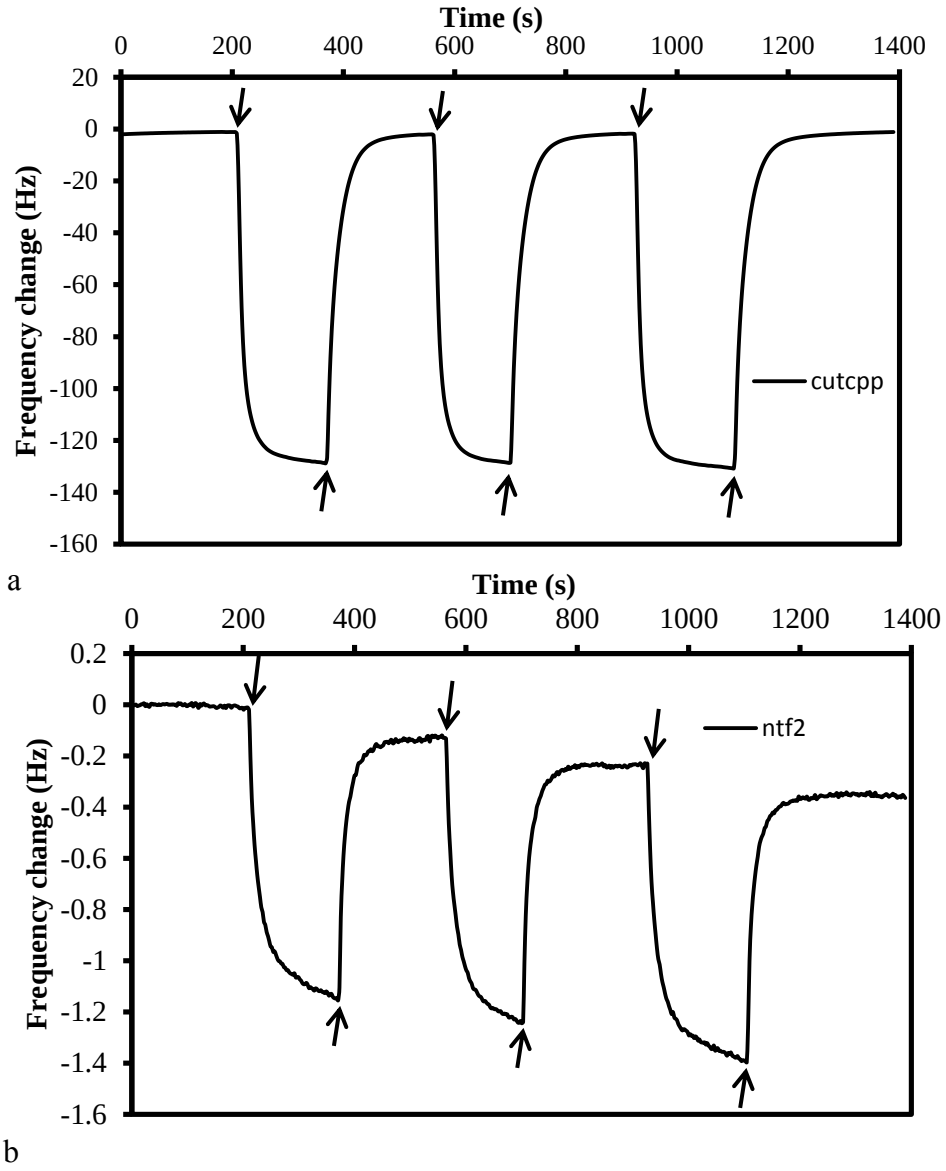

Figure 4.7 Changes in the first harmonic frequency of QCM-D sensors on repeated (3 times) exposure to 10% methanol. Amount of coating materials: (a) 70 μg.cm^{-2} of $[P66614]_4[CuTCPP]$ and (b) 13 μg.cm^{-2} of [P66614][TFSI]. Downward arrows represent the point where the sensor is exposed to methanol, and the upward arrows represent the start of removal of methanol by blowing argon.

these materials provide much higher sensitivity compared to nonionic porphyrins and phthalocyanines. One reason for obtaining higher sensitivity is an increase in amount of coating material, and another reason is an increase in free volume within these materials. As a result, we saw an overall improvement in sensitivity up to two orders of magnitude. A decrease in response

time was obtained with these materials which may be attributed to the increase free volume. Finally, the deposition procedure for GUMBOS onto the surface of the quartz crystal is simple and the thickness can be easily controlled. We note that complex deposition procedures such as thermal evaporation, plasma polymerization, and electropolymerization have been practiced by others in the past.[15,17,20] Drop casting is a simple procedure that has also been widely used. However, major concerns in previous studies are lack of reproducibility and imperfect adhesion of the film on the substrate.[20]

4.4 Conclusion

In this study, we have synthesized two novel GUMBOS using cyclic tetrapyrroles, and have evaluated the vapor-sensing characteristics of these compounds using a QCM transducer. One GUMBOS was synthesized using a porphyrin derivative, while the other was synthesized using a phthalocyanine derivative. These GUMBOS showed excellent sensing characteristics. In addition, these compounds exhibited cross-reactive responses to different vapors, making these type of materials ideal for array-based differential sensing. Porphyrins and phthalocyanine are versatile classes of compounds, and a large set of compounds can be easily synthesized by changing the central metal atom and the peripheral substitution pattern in order to tune the selectivity pattern towards different chemical analytes. Hence, these materials show considerable promise for use in construction of cross-reactive sensor arrays for detection and discrimination of a wide range of organic vapors. Future work includes synthesizing a diverse range of GUMBOS and creating sensor arrays to analyze real-world samples.

4.5 References

(1) Rakow, N. A.; Suslick, K. S.: A colorimetric sensor array for odour visualization. *Nature* **2000**, *406*, 710-713.

(2) Zhou, R.; Josse, F.; Göpel, W.; Öztürk, Z.; Bekaroğlu, Ö.: Phthalocyanines as sensitive materials for chemical sensors. *Applied Organometallic Chemistry* **1996**, *10*, 557-577.

(3) Spadavecchia, J.; Ciccarella, G.; Siciliano, P.; Capone, S.; Rella, R.: Spin-coated thin films of metal porphyrin–phthalocyanine blend for an optochemical sensor of alcohol vapours. *Sensors and Actuators B: Chemical* **2004**, *100*, 88-93.

(4) Bouvet, M.: Phthalocyanine-based field-effect transistors as gas sensors. *Analytical and Bioanalytical Chemistry* **2006**, *384*, 366-373.

(5) Campbell, W. M.; Jolley, K. W.; Wagner, P.; Wagner, K.; Walsh, P. J.; Gordon, K. C.; Schmidt-Mende, L.; Nazeeruddin, M. K.; Wang, Q.; Grätzel, M.: Highly efficient porphyrin sensitizers for dye-sensitized solar cells. *The Journal of Physical Chemistry C* **2007**, *111*, 11760-11762.

(6) Wang, X.-F.; Tamiaki, H.: Cyclic tetrapyrrole based molecules for dye-sensitized solar cells. *Energy & Environmental Science* **2010**, *3*, 94-106.

(7) Mori, S.; Nagata, M.; Nakahata, Y.; Yasuta, K.; Goto, R.; Kimura, M.; Taya, M.: Enhancement of incident photon-to-current conversion efficiency for phthalocyanine-sensitized solar cells by 3D molecular structuralization. *Journal of the American Chemical Society* **2010**, *132*, 4054-4055.

(8) Law, K. Y.: Organic photoconductive materials: recent trends and developments. *Chemical Reviews* **1993**, *93*, 449-486.

(9) Choi, S. J.; Lee, Y. C.; Seol, M. L.; Ahn, J. H.; Kim, S.; Moon, D. I.; Han, J. W.; Mann, S.; Yang, J. W.; Choi, Y. K.: Bio-inspired complementary photoconductor by porphyrin-coated silicon nanowires. *Advanced Materials* **2011**, *23*, 3979-3983.

(10) Li, B.; Li, J.; Fu, Y.; Bo, Z.: Porphyrins with four monodisperse oligofluorene arms as efficient red light-emitting materials. *Journal of the American Chemical Society* **2004**, *126*, 3430-3431.

(11) Bown, S.; Tralau, C.; Smith, P.; Akdemir, D.; Wieman, T.: Photodynamic therapy with porphyrin and phthalocyanine sensitisation: quantitative studies in normal rat liver. *British Journal of Cancer* **1986**, *54*, 43-52.

(12) Spikes, J. D.: Phthalocyanines as photosensitizers in biological systems and for the photodynamic therapy of tumors. *Photochemistry and Photobiology* **1986**, *43*, 691-699.

(13) Liu, M. O.; Hu, A. T.: Microwave-assisted synthesis of phthalocyanine–porphyrin complex and its photoelectric conversion properties. *Journal of Organometallic Chemistry* **2004**, *689*, 2450-2455.

(14) Harbeck, M.; Taşaltın, C.; Gürol, I.; Musluoğlu, E.; Ahsen, V.; Öztürk, Z. Z.: Preferential sorption of polar compounds by fluoroalkyloxy substituted phthalocyanines for the use in sorption based gas sensors. *Sensors and Actuators B: Chemical* **2010**, *150*, 616-624.

(15) Kurosawa, S.; Kamo, N.; Matsui, D.; Kobatake, Y.: Gas sorption to plasma-polymerized copper phthalocyanine film formed on a piezoelectric crystal. *Analytical Chemistry* **1990**, *62*, 353-359.

(16) Schiebaum, K-D.; Zhou, R.; Knecht, S.; Dieing, R.; Hanack, M.; Göpel, W.: The interaction of transition metal phthalocyanines with organic molecules: a quartz-microbalance study. *Sensors and Actuators B: Chemical* **1995**, *24*, 69-71.

(17) Fietzek, C.; Bodenhöfer, K.; Haisch, P.; Hees, M.; Hanack, M.; Steinbrecher, S.; Zhou, F.; Plies, E.; Göpel, W.: Soluble phthalocyanines as coatings for quartz-microbalances: specific and unspecific sorption of volatile organic compounds. *Sensors and Actuators B: Chemical* **1999**, *57*, 88-98.

(18) Paolesse, R.; Di Natale, C.; Macagnano, A.; Davide, F.; Boschi, T.; D'Amico, A.: Self-assembled monolayers of mercaptoporphyrins as sensing material for quartz crystal microbalance chemical sensors. *Sensors and Actuators B: Chemical* **1998**, *47*, 70-76.

(19) Brunink, J.; Di Natale, C.; Bungaro, F.; Davide, F.; D'Amico, A.; Paolesse, R.; Boschi, T.; Faccio, M.; Ferri, G.: The application of metalloporphyrins as coating material for quartz microbalance-based chemical sensors. *Analytica Chimica Acta* **1996**, *325*, 53-64.

(20) Paolesse, R.; Di Natale, C.; Campo Dall'Orto, V.; Macagnano, A.; Angelaccio, A.; Motta, N.; Sgarlata, A.; Hurst, J.; Rezzano, I.; Mascini, M.: Porphyrin thin films coated quartz crystal microbalances prepared by electropolymerization technique. *Thin Solid Films* **1999**, *354*, 245-250.

(21) Di Natale, C.; Brunink, J. A.; Bungaro, F.; Davide, F.; d'Amico, A.; Paolesse, R.; Boschi, T.; Faccio, M.; Ferri, G.: Recognition of fish storage time by a metalloporphyrins-coated QMB sensor array. *Measurement Science and Technology* **1996**, *7*, 1103-1114.

(22) Di Natale, C.; Macagnano, A.; Repole, G.; Saggio, G.; D'Amico, A.; Paolesse, R.; Boschi, T.: The exploitation of metalloporphyrins as chemically interactive material in chemical sensors. *Materials Science and Engineering: C* **1998**, *5*, 209-215.

(23) Paolesse, R.; Di Natale, C.; Macagnano, A.; Sagone, F.; Scarselli, M. A.; Chiaradia, P.; Troitsky, V. I.; Berzina, T. S.; D'Amico, A.: Langmuir-Blodgett films of a manganese corrole derivative. *Langmuir* **1999**, *15*, 1268-1274.

(24) Di Natale, C.; Macagnano, A.; Martinelli, E.; Paolesse, R.; D'Arcangelo, G.; Roscioni, C.; Finazzi-Agrò, A.; D'Amico, A.: Lung cancer identification by the analysis of breath by means of an array of non-selective gas sensors. *Biosensors and Bioelectronics* **2003**, *18*, 1209-1218.

(25) Montmeat, P.; Madonia, S.; Pasquinet, E.; Hairault, L.; Gros, C. P.; Barbe, J.-M.; Guilard, R.: Metalloporphyrins as sensing material for quartz-crystal microbalance nitroaromatics sensors. *Sensors Journal, IEEE* **2005**, *5*, 610-615.

(26) Capan, I.; Tarımcı, Ç.; Capan, R.: Fabrication of Langmuir–Blodgett thin films of porphyrins and investigation on their gas sensing properties. *Sensors and Actuators B: Chemical* **2010**, *144*, 126-130.

(27) Özmen, A.; Tekce, F.; Ebeoğlu, M.; Taşaltın, C.; Öztürk, Z.: Finding the composition of gas mixtures by a phthalocyanine-coated QCM sensor array and an artificial neural network. *Sensors and Actuators B: Chemical* **2006**, *115*, 450-454.

(28) Potyrailo, R. A.; Surman, C.; Nagraj, N.; Burns, A.: Materials and transducers toward selective wireless gas sensing. *Chemical Reviews* **2011**, *111*, 7315-7354.

(29) Albert, K. J.; Lewis, N. S.; Schauer, C. L.; Sotzing, G. A.; Stitzel, S. E.; Vaid, T. P.; Walt, D. R.: Cross-reactive chemical sensor arrays. *Chemical Reviews* **2000**, *100*, 2595-2626.

(30) Persaud, K.; Dodd, G.: Analysis of discrimination mechanisms in the mammalian olfactory system using a model nose. *Nature* **1982**, *299*, 352-355.

(31) Sauerbrey, G.: The use of quartz oscillators for weighing thin layers and for microweighing. *Zeitschrift Fur Physik* **1959**, *155*, 206-222.

(32) Keiji Kanazawa, K.; Gordon II, J. G.: The oscillation frequency of a quartz resonator in contact with liquid. *Analytica Chimica Acta* **1985**, *175*, 99-105.

(33) Bandey, H. L.; Martin, S. J.; Cernosek, R. W.; Hillman, A. R.: Modeling the responses of thickness-shear mode resonators under various loading conditions. *Analytical Chemistry* **1999**, *71*, 2205-2214.

(34) Voinova, M. V.; Rodahl, M.; Jonson, M.; Kasemo, B.: Viscoelastic acoustic response of layered polymer films at fluid-solid interfaces: continuum mechanics approach. *Physica Scripta* **1999**, *59*, 391-396.

(35) Regmi, B. P.; Monk, J.; El-Zahab, B.; Das, S.; Hung, F. R.; Hayes, D. J.; Warner, I. M.: A novel composite film for detection and molecular weight determination of organic vapors. *Journal of Materials Chemistry* **2012**, *22*, 13732-13741.

(36) Regmi, B.P.; Speller, N.C.; Anderson, M. J.; Btutus, J. O.; Merid, Y.; Das, S.; El-Zahab, B.; Hayes, D. J.; Murray, K. K.;Warner, I. M.: Molecular weight sensing properties of ionic liquid-polymer composite films: theory and experimen. *Journal of Materials Chemistry C* **2014**, *2*, 4867-4878.

(37) Galpothdeniya, W. I. S.; McCarter, K. S.; de Rooy, S. L.; Regmi, B. P.; Das, S.; Hasan, F.; Tagge, A.; Warner, I. M.: Ionic liquid-based optoelectronic sensor arrays for chemical detection. *RSC Advances* **2014**, *4*, 7225-7234.

(38) Schäferling, M.; Bäuerle, P.: Porphyrin-functionalized oligo-and polythiophenes. *Journal of Materials Chemistry* **2004**, *14*, 1132-1141.

(39) Guillen, G. R.; Pan, Y.; Li, M.; Hoek, E. M.: Preparation and characterization of membranes formed by nonsolvent induced phase separation: a review. *Industrial & Engineering Chemistry Research* **2011**, *50*, 3798-3817.

(40) Zhao, J.; Luo, G.; Wu, J.; Xia, H.: Preparation of microporous silicone rubber membrane with tunable pore size via solvent evaporation-induced phase separation. *ACS Applied Materials & Interfaces* **2013**, *5*, 2040-2046.

(41) Bodenhöfer, K.; Hierlemann, A.; Juza, M.; Schurig, V.; Göpel, W.: Chiral discrimination of inhalation anesthetics and methyl propionates by thickness shear mode resonators: new insights into the mechanisms of enantioselectivity by cyclodextrins. *Analytical Chemistry* **1997**, *69*, 4017-4031.

(42) Xu, H-J.; Gros, C. P.; Brandès, S.; Ge, P-Y.; Girault, H. H.; Barbe, J-M.: Room temperature ionic liquids based on cationic porphyrin derivatives and tetrakis (pentafluorophenyl) borate anion. *Journal of Porphyrins and Phthalocyanines* **2011**, *15*, 560-574.

CHAPTER 5 CONCLUSIONS AND FUTURE WORK

5.1 Conclusion

Volatile organic compounds (VOCs) are emitted from a wide array of natural and anthropogenic sources. There is an urgent need for the development of reliable sensors for accurate and real-time monitoring of VOCs in different environments. A typical vapor sensor comprises a chemosensitive layer immobilized onto the surface of suitable physical transducer. Among a number of different transducers, the quartz crystal microbalance (QCM) has become popular in recent years because it is a simple and low-cost device that is amenable to miniaturization and creation of sensor arrays. With regard to the sensing materials, the use of ionic liquids (ILs) and a group of uniform materials based on organic salts (GUMBOS) for the QCM device is rapidly growing. Tunable physicochemical properties, negligible volatility, thermal and chemical stabilities, and ease of preparation make ILs attractive for use in highly sensitive chemical sensing devices..

Preparation, characterization, and vapor-sensing characteristics of a GUMBOS-polymer composite film immobilized on the QCM surface are presented in Chapter 2. These studies revealed for the first time that the QCM device can act not only a mass sensor but also a molecular weight sensor. In particular, the frequency shift (Δf) and motional resistance change (ΔR) of the sensor were simultaneously measured during exposure to a number of VOCs. The Δf-versus-ΔR plot was observed to be distinct for each vapor. Interestingly, the Δf-to-ΔR ratio was found to be proportional to the molecular weight of vapor absorbed, provided that the sensor is exposed to relatively low concentrations of vapors. These interesting observations led us to conduct further studies in this area.

More detailed studies aimed at understanding the theoretical basis for the aforementioned observations are described in Chapter 3. In this regard, a number of different ILs and two different polymers were evaluated. An extended range of concentration of analytes was investigated, and a quadratic equation to estimate molecular weight of organic vapors was developed. Additionally, the frequency and dissipation at multiple harmonics were measured during vapor absorption, and these data were fitted to different materials models. It revealed that the composite films behave like Maxwell viscoelastic materials. With these data, a plausible explanation is proposed to account the relationship between QCM variables and molecular weight of vapors.

Synthesis and vapor-sensing applications of two representative GUMBOS prepared from cyclic tetrapyrroles are described in Chapter 4. One of these GUMBOS was prepared from porphyrin, while the other was prepared from phthalocyanine. The vapor-sensing studies of these compounds were conducted using the QCM transducer, and a significant improvement is sensitivity and response time was observed compared to previous reports. In addition, these two sensors display cross-reactive responses to different analyte vapors, thereby showing great promise for electronic nose applications.

5.2 Suggestions for Future Research

The results presented in this dissertation demonstrate the true potential of ILs and GUMBOS for sensing applications. Future research is needed to extend these findings and develop high performance sensing devices. As discussed above IL or GUMBOS-based QCM sensors exhibit two-parameter response i.e. Δf and ΔR (or ΔD). Two responses per sensor element provide more information during array-based vapor sensing. It must be noted that currently reported QCM-based sensor arrays are based on the measurement of only Δf. Future

studies should therefore focus on creating sensor arrays using these materials for efficient discrimination of closely related samples. This approach should be useful for discrimination between different organic compounds belonging to the same class. The discrimination between the members—since they possess similar chemical structures—of a homologous series is difficult using currently available sensor arrays which are based on difference in binding affinity.

In addition, preliminary studies indicate the possibility of discrimination of different analytes based on the multiple harmonic data obtained using an IL-coated QCM-D sensor. Further studies should focus on devising more experiments and analyzing the data using suitable pattern recognition techniques. Again, this approach should be useful for the discrimination of compounds within a given chemical class. In Chapter 4, it has been demonstrated that GUMBOS based on cyclic tetrapyrroles are very sensitive for vapor detection. Additional experiments should be designed focusing on synthesis of similar new GUMBOS and creating sensor arrays for characterization of real samples.

APPENDIX A SUPPORTING INFORMATION FOR CHAPTER NUMBER TWO: TABLE AND FIGURES

Table A1: Detection limits, sensitivities, and ranges studied for different VOCs

VOC	Detection limit (mg/L)	Range studied (mg/L)	Sensitivity (Hz.L/mg)
acetone	0.0806	0.19-60.8	6.7
acetonitrile	0.0267	0.19-15.2	24.6
chloroform	0.1271	0.36-57.0	4.1
ethanol	0.1189	0.19-60.8	5.4
methanol	0.1611	0.19-61.1	3.8
toluene	0.0508	0.21-16.7	11.2

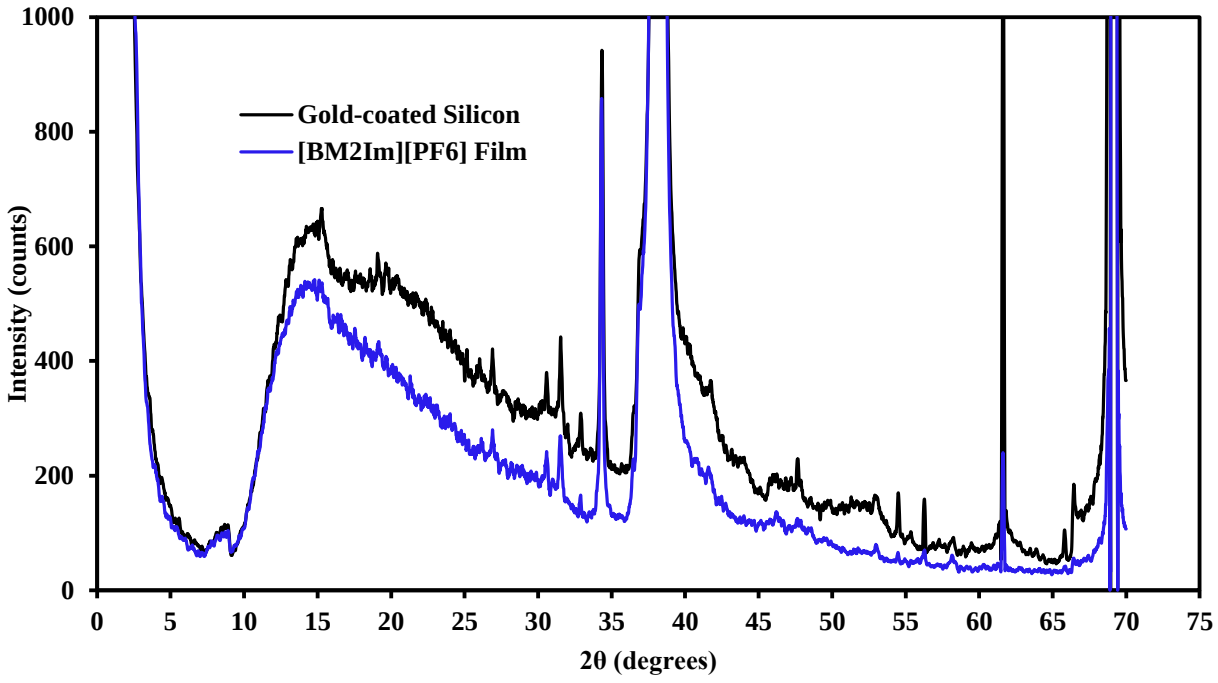

Figure A1 XRD diffractograms of gold-coated silicon, and $[BM_2Im][PF_6]$ film deposited on the same substrate.

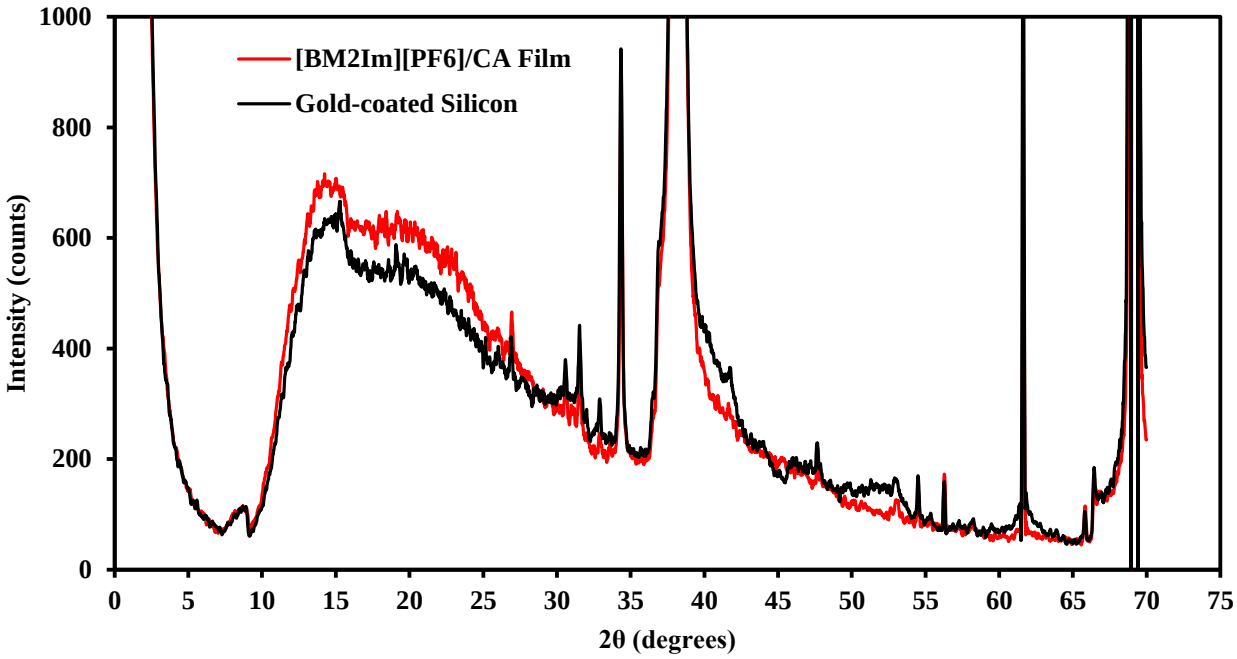

Figure A2 XRD diffractograms of gold-coated silicon, and $[BM_2Im][PF_6]$-CA film deposited on the same substrate.

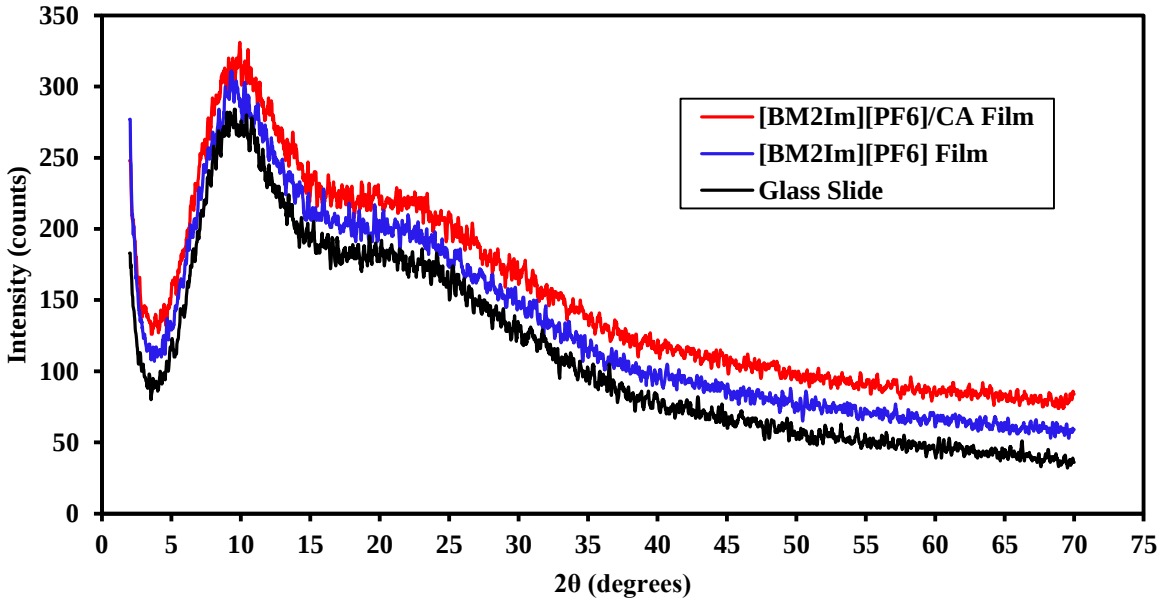

Figure A3 XRD diffractograms of glass slide, $[BM_2Im][PF_6]$, and $[BM_2Im][PF_6]$-CA films deposited on the glass slide.

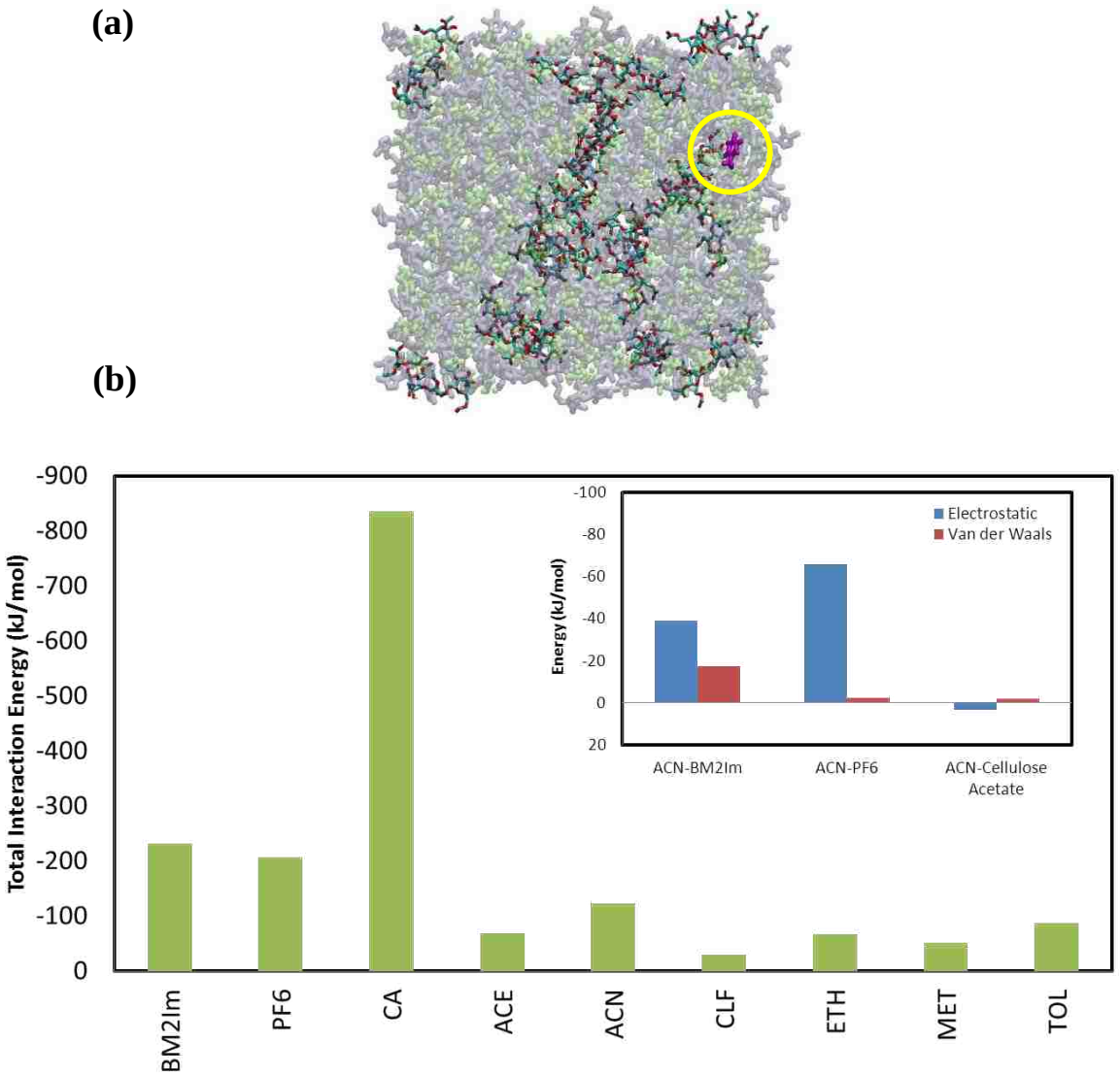

Figure A4 (a) Simulation snapshot showing 500 [BM_2Im][PF_6] pairs with 18 oligomers of CA and one molecule of VOC (toluene, circled in yellow). (b) Total interaction energy (i.e., sum of electrostatic and van der Waals interactions) exerted by all molecules present in the system to a single molecule of any given species. Shown in order (x-axis): a randomly chosen cation; a randomly chosen anion; a randomly chosen oligomer of cellulose acetate; and a molecule of analyte (in order: acetone, acetonitrile, chloroform, ethanol, methanol and toluene). The inset shows the electrostatic and van der Waals interactions experienced by a molecule of acetonitrile due to all the cations, anions and oligomers of cellulose acetate present in the system; the sum of all these energies give the total interaction energy experienced by the molecule of acetonitrile.

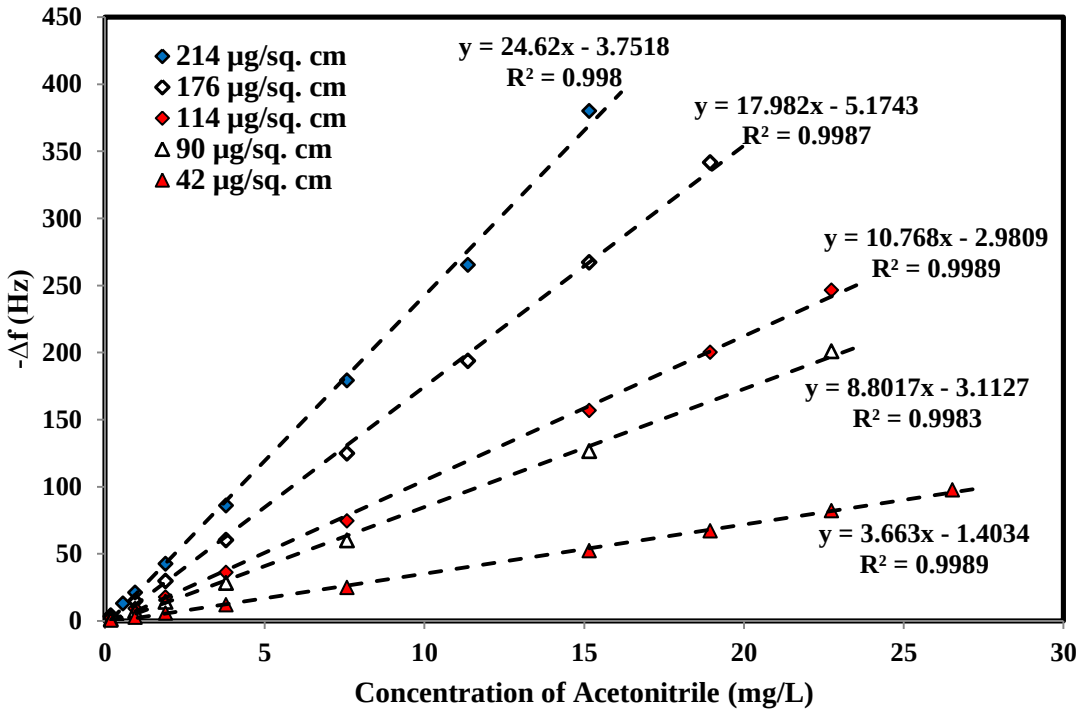

Figure A5 Frequency shift versus acetonitrile vapor concentration for films containing different masses of the composite material. Legend shows the mass of the sensing material in each film.

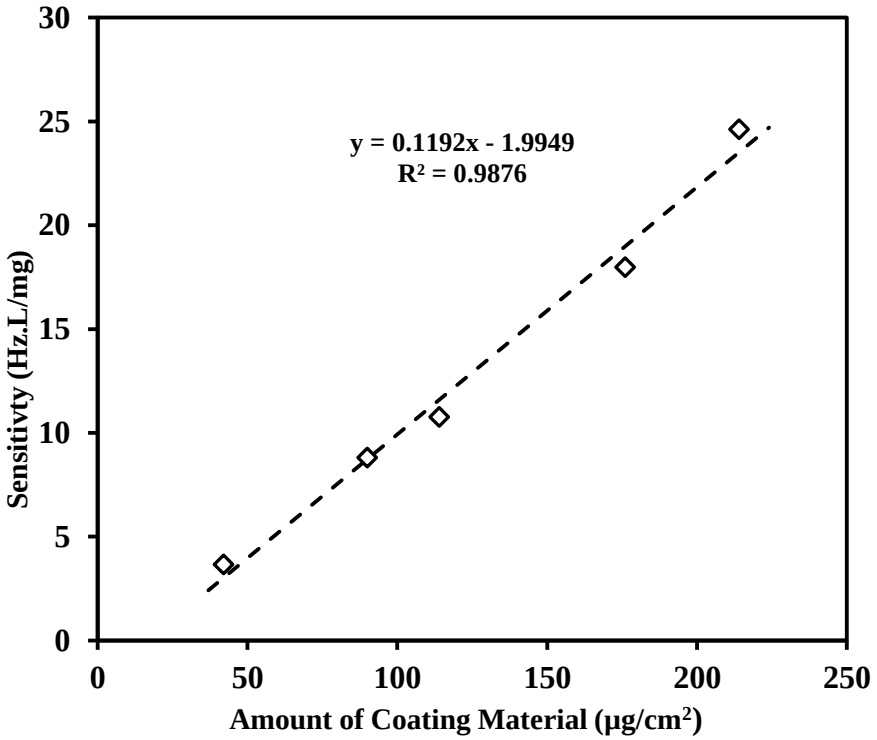

Figure A6 Variation of sensitivity to acetonitrile vapors as a function of mass of sensing material.

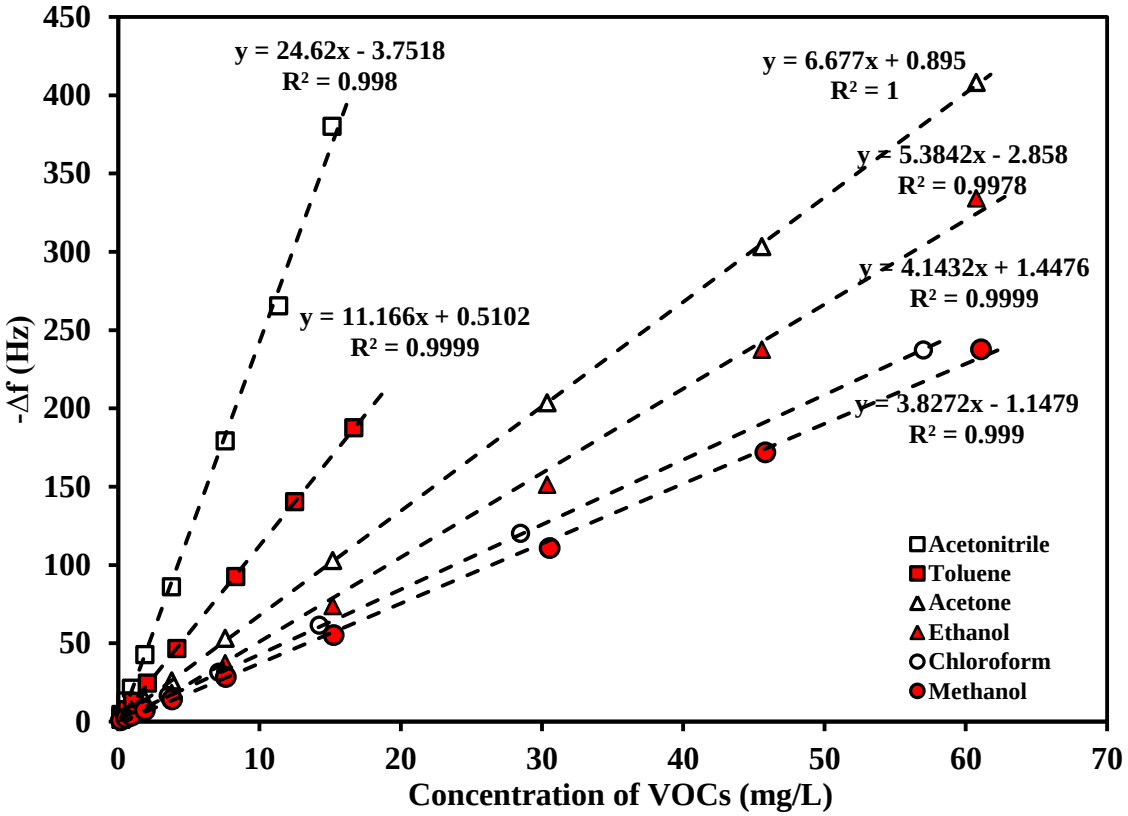

Figure A7 Frequency shift as a function of vapor concentrations for various VOCs.

[In Figure A4b, interaction energies are expressed in units of kJ/mol, while the slopes here are in units of Hz/(mg/L). For comparison, the slopes should be converted to moles of analyte absorbed per cm^2 for the same molar concentration of each vapor. Since Δf/(mg/L) is proportional to (moles/cm^2)/ (moles/L), the order remains the same].

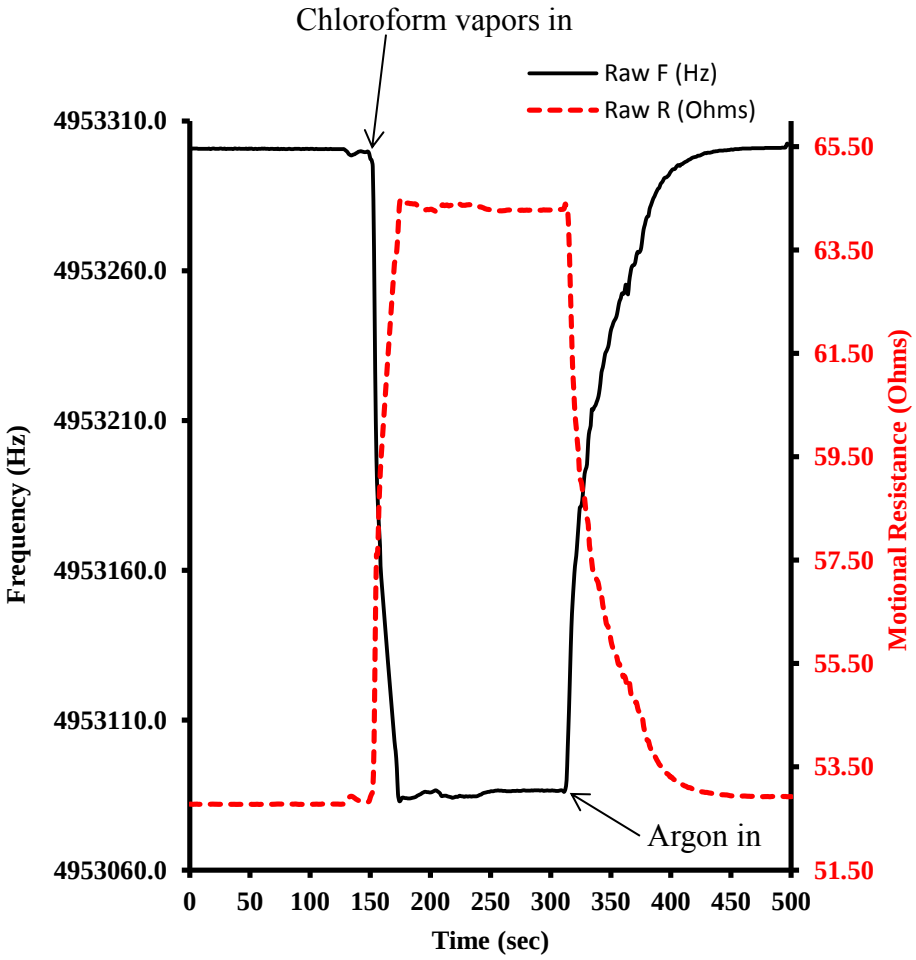

Figure A8 Frequency and motional resistance responses of the sensor when premade chloroform vapors are introduced into the measuring chamber.

APPENDIX B SUPPORTING INFORMATION FOR CHAPTER NUMBER THREE: FIGURES

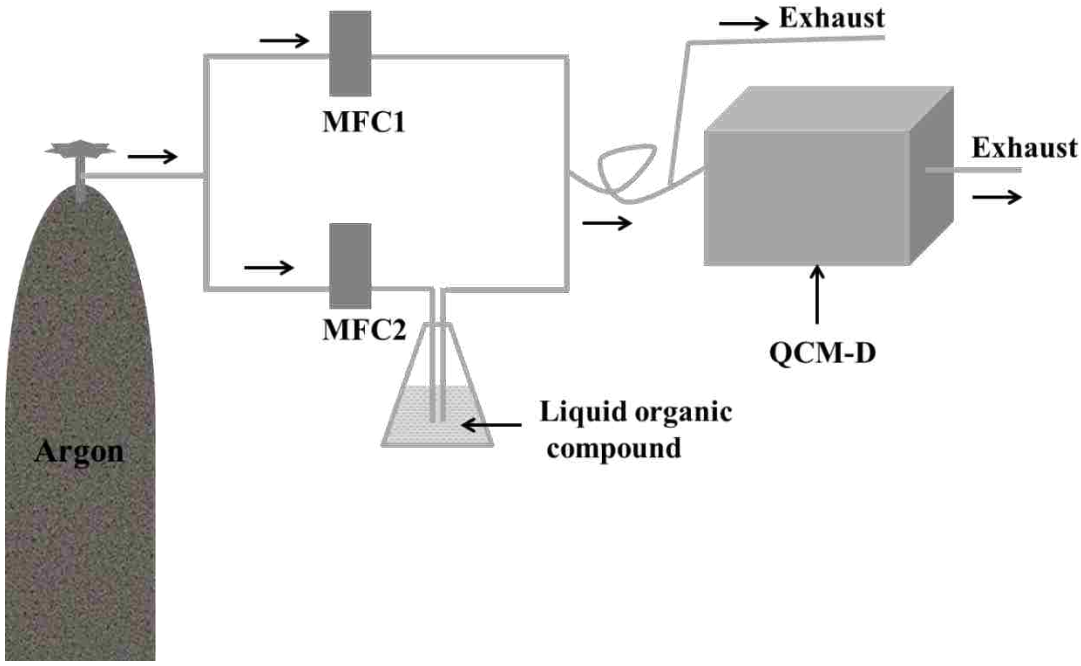

Figure B1 Schematic of experimental setup used for vapor generation and measurement.

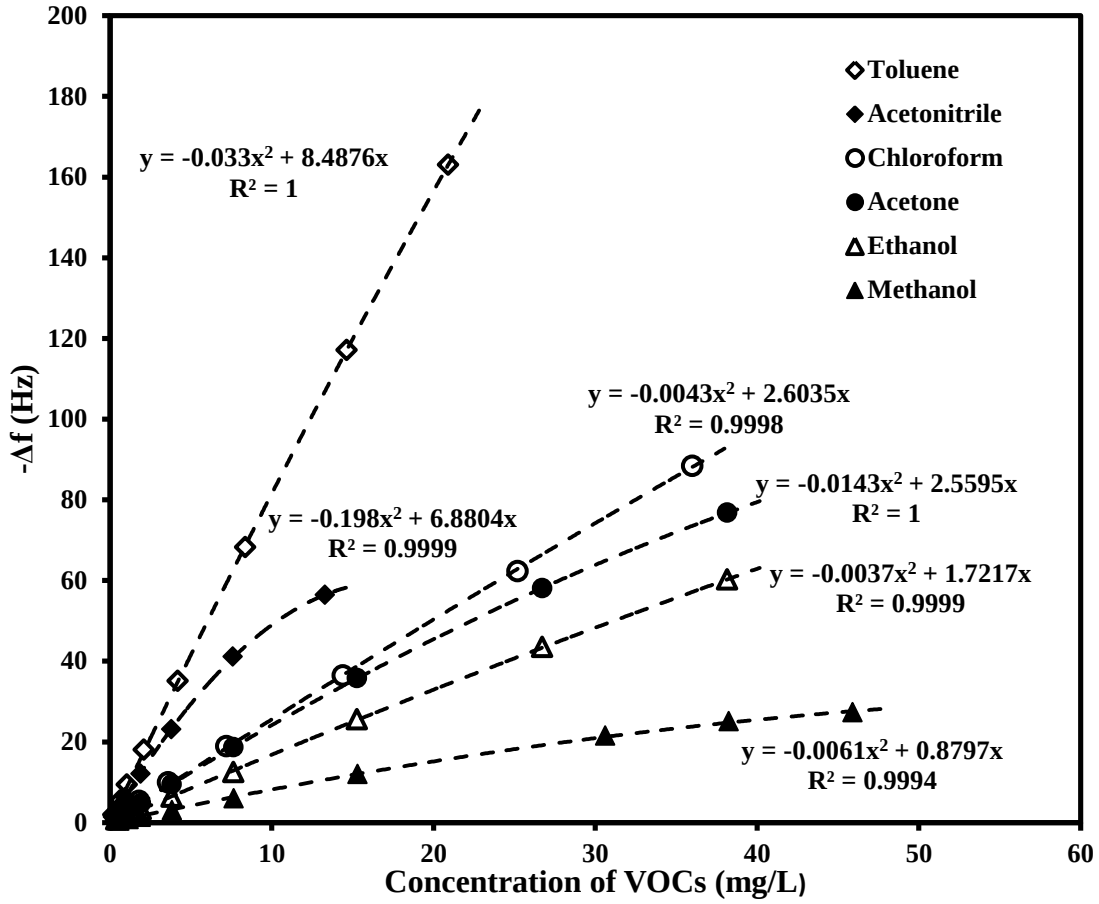

Figure B2 Plots showing the variation of Δ*f* with concentration of VOCs for a QCM sensor coated with [HMPyr][PF_6]. Amount of coating material: 83 µg.cm^{-2}. Each analyte exhibits a second-degree polynomial relationship between Δ*f* and concentration.

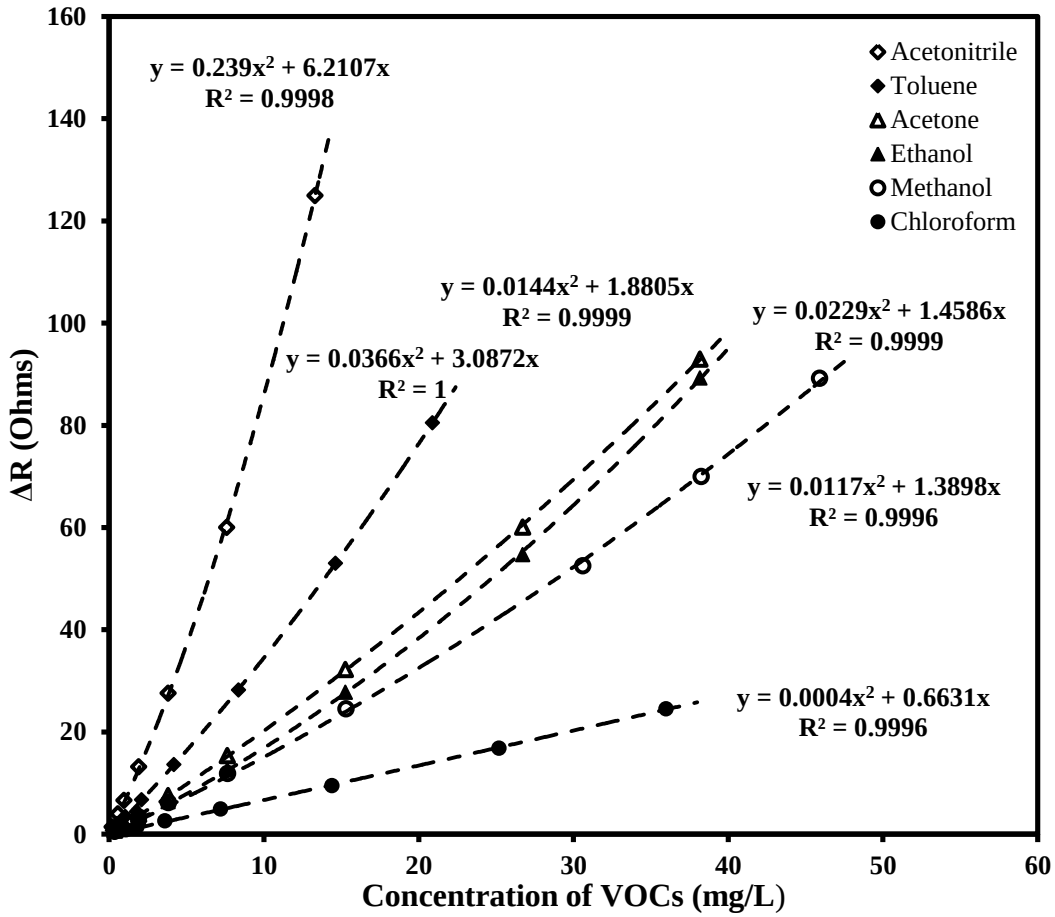

Figure B3 Plots showing the variation of Δ*R* with concentration of VOCs for the same sensor shown in Figure B2. Each analyte is showing a second-degree polynomial relationship between Δ*R* and concentration.

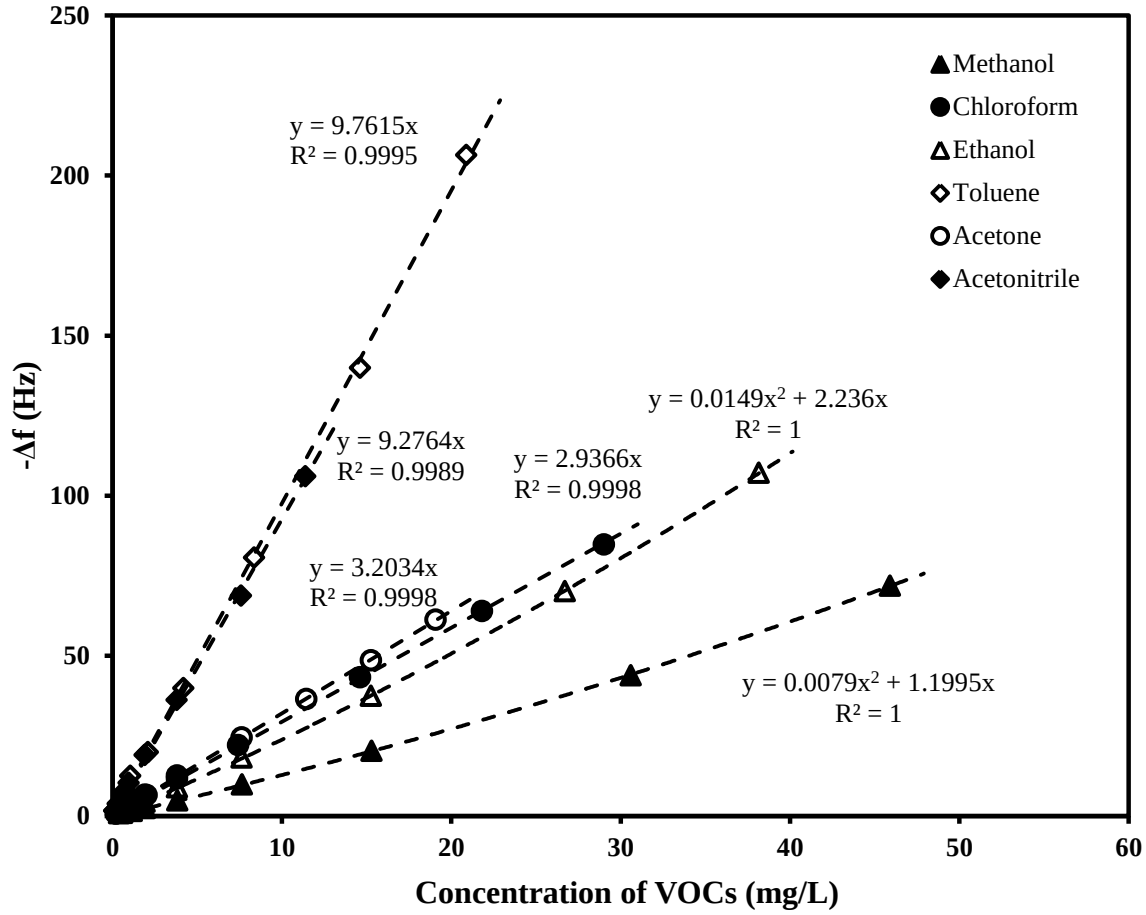

Figure B4 Plots showing the magnitude of frequency shift of a QCM sensor coated with [HMPyr][PF_6]-PMMA on exposure to varying concentration of organic vapor. Amount of sensing material: 90 µg.cm^{-2}. Methanol and ethanol are slightly more polynomial, while others are linear.

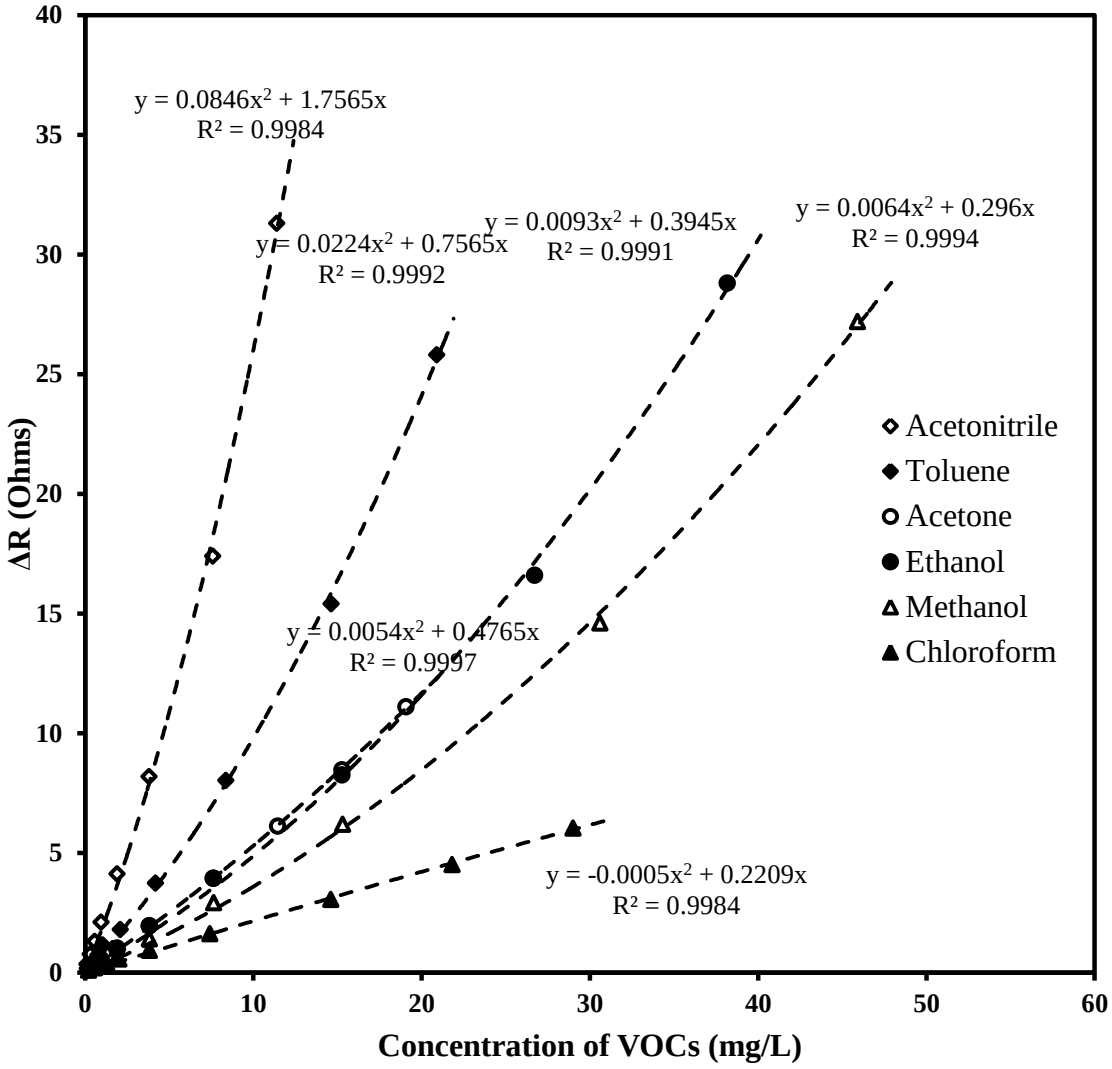

Figure B5 Plots showing the motional resistance shift of a QCM sensor coated with [HMPyr][PF_6]-PMMA on exposure to varying concentration of organic vapor. Amount of sensing material: 90 μg.cm^{-2}. Each analyte shows a second-order polynomial relationship between motional resistance shift and the vapor concentration.

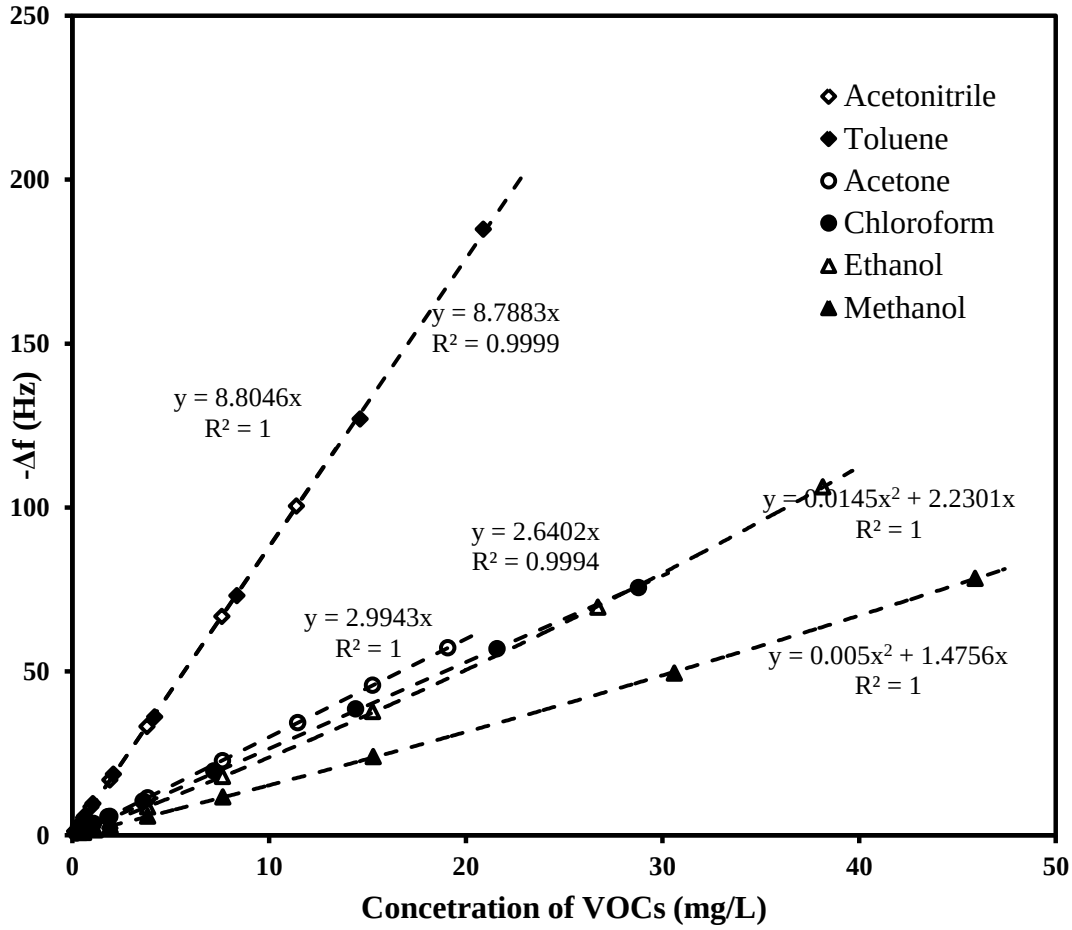

Figure B6 Plots showing the magnitude of frequency shift of a QCM sensor coated with [HMPyr][PF_6]-CA on exposure to varying concentration of organic vapor. Amount of sensing material: 85 µg.cm^{-2}. Each analyte shows a second-order polynomial relationship between the frequency shift and the vapor concentration.

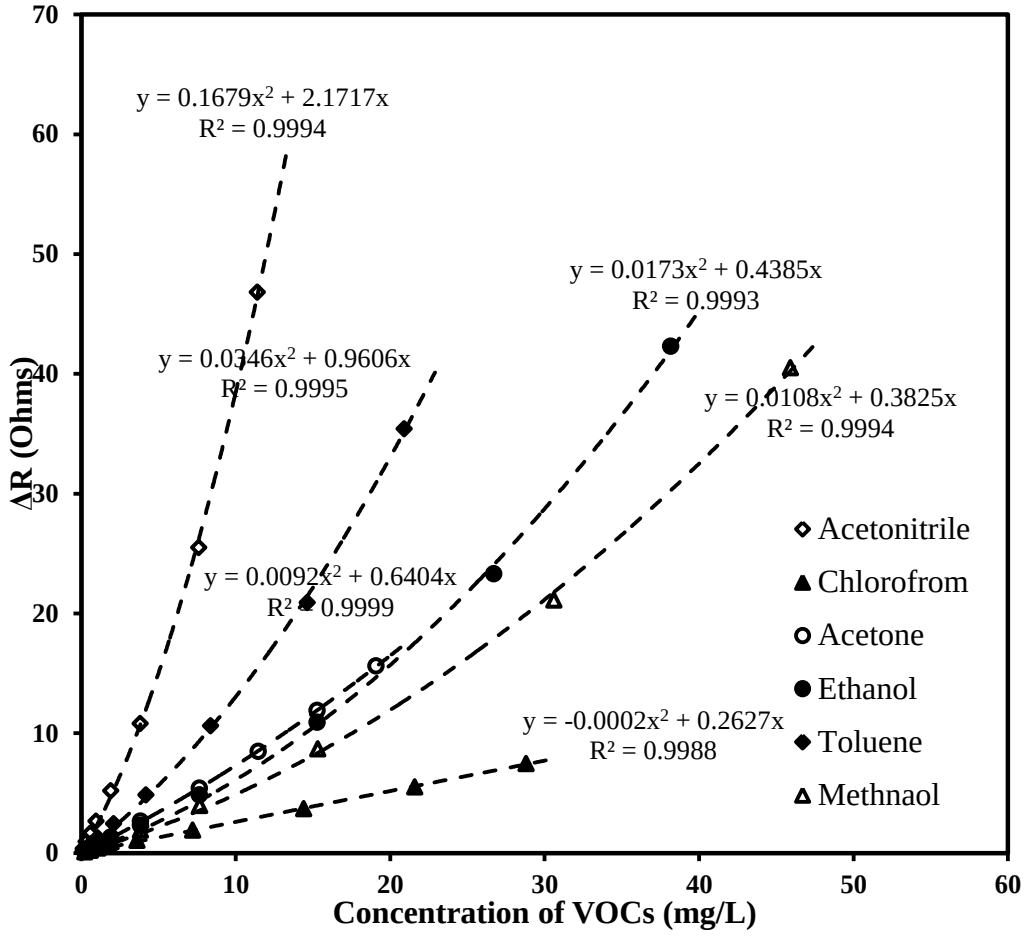

Figure B7 Plots showing the frequency shift of a QCM sensor coated with [HMPyr][PF_6]-CA on exposure to varying concentration of organic vapor. Amount of sensing material: 85 µg.cm^{-2}.

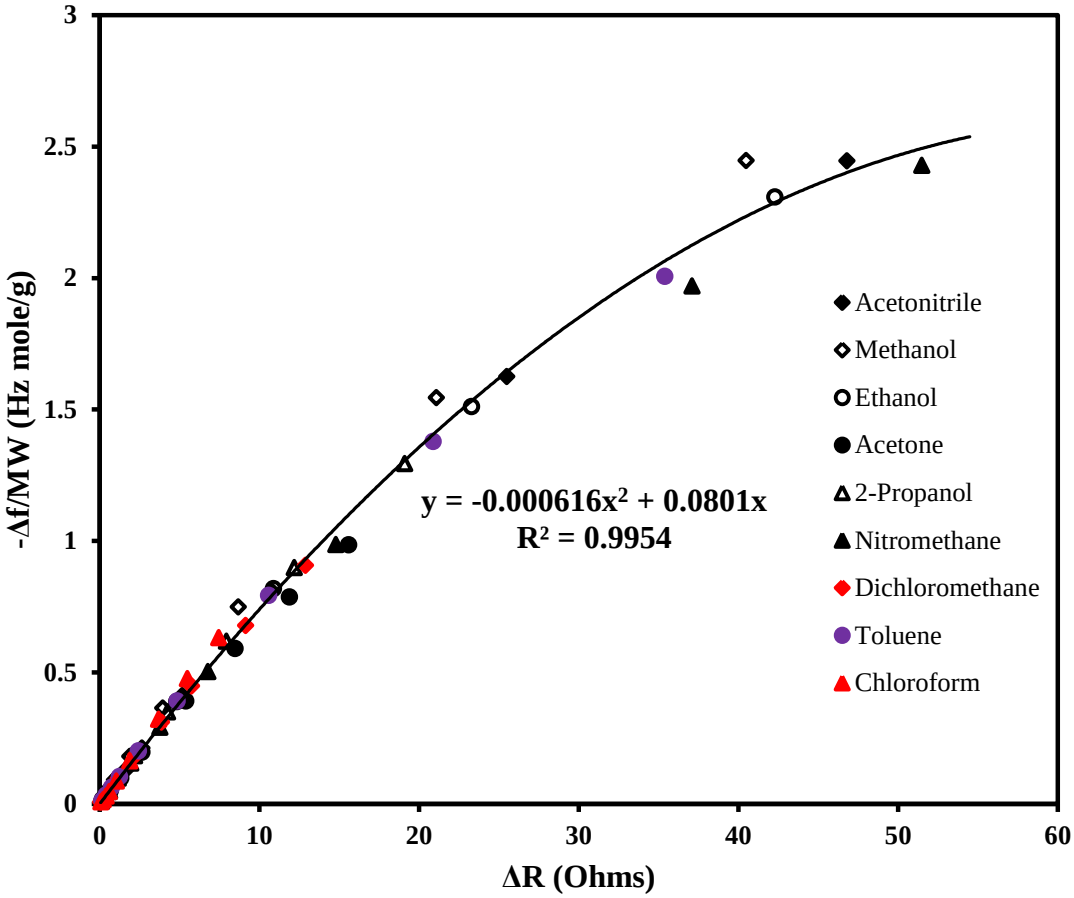

Figure B8 Plot of the ratio of frequency shift to molecular weight against motional resistance shift of a QCM sensor coated with [HMPyr][PF_6]-CA for nine different organic vapors. Concentration ranges of the vapors are 0.574 to 45.9 mg.L^{-1} for methanol, 0.114 to 11.4 mg.L^{-1} for acetonitrile 0.382 to 38.2 mg.L^{-1} for ethanol, 0.191 to 19.1 mg.L^{-1} for acetone, 0.190 to 26.6 mg.L^{-1} for 2-propanol, 0.138 to 6.88 mg.L^{-1} for nitromethane, 0.321 to 64.2 mg.L^{-1} for dichloromethane, 0.125 to 20.9 mg.L^{-1} for toluene, and 0.216 to 29.0 mg.L^{-1} for chloroform.

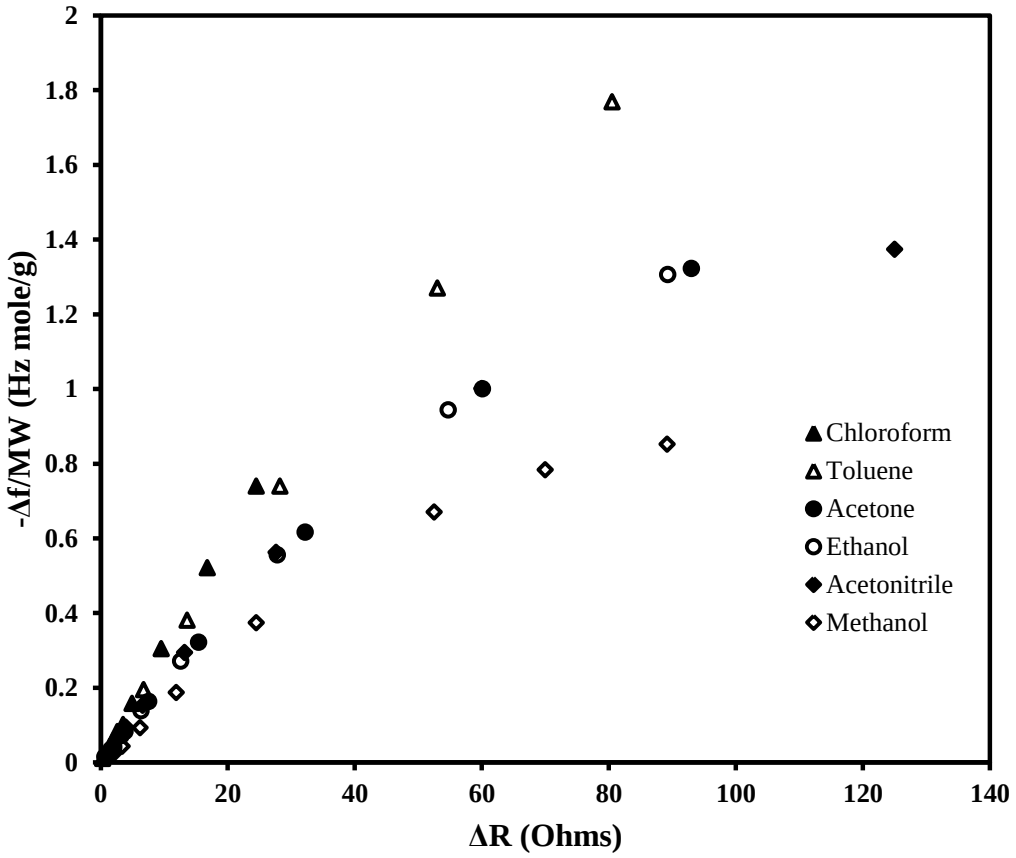

Figure B9 Plot of the ratio of frequency shift to molecular weight against motional resistance shift of a QCM sensor coated with [HMPyr][PF_6]-only for six different organic vapors.

.

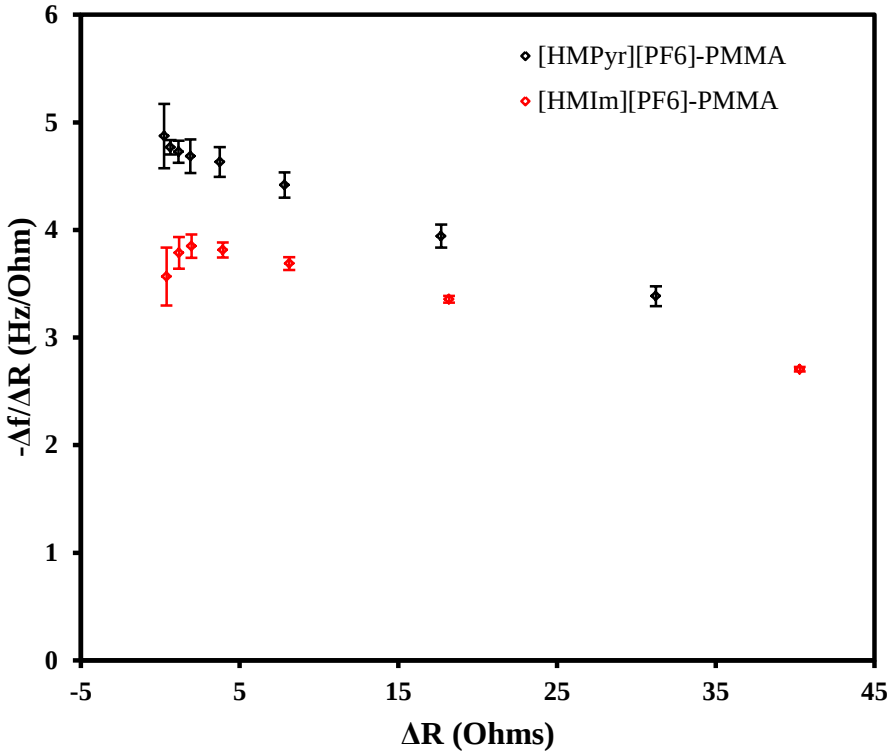

Figure B10 Plot of $\frac{\Delta f}{\Delta R}$ versus ΔR (mean) for two different coatings during the absorption of acetonitrile vapors. Error bars represent the standard deviation of three replicate measurements. Except for the first point, for each coating, which lies near the detection limit, the relative standard deviation of other points lies between 1 to 4 percent. For [HMPyr][PF_6]-PMMA coated sensor each set of measurements were taken in an interval of three hours, while for [HMPIm][PF_6]-PMMA the measurements were taken in an interval of 1 hour. The larger standard deviations may be due to fluctuations in temperature.

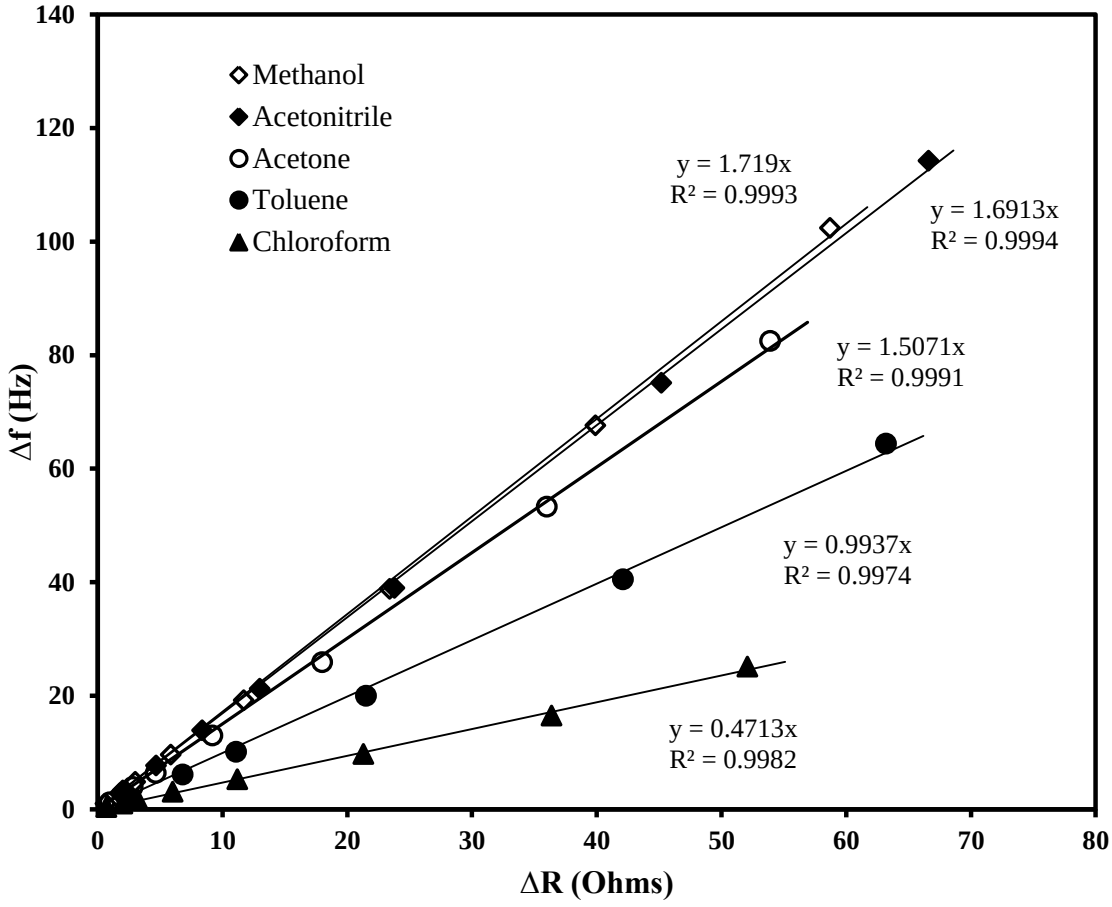

Figure B11 Plots showing the variation of Δ*f* with Δ*R* for a QCM sensor coated with [HMPyr][TFSI] upon exposure to five different organic vapors. Concentration ranges of the vapors are 0.191 to 19.1 mg L^{-1} for methanol, 0.114 to 5.70 mg L^{-1} for acetonitrile 0.191 to 11.4 mg L^{-1} for acetone, 0.210 to 6.27 mg L^{-1} for toluene, and 0.360 to 36.0 mg L^{-1} for chloroform.

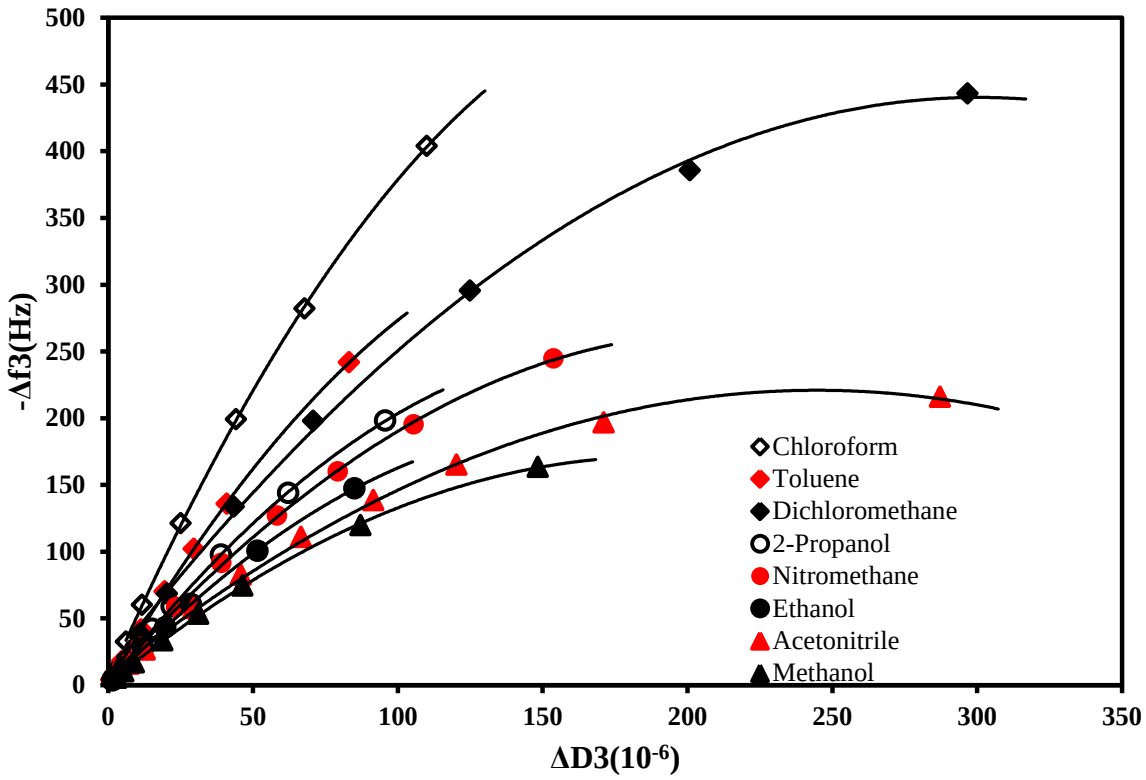

Figure B12 Third harmonic Δ*f* versus Δ*D* plots for different analytes.

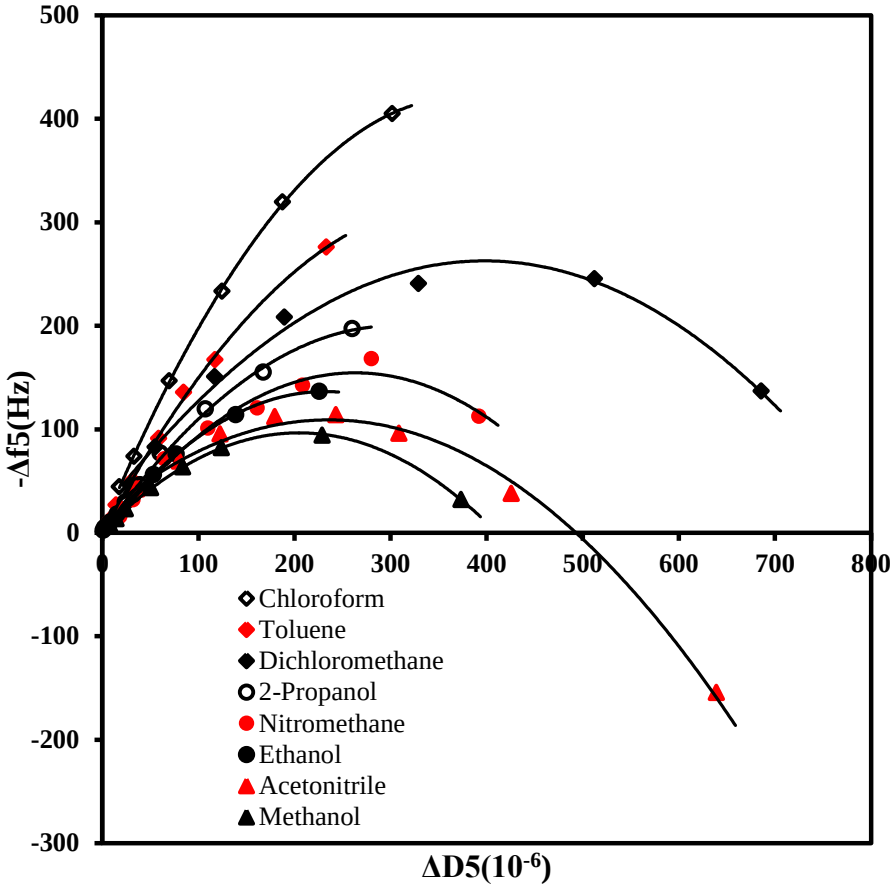

Figure B13 Fifth harmonic Δ*f* versus Δ*D* plots for different analytes.

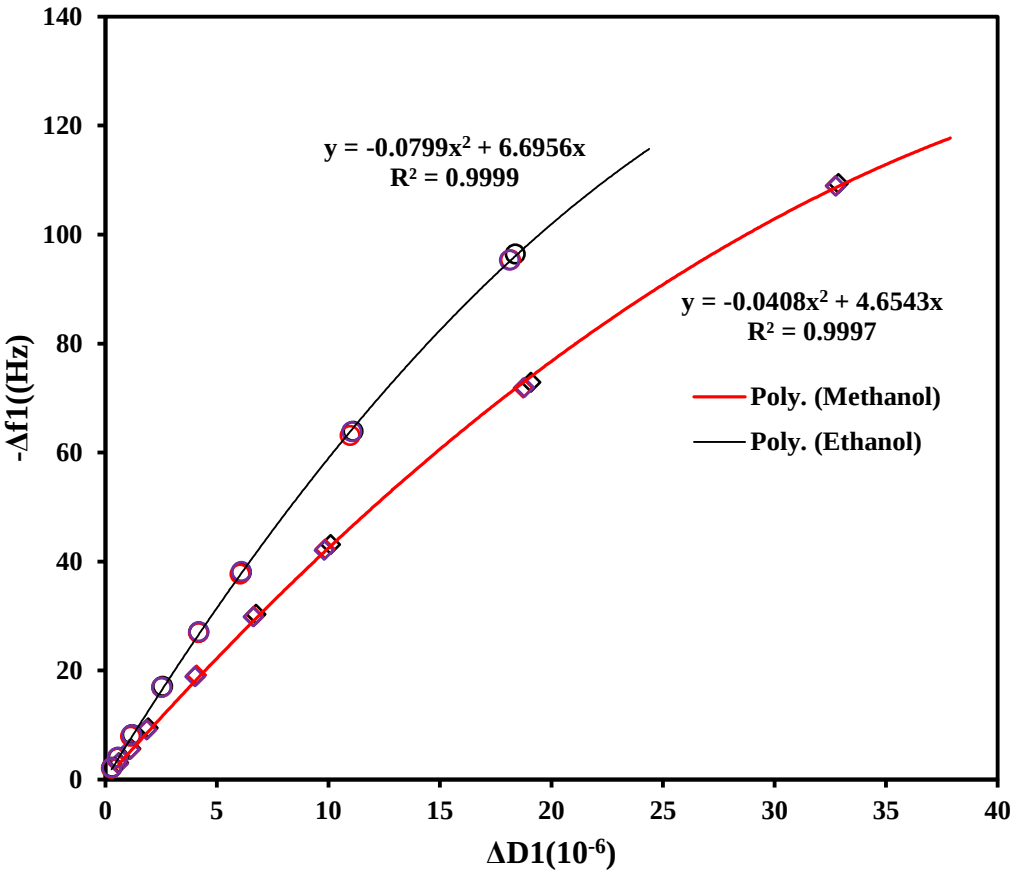

Figure B14 Frequency shift versus dissipation shift plots for the first harmonic of a QCM-D coated with [HMPyr][PF_6]-PMMA during absorption of methanol and ethanol vapors. For each compound, three replicate measurements were performed in the concentration range of 1.5% to 40% of the saturated vapor concentration. The relative standard deviation of $\frac{\Delta f}{\Delta R}$ for each concentration tested was found to be between 0.1% and 1%.

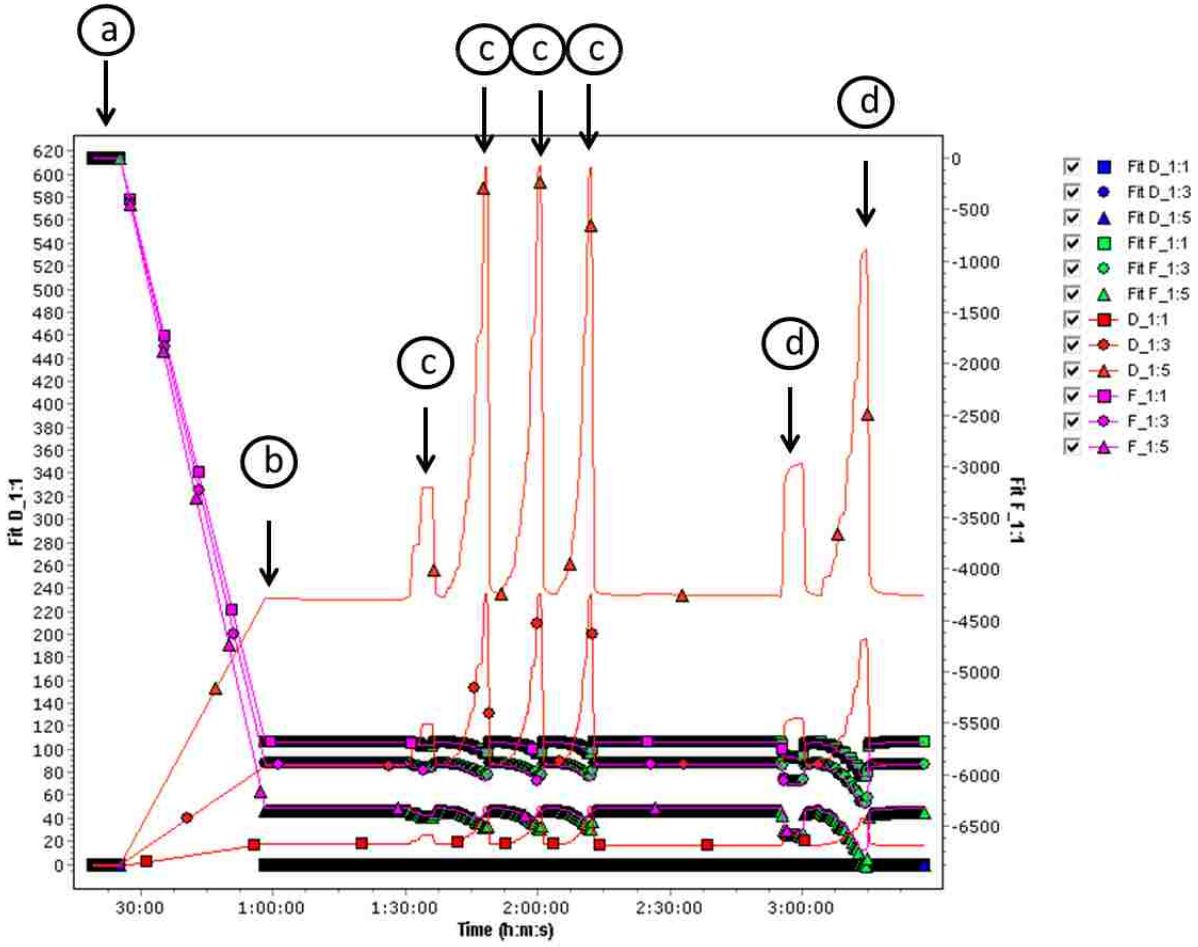

Figure B15 Representative QCM-D data displaying experimental and fit values frequency and dissipation changes for the first, third, and fifth harmonics. The film was assumed to be purely elastic. Arrows represent: (a) bare quartz crystal, (b) after coating with [HMPyr][PF_6]-PMMA, (c) during exposure to methanol vapors, and (d) during exposure to chloroform vapors.

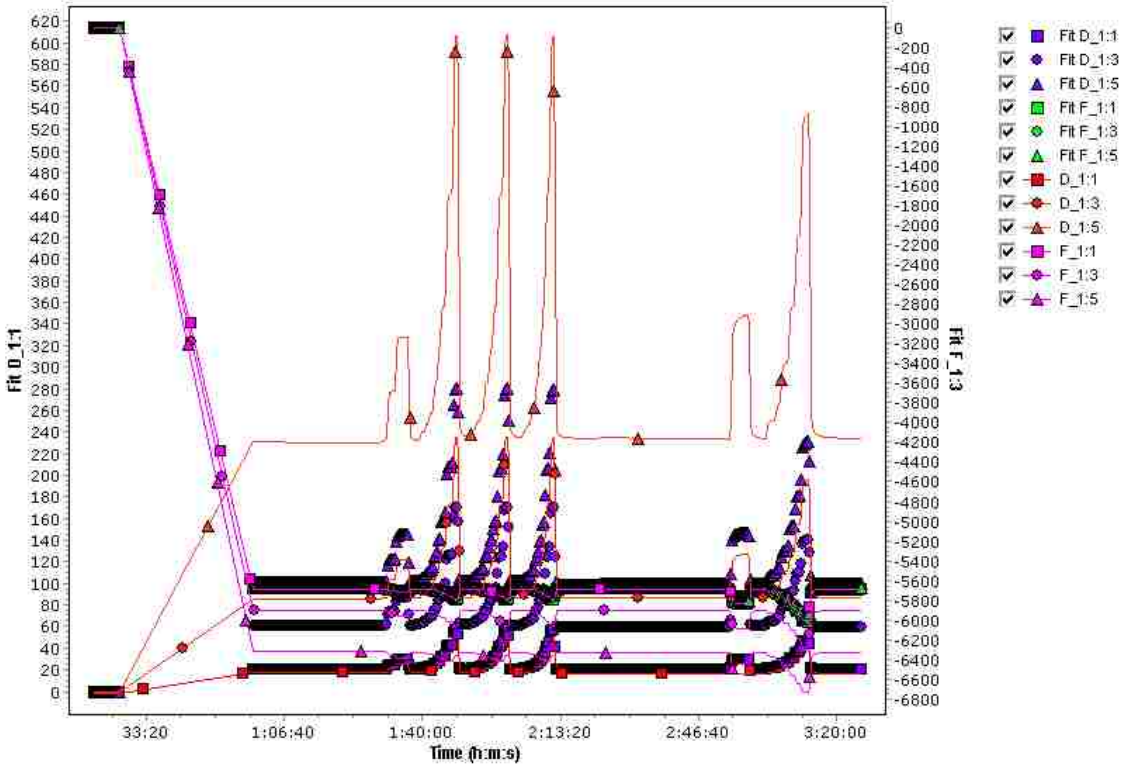

Figure B16 The experimental and fit values of Δf and ΔD by assuming the film to be purely viscous.

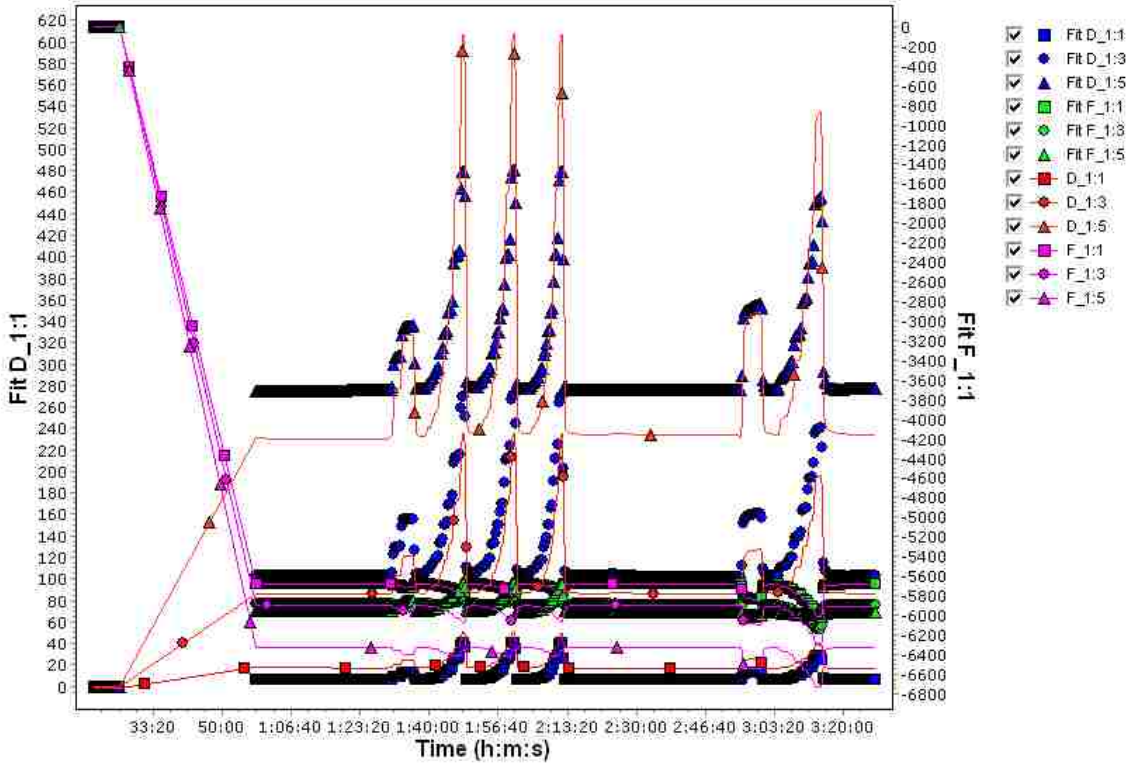

Figure B17 The experimental and fit values of Δf and ΔD by assuming the film follows the Voigt viscoelastic model.

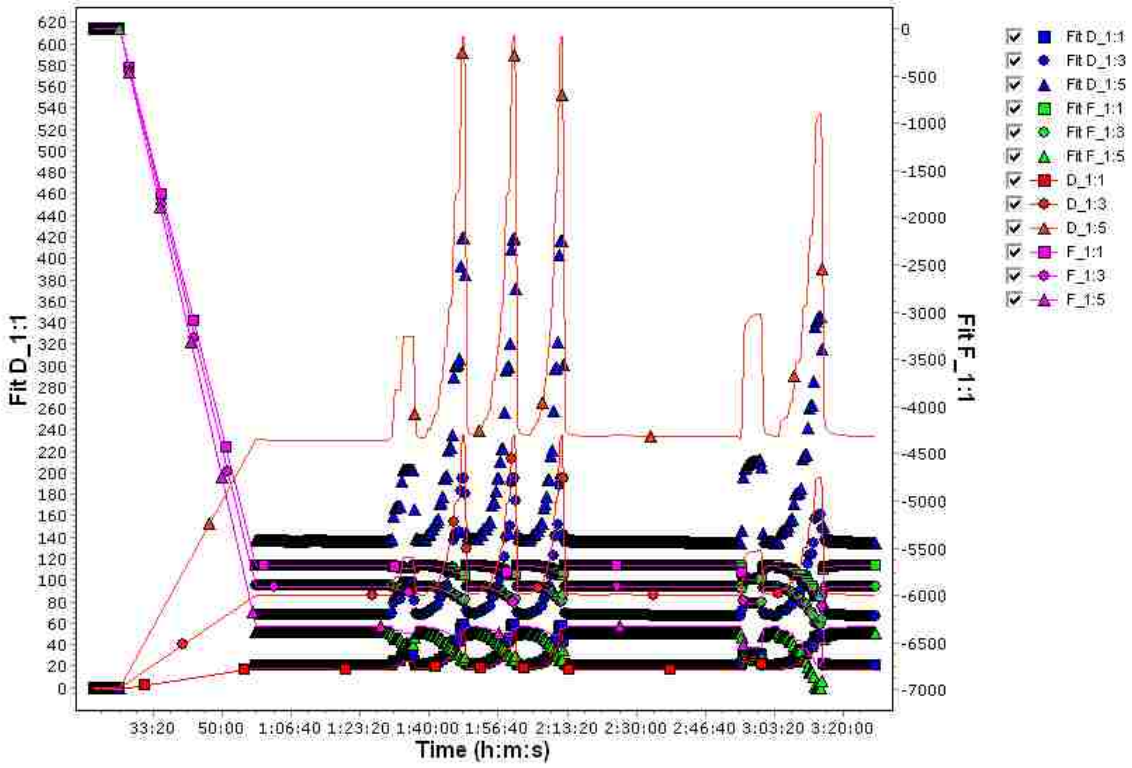

Figure B18 The experimental and fit values of Δf and ΔD by assuming the film follows the Maxwell viscoelastic model.

a

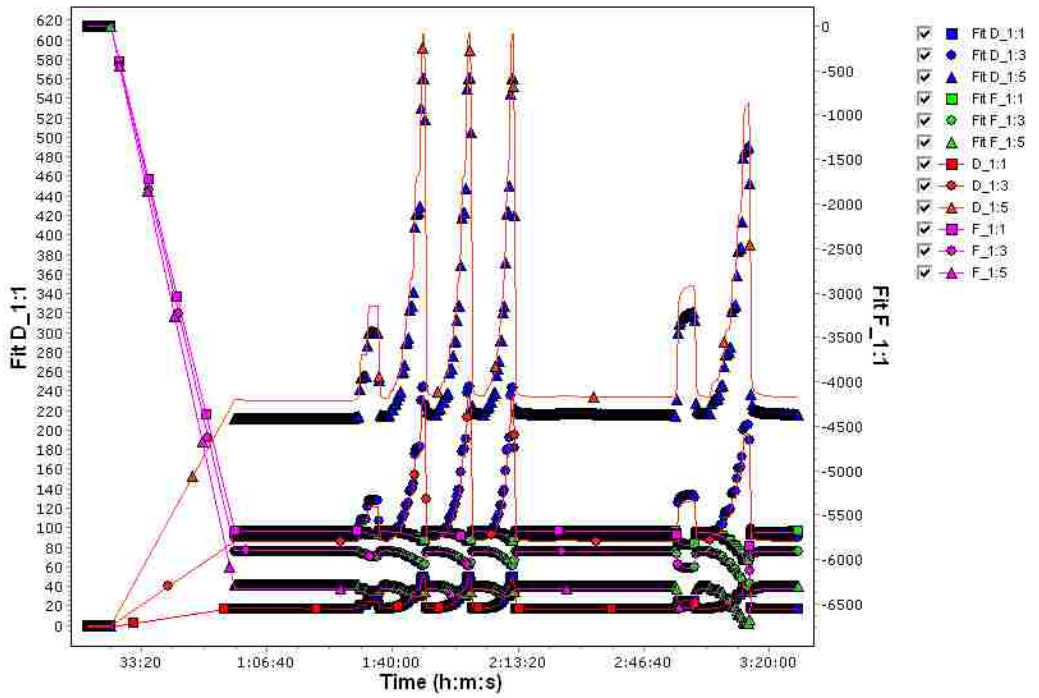

b

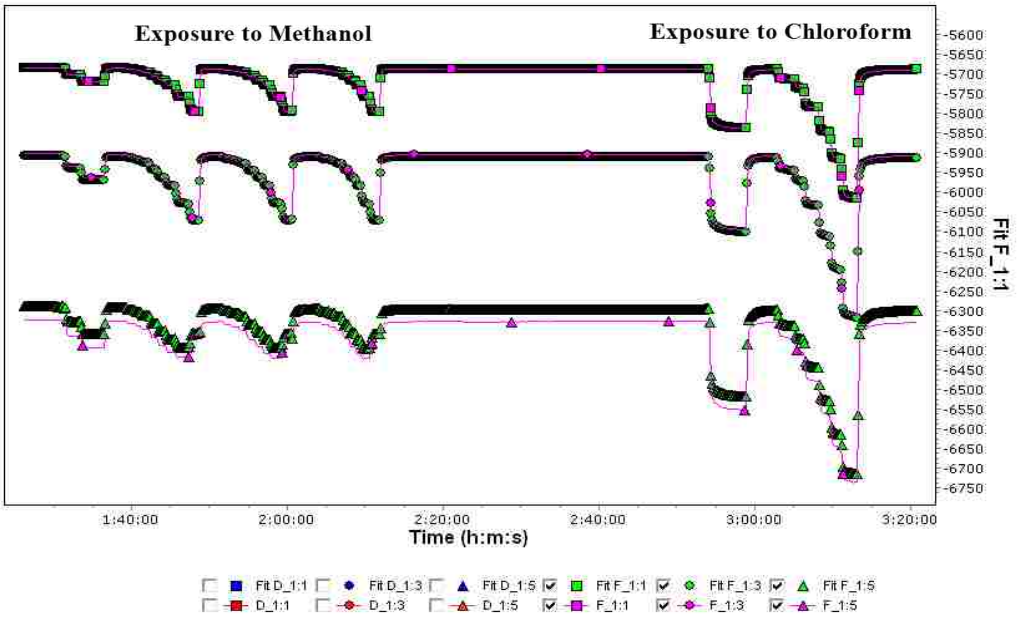

Figure B19 (a) The experimental and fit values of Δ*f* and Δ*D* using the extended Voigt viscoelastic model, (b) experimental and fit values of Δ*f*, and (c*)* experimental and fit values of Δ*D* shown for clarity.

(c)

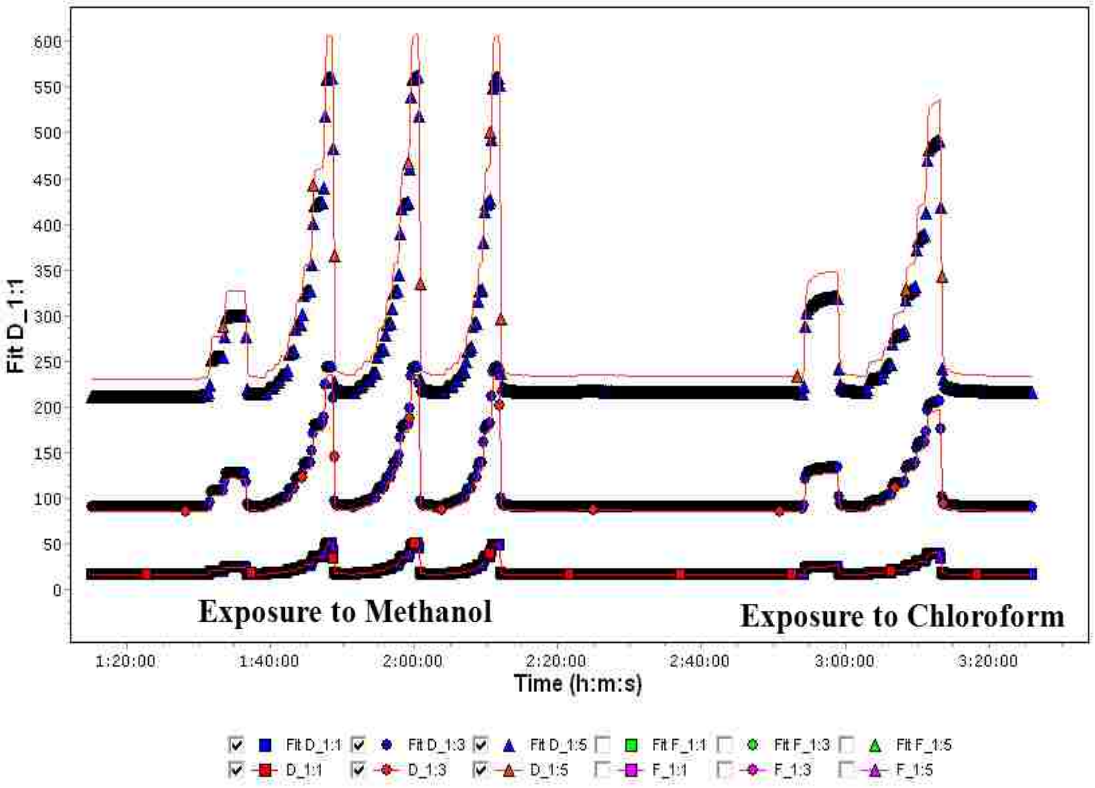

Figure B19 (continued)

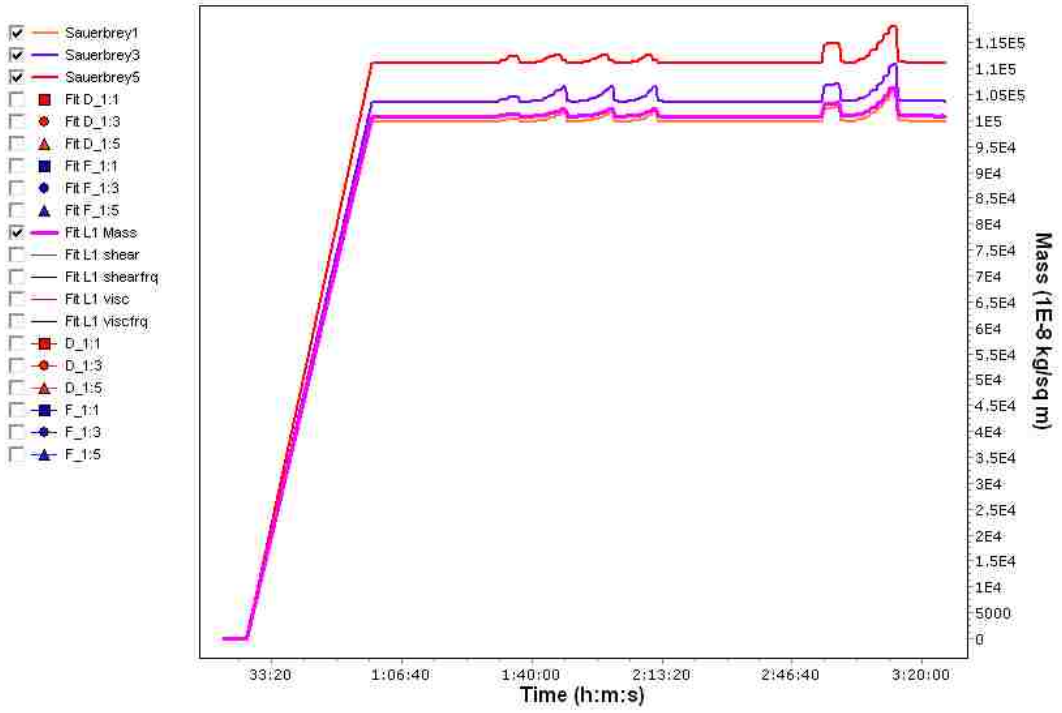

Figure B20 Mass of the film before and after the uptake of vapors as determined by the Sauerbrey equation at the first, third, and fifth harmonics. The fit mass obtained by using the extended Maxwell viscoelastic model is represented by the bold line.

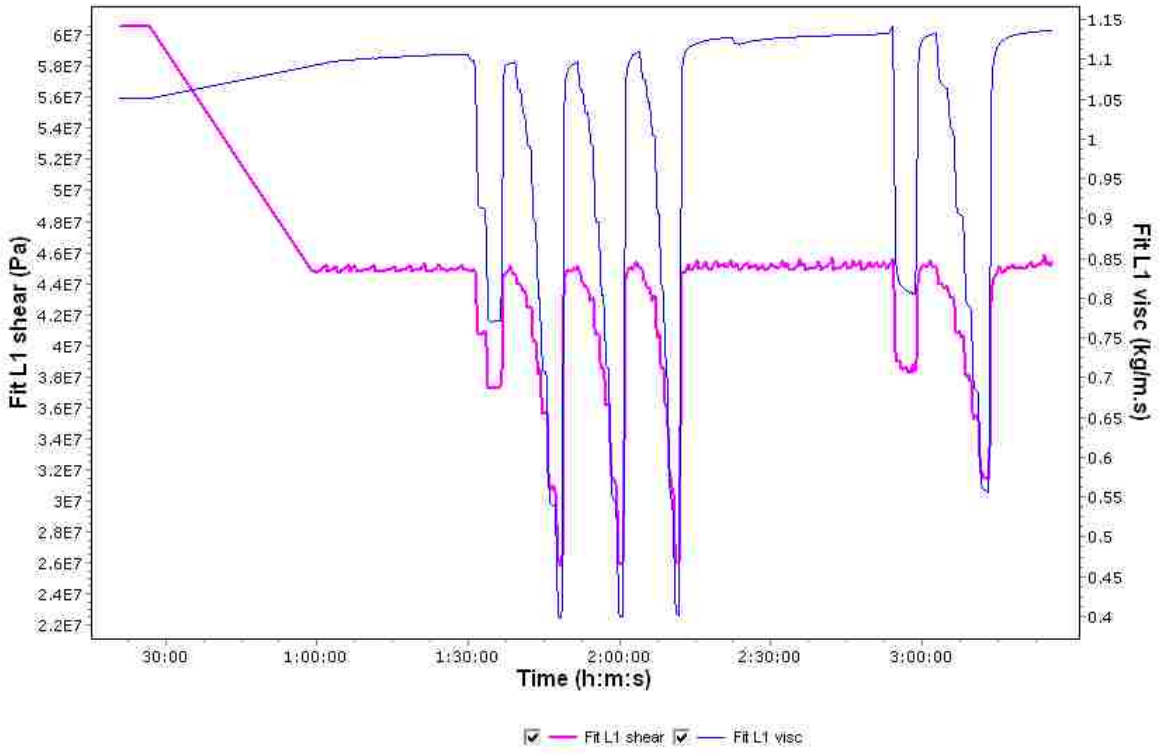

Figure B21 Changes in elastic shear modulus and viscosity of the film during vapor absorption as predicted by the extended Maxwell viscoelastic model.

APPENDIX C PERMISSION LETTER

CONTRACTS-COPYRIGHT (shared) <Contracts-Copyright@rsc.org> Jun 18 (5 days ago)

to me

Dear Bishnu

The Royal Society of Chemistry (RSC) hereby grants permission for the use of your paper(s) specified below in the printed and microfilm version of your thesis. You may also make available the PDF version of your paper(s) that the RSC sent to the corresponding author(s) of your paper(s) upon publication of the paper(s) in the following ways: in your thesis via any website that your university may have for the deposition of theses, via your university's Intranet or via your own personal website. We are however unable to grant you permission to include the PDF version of the paper(s) on its own in your institutional repository. The Royal Society of Chemistry is a signatory to the STM Guidelines on Permissions (available on request).

Please note that if the material specified below or any part of it appears with credit or acknowledgement to a third party then you must also secure permission from that third party before reproducing that material.

Please ensure that the thesis states the following:

Reproduced by permission of The Royal Society of Chemistry

and include a link to the paper on the Royal Society of Chemistry's website.

Please ensure that your co-authors are aware that you are including the paper in your thesis.

Regards

Gill Cockhead
Publishing Contracts & Copyright Executive

Gill Cockhead

Publishing Contracts & Copyright Executive

Royal Society of Chemistry,

Thomas Graham House,

Science Park, Milton Road,

Cambridge, CB4 0WF, UK

Tel +44 (0) 1223 432134

Follow the Royal Society of Chemistry:

www.rsc.org/follow

Winner of The Queen's Award for Enterprise, International Trade 2013

-----Original Message-----

From: bregmi2@tigers.lsu.edu [mailto:bregmi2@tigers.lsu.edu]

Sent: 16 June 2014 22:19

To: CONTRACTS-COPYRIGHT (shared)

Subject: Permission Request Form: Bishnu P. Regmi

Name : Bishnu P. Regmi

Address :

436 Choppin Hall

Baton Rouge, LA 70803

Tel : 2255783919

Fax :

Email : bregmi2@tigers.lsu.edu

I am preparing the following work for publication:

Article/Chapter Title :

Journal/Book Title :

Editor/Author(s) :

Publisher :

I would very much appreciate your permission to use the following material:

Any Additional Comments :

To whom it may concern:

I am the first author of the following two articles published in RSC journals:

1. Bishnu P. Regmi, Nicholas Speller, Michael John Anderson, Jean Olivier Brutus, Yonathan Merid, Susmita Das, Bilal El-Zahab, Daniel J. Hayes, Kermit K. Murray, and Isiah M. Warner. Molecular weight sensing properties of ionic liquid-polymer composite films: theory and experiment. Journal of Materials Chemistry C 2014, 2, 4867-4878.

2.Bishnu P. Regmi, Joshua Monk, Bilal El-Zahab, Susmita Das, Franscisco R. Hung, Daniel J. Hayes, and Isiah M. Warner. A novel composite film for detection and molecular weight determination of organic vapors. Journal of Materials Chemistry 2012, 22, 13732-13741.

I would very much appreciate your permission to use these materials in my PhD dissertation.

Regards,

Bishnu Regmi

Warner research Group

Louisiana State University

Baton Rouge, LA 70803

USA

VITA

Bishnu Regmi was born to Damawati and Devi Prasad Regmi. He grew up in a small town in Syangja, Nepal. He began his undergraduate work at Tribhuvan University, and graduated majoring in Physical Chemistry in 1997. After teaching for seven years in high school and college levels, he moved to Utah State University and graduated with a Master's degree in Biocehmistry in 2008. In the same year, he was admitted to Louisiana State University where he began his research in Analytical Chemistry under the guidance of Professor Isiah M. Warner. He worked on development of GUMBOS- and ionic liquid-based quartz crystal microbalance sensor for detection and molecular weight estimation of volatile organic compounds. During this time, he published five manuscripts in peer-reviewed journals, and more than five manuscripts are under different stages of preparation and one pending patent.

Bishnu is a member of the American Chemical Society. He has presented his research in several regional and national conferences. He was awarded 2013-2014 Kiran Allam International Award for outstanding contribution is research and teaching at LSU Chemistry. He expects to graduate with the degree of Doctor of Philosophy in Chemistry on August 8, 2014 at the LSU summer commencement. After graduation, Bishnu plans to work with Professor David R. Walt at Tufts University as a postdoctoral scholar.